Master Thesis in Geographical Information Science nr 153

WILDFIRE GROWTH MODELLING IN SWEDEN

– a suitability assessment of available data –

Henrik Hagelin

2023
Department of
Physical Geography and Ecosystem Science
Centre for Geographical Information Systems
Lund University
Sölvegatan 12
S-223 62 Lund
Sweden

Henrik Hagelin (2023). Wildfire growth modelling in Sweden – a suitability assessment of available data
Master degree thesis, 30 ECTS credits in Master in Geographical Information Science
Department of Physical Geography and Ecosystem Science, Lund University

WILDFIRE GROWTH MODELLING IN SWEDEN

– a suitability assessment of available data –

Henrik Hagelin

Master degree thesis, 30 ECTS credits

in Geographical Information Science

Dept. of Physical Geography & Ecosystem Science

Centre for Geographical Information Systems

Lund University

Sweden

2023

Supervisor

Veiko Lehsten

veiko.lehsten@nateko.lu.se

Chairperson examining committee

Jonas Ardö

jonas.ardo@nateko.lu.se

Preface

I, the author, have a BSc degree in physical geography and ecosystem analysis, a certificate in fire, rescue and safety work (i.e. civil protection training programme governed by the Swedish regulation SFS 2003:447), and work experience as a firefighter at a Swedish municipal fire and rescue service. In 2018, I begun the development of WiSE-FASS. WiSE-FASS is tested for the first time in this study.

This thesis project marks the end of the MSc programme in geographical information science. The course is given at the Department of Physical Geography and Ecosystem Science at Lund University, Sweden, and comprises 30 ECTS credits. I, the author, would like to thank the following persons for their support and guidance. Without your input, the thesis work would have been more difficult to complete.

⋆ **Veiko Lehsten** (PhD) [*Department of Physical Geography and Ecosystem Science, Lund University*]
Thank you for supervising the work.

⋆ **Ulrik Mårtensson** [*Department of Physical Geography and Ecosystem Science, Lund University*]
Thank you for reviewing the manuscript and for providing inputs on how to enhance the manuscript.

⋆ **Martin Haag** (PhD) [*European Space Research and Technology Centre, the European Space Agency*]
Thank you for reviewing the manuscript and for providing inputs on how to enhance the manuscript.

⋆ **Oscar Elias**
Thank you for proofreading the thesis.

⋆ **Britta Smångs** [*Geolibrary, Lund University*]
Thank you for providing guidelines about reference writing and for assisting me finding articles seemingly impossible to acquire.

⋆ **Family and friends**
Thank you for giving useful inputs, love and support during this hectic time.

Summary

Wildfires are worldwide problems that stress societies by damaging their economies and they cause serious, sometimes fatal, health implications among the populations. In recent years, the rate of wildfire occurrence has increased as the global average temperature has risen. Because of global climate change, this rate is expected to continue rising. In Sweden, in the aftermath of the 2014 Västmanland wildfire, the Swedish Civil Contingencies Agency called for an urgent need to develop the national emergency preparedness for disastrous events like wildfires. Maps of forecasted wildfire growth can facilitate the work of emergency services trying to limit the consequences of a wildfire. Hence, the introduction of a wildland fire growth simulation model has the potential to strengthen the Swedish societal resilience to wildfires. However, no Swedish guidelines outlining the necessary collection and preparation of spatial information, required by wildland fire growth simulation models, currently exist. Therefore, the aim of this thesis project was to assess the suitability of available spatial data in Sweden for wildfire growth modelling. This was achieved by first reviewing literature to gain the needed understanding of general wildfire behaviour to allow for the theorising of an expected wildfire propagation in the area burnt by the 2014 Västmanland wildfire. Then, the 2014 Västmanland wildfire was modelled using two wildland fire growth simulation models. Their modelled extents were reviewed and compared with real final perimeter of the modelled wildfire. Finally, based on observed deviations, weaknesses in the spatial data were identified. The study concludes that the, in Sweden, available spatial data is sufficient to allow for wildfire growth modelling. However, the temporal resolution of the ground cover information must increase to reflect changes in vegetation before the modelled forecasts can be suitable for any use.

Keywords
Geography · GIS · Geographic Information Science · Physical geography · Prometheus · WiSE-FASS · The 2014 Västmanland wildfire · Wildfire growth modelling · Wildfire suppression support · Wildfire behaviour · MESAN

Sammanfattning

Vegetationsbränder är världsomspännande problem som skakar samhällen genom att skada deras ekonomier och orsaka allvarliga, ibland dödliga, hälsokomplikationer bland deras befolkningar. Takten av vegetationsbrandsförekomst har ökat de senaste åren till följd av en stigande global medeltemperatur. Denna takt förväntas att fortsätta öka på grund av den globala uppvärmningen. I efterdyningarna av branden i Västmanland, 2014, rapporterade Myndigheten för Samhällsskydd och Beredskap om ett akut behov av att öka den nationella krisberedskapen i Sverige för katastrofala händelser såsom vegetationsbränder. Kartor över prognostiserad vegetationsbrandstillväxt kan underlätta räddningstjänstens arbete med att begränsa konsekvenserna av löpeld. Om ett modellsystem för simulering av löpeldstillväxt implementeras i Sverige kan motståndskraften i samhället mot vegetationsbränder stärkas. Det finns dock inga riktlinjer som beskriver den nödvändiga insamlingen och beredningen av de rumsliga datamängder som krävs av ett sådant modellsystem. Därför var syftet med detta examensarbete att bedöma lämpligheten av tillgänglig rumslig data för modellering av vegetationsbrandstillväxt. Detta uppnåddes genom att först utföra litteraturstudier för att skapa en nödvändig teoretisk förståelse av förväntad brandtillväxt under en referensbrand. Därefter modellerades referensbranden med hjälp av två befintliga simuleringsmodeller. Den prognostiserade löpeldstillväxten jämfördes med referensbrandens kända perimeter och med hjälp av den teoretiska förväntningen kunde slutligen svagheter i den rumsliga datan identifieras. I detta arbete dras slutsatsen att upplösningen av den geografiska data som finns tillgänglig i Sverige är tillräcklig för modellering av brandtillväxt i vegetation. Däremot måste marktäckesinformationens temporala upplösning öka från dagens fem år till en upplösning som kan återspegla naturliga variationer i vegetationen. Fram till dess förblir modellering av vegetationsbränder olämpligt för all typ av användning i Sverige.

Nyckelord

Geografi · GIS · Geografisk informationsvetenskap · Naturgeografi · Prometheus · WISE-FASS · Skogsbranden i Västmanland 2014 · Modellerad tillväxt av vegetationsbrand · Understödd brandbekämpning i vegetation · Brandbeteende i vegetation · MESAN

Table of Contents

Nomenclature

Abbreviations & definitions

BUI	Buildup Index - component of the FWI system.
CFFDRS	Canadian Forest Fire Danger Rating System.
DC	Drought Code - component of the FWI system.
DEM	Digital Elevation Model.
DMC	Duff Moisture Code - component of the FWI system.
EPSG	European Petroleum Survey Group.
Esri	Environmental Systems Research Institute.
FBP System	Canadian Forest Fire Behaviour Prediction System.
FFMC	Fine Fuel Moisture Code - component of the FWI system.
FWI System	Canadian Forest Fire Weather Index System.
GIScience	Geographic Information Science.
GIS	Geographic Information System.
IDW	Inverse Distance Weighting - an interpolation method.
IPCC	Intergovernmental Panel on Climate Change.
ISI	Initial Spread Index - component of the FWI system.
Lantmäteriet	Land Survey of Sweden.
MASL	Metre above sea level.
MESAN	Mesoscale Analysis.
MSB	Swedish Civil Contingencies Agency.
NFDRS	National Fire Danger Rating System.
NWCG	National Wildfire Coordinating Group.

Prometheus	The Canadian Wildland Fire Growth Simulation Model.
SLU	Swedish University of Agricultural Sciences.
SMHI	Swedish Meteorological and Hydrological Institute.
TIN	Triangulated Irregular Network - an interpolation method.
WiSE-FASS	Wildfire State Estimator & Fire Attack Support System.

Terminology

Dead fuel moisture of extinction	*Fuel type* specific threshold marking the highest level of moisture content at which *pyrolysis* can occur.
Fire break	Barrier to *wildfire* propagation. Interchangeable with barrier.
Fire flanks	Sides of the burning perimeter. Often parallel to the *fire front*.
Fire front	Part of the burning perimeter having the highest rate of propagation. It constitutes the main direction of propagation.
Fire head / Head of a fire	Part of the burning perimeter having a higher rate of propagation than its surroundings. Visible as a bulge on the burning perimeter.
Fire point	Temperature threshold at which the energy release from combustion of *fuel* can keep a *flame* alive for a minimum of five seconds.
Fire rear	Part of the burning perimeter located 180° from the *fire front*.
Fire spotting	Burning matter uplifted and transported by the wind.
Flame	Smallest component of a fire.
Flash point	Threshold value specifying the lowest temperature at which ignition of *fuel* can occur.
Fuel type	Set of instructions describing the combustion of a ground cover class.
Fuel	Carbon molecules released through *pyrolysis* of organic matter.
Hotspot	Burning cell/pixel.
Ignition point	Location of *wildfire* initiation.
Pyrolysis	Thermochemical process in which matter decomposes into gas.
The 2014 Västmanland wildfire	Catastrophic *wildfire* that ravage the Västmanland County, Sweden, in 2014. Used as reference fire in the present study.
u component of wind	Zonal (i.e. latitudinal) wind flow.
v component of wind	Meridional (i.e. longitudinal) wind flow.
Wildfire	Non-urban fire growing uncontrolled, in all directions, in vegetation.
Wildland fire	Umbrella term encompassing prescribed fire and *wildfire*.

Chapter 1

Introduction

Prolonged periods of higher than normal temperatures and a fourth of the normal precipitation amounts were reasons to the overall high fire risk level during the summer of 2014 in Sweden (SMHI 2014a; MSB 2015). On 31 July, the Swedish Meteorological and Hydrological Institute (SMHI) increased the fire risk level to extreme in the Västmanland County as a result of the recent weather situation. Later the same day, a sparkle from a forest scarifier ignited a wildfire, commonly referred to as the *2014 Västmanland wildfire*, that grew in size for six days to become the largest single wildfire disaster in Sweden since the middle of the 20th century. The disaster quickly overwhelmed the local emergency services and the Swedish authorities because of its rapid growth and the complexity to strategically plan and deploy fire extinguishing resources in the remote terrain in which the wildfire raged. Extensive resources were required to protect inhabitants and assets in the area, including four firefighting airplanes flown in from abroad to facilitate the extinguishing work (MSB 2015, 2018). In total, about 9 600 ha of forest were damaged by the conflagration meaning an estimated cost of damage of SEK 1 billion for forest owners (Länsstyrelsen i Västmanlands län 2014). Following the severe incident, the Swedish Civil Contingencies Agency (MSB) reported a need to increase the emergency preparedness in Sweden for complex events such as wildfires (MSB 2016). Two years later, in the summer of 2018, the wildfire risk level, in Sweden, were once again extreme because of long lasting heatwaves and small amounts of precipitation. Open burning prohibition orders were issued in all Swedish counties to reduce the risk of wildfire occurrences (MSB 2018). However, despite these measures, a large number of wildfires raged during this summer in most counties. For example, 75 wildfires were reported to the Swedish authorities in mid July (Malmstedt and Hedlund 2018) and the total area affected by wildfires became the largest ever statistically compiled in Sweden (MSB 2018). About 20 000 ha, representing four fifths of the total area, were burnt in the counties Dalarna, Gävleborg, Jämtland and Västernorrland (López et al. 2018). Furthermore, wildfire hazard constitutes a major worldwide threat to urban societies, forests and other terrestrial ecosystems (Krivtsov et al. 2009). Every year, wildfires stress societies around the world by straining their economies and causing an increased risk of impaired health, and even fatality, among its populations. A recent example is *Camp Fire*, one of the many wildfires raging in California, USA, during the summer of 2018, that completely combusted the city *Paradise* and forced tens of thousands of people to evacuate (Lam et al. 2018). In a warming climate, the wildfire risk increases meaning that the occurrence of catastrophic wildfires, like those affecting Sweden in 2014 and 2018, can be expected (IPCC 2014, 2018; MSB 2018). Wildfire growth modelling can be applied to forecast wildfire propagation, hence it has the potential

facilitating both the process of allocating fire extinguishing resources and the evacuation of urban areas (Vakalis et al. 2004; Reinhardt and Dickinson 2010). Perhaps the introduction of a wildland fire growth simulation model would make the Swedish society better prepared for wildfires.

Prometheus, FARSITE and Wildfire Analyst are three of the most commonly used wildland fire growth simulation models throughout the world (Finney 2004; Opperman et al. 2006; Tymstra et al. 2010; Ramirez et al. 2011). None of these are adapted to simulate wildfire growth in Swedish vegetation (Hansen 2008; Burman et al. 2016; Hagelin and Cluzel 2016). However, since Prometheus is developed for use in Canada, a country with similar vegetation and climate as Sweden, it has been assumed to be the most suitable wildland fire growth simulation model for use in Sweden (Burman et al. 2016; Hagelin and Cluzel 2016). Prometheus was chosen as the main simulation model in this study. Information of why a simulation model was needed is described by the study aim and research objectives in section 1.1. A second wildland fire growth simulation model was tested as it is designed for use in Sweden. It is unpublished and incomplete meaning a poor simulation performance is expected. Thus, a comparison between the simulation models is unreasonable. This is specified as one of five limitations in section 1.2.

1.1 Aim and research objectives

Despite the fact that wildland fire growth simulation models have the potential constituting crucial tools when trying to limit the consequences of wildfires, no such models are currently used in Sweden and no national guidelines for the data preparation, required for wildfire growth modelling, exist. Therefore, the aim of this thesis project was to assess the suitability of available spatial data in Sweden for wildfire growth modelling. The following six objectives were established to ease the fulfilment of this aim:

Objective 1: *Review the literature and describe wildfire influential factors by introducing the theory of general fires, wildfires and some concepts of wildfire modelling to gain an understanding of how wildfires propagate in different environments, and, based on this understanding, summarise the prerequisites for wildfire growth in the study area (i.e. the region affected by the 2014 Västmanland wildfire), to theorise an expected wildfire propagation, in the study area, needed when interpreting the performed simulations.*

Objective 2: *Retrieve the spatial information needed for the creation of all input data sets, and perform the necessary preprocessing of this information, required by the two wildland fire growth simulation models.*

Objective 3: *Compare one of the simulations, performed in this study, with a comparable simulation, by Hagelin and Cluzel (2016), that used a different weather data input and evaluate whether the weather data used in the present study better reflects the actual weather conditions during the 2014 Västmanland wildfire.*

Objective 4: *Contrast the extents modelled in two comparable simulations, performed in the present study, focusing on the influence of fire breaks, contained in a barrier input used in one of the simulations, on the modelled wildfire growth and form recommendations regarding future collection of barrier information.*

Objective 5: *Analyse the performance of the novel wildland fire growth simulation model by comparing its modelled extent to the real fire perimeter and try explaining noticeable deviations using its data inputs.*

Objective 6: *Evaluate whether the spatial and temporal resolutions of the in Sweden available spatial information are sufficient to allow for wildfire growth modelling intended to support wildfire suppression.*

1.2 Project limitations

Wildfire modelling is an interdisciplinary field involving aspects from, among others, pyrology, physical geography, GIScience, mathematics and computer science. It was not feasible covering all aspects within this project. The following sections 1.2.1 to 1.2.5 detail the five limitations that delineated the project.

1.2.1 Ground truth availability

In Sweden, the 2014 Västmanland wildfire is the only wildfire sufficiently documented to allow for wildfire growth modelling. Also, only its final perimeter is made available by the Swedish authorities. Consequently, the 2014 Västmanland wildfire is the only wildfire used as reference fire in the present study and the interpretation of the modelled wildfire growths is restricted to its outermost perimeter.

1.2.2 A lack of comparable studies

Only the paper by Hagelin and Cluzel (2016) describes a simulation of the 2014 Västmanland wildfire using Prometheus and unmodified input data. Hence, only one of the Prometheus simulations detailed in that study was used as comparative simulation when assessing the weather data input according to objective 3. In contrast, WiSE-FASS (i.e. simulation model 2) has not been described in literature.

1.2.3 Incomparable simulation models

The tested wildland fire growth simulation models differ widely in terms of their completeness. Hence, a thorough intercomparison of the models cannot be made. Instead, area measurements of their modelled wildfire growths are summarised and compared to the surface burnt by the 2014 Västmanland wildfire.

1.2.4 Challenging data interpolation

Most wildland fire growth simulation models require data inputs having the same spatial resolution. Therefore, data interpolation is often part of the input data creation process. However, the conventional deterministic and stochastic interpolation techniques (e.g. IDW; Kriging; TIN; Trend surface analysis), found in major GIS, are not always suitable options when an increased spatial resolution is needed. Wind velocity and direction are correlated to other spatial information (Song et al. 2013) meaning analyses designed to deal with wind data should preferably be used when an increased spatial resolution of such indices is needed. Unfortunately, application of a proper wind model, such as WindNinja, could not be performed because of the confined time frame of this thesis work. Instead, the present study implements a method that increases the data pixel resolution without altering the original information.

1.2.5 Incompleteness of the barrier input

An input containing fire breaks is included in one of the simulations performed in the present study. These fire breaks are represented by line features digitised on estimated locations interpreted from the summary by MSB (2015). Their exact coordinates are not detailed in this summary meaning they may

not be correctly rendered. Also, the active wildfire suppression, carried out by the emergency services in the field, is not reflected in the barrier input. Thus, the simulation including the barrier input should not be considered to accurately reflect the real course of events during the 2014 Västmanland wildfire.

Chapter 2

Theoretical background

Simulation of wildfires requires preparation of large amounts of data, often in model specific formats, that are based on terrain, ground cover and weather information (Finney 2004; Tymstra et al. 2010; Ramirez et al. 2011; Andrews 2018). This preparatory task is a time consuming process, even for trained GIS professionals, that often delays the simulation start. Consequently, the modelled forecasts, that potentially facilitates the work of fire officials to correctly coordinate personnel and resources for an effective fire attack and early fire suppression, are delivered too late. Since wildfires growing in size often exceed the fire fighting capabilities of emergency services within hours from their ignitions (MSB 2018), it is clear that automatic preparation of model inputs would allow for immediate initiation of a simulation when desired. However, none of the most commonly used wildland fire growth simulation models are designed for someone actively combating an intensifying wildfire (Finney 2004; Opperman et al. 2006; Tymstra et al. 2010; Ramirez et al. 2011). They have cluttered, typically due to feature-packed, user interfaces, require multistep configuration, and lack functionality to automatically prepare their data inputs. Also, their inputs cannot be updated by a user during a simulation because simulations are executed in a virtual representation of the study area that is stored in computer memory.

The first section (2.1) of this chapter depicts the complex task to model the growth of a wildfire. It introduces basic fire theory, the physical factors influencing wildfire behaviour, and some field related concepts to increase the understanding of why forecasting of wildfire growth is difficult to perform. The subsequent sections 2.2 and 2.3 briefly introduce the simulation models that were used in the data suitability assessment of this study. These simulation models incorporate some similar functionality such as the option to terminate a simulation if the simulation reaches the outer extent of the input data, and they can export geometries representing the modelled wildfire perimeter at different time stamps.

2.1 Wildfire theory and modelling

A general fire consists of a constellation of flames. Its smallest component, a single *flame*, requires a certain mixture of oxygen, *fuel* and energy to stay alive. This mixture is often illustrated as an equilateral triangle in which the energy component is referred to as heat (see figure 2.1). Oxygen is typically taken from the ambient air and fuel is the carbon molecules released through *pyrolysis* (i.e. vaporisation of matter to gas; energy demanding process). Pyrolysis takes place as soon as enough heat is present for a particular matter to volatilise and ignition of the fuel occurs as soon as the *flash point* is reached. The rate of pyrolysis is determined by *fuel type* characteristics such as porosity, mineral composition, moisture content and surface area to volume ratio. An external heat source is needed for the initial ignition while the energy released during combustion is usually sufficient for the flame to keep burning. The latter is true as long as the *fire point* has been reached. It means a general fire is controlled by its fuel and oxygen supply when it is self contained in regards of energy (Ondrus and Gylldorff 1996; Bengtsson 2001). Furthermore, in addition to pyrolysis and ignition, heat is needed for the warming of surrounding matter. When energy from a fire warms nearby matter, the matter moisture content is reduced due to evaporation and, soon, pyrolysis of the matter begins. Then, if the flash point is reached, a new ignition occurs. The needed heat amount depends on the moisture content of the matter. Wet or damp matter must dry to a specific moisture content, referred to as *dead fuel moisture of extinction* within the field of wildland fire growth modelling, before pyrolysis begins (Anderson 1982; Scott and Burgan 2005; Andrews 2018). A moisture content above that level prevents ignition meaning only dead matter is ignitable. Hence, no fire growth occurs if the fire intensity is lower that what is required for heating of adjacent matter to their flash points. Similarly, the rate of pyrolysis is reduced as a response to a falling fire intensity. Eventually, the pyrolysis gas becomes insufficient (i.e. the fuel supply is disrupted), to maintain continued combustion, and the fire goes out.

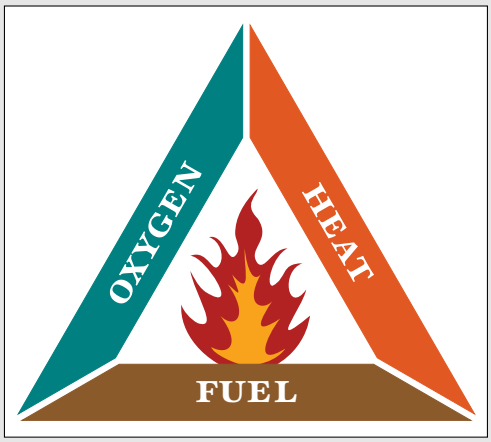

Figure 2.1: The three components of a general fire illustrated as the legs of an equilateral triangle. Heat is the energy needed for warming of adjacent matter, pyrolysis, and ignition. Fuel is made up of the carbon molecules released through pyrolysis. When oxygen reacts with the fuel, energy is released. This process is repeated until the mixture composition becomes unbalanced (Bengtsson 2001).

Limited ventilation and availability of pyrolysable matter often control the behaviour of fires in urban environments (Davis et al. 1959; Chandler et al. 1983; Bengtsson 2001). Those are two important factors that firefighters try to diminish when combating construction fires. In contrast, wildfires usually have access to immense quantities of pyrolysable matter and an almost infinite amount of oxygen (Davis et al. 1959; Chandler et al. 1983; Hansen 2003). Instead, wildfires are controlled by factors related to the physical geography of the environment in which they rage. The subsequent section 2.1.1 introduces wildfire behaviour while some concepts about wildfire growth modelling are described in section 2.1.2.

2.1.1 Factors controlling wildfire behaviour

As illustrated by figure 2.2, wildfires are controlled by recent and current weather, their fuel supply and the terrain in which they rage. The direction of propagation varies with wind direction and aspect of slopes, while the growth rate is influenced by fuel type characteristics, degree of upslope and wind velocity. The level of fuel type moisture is a critical factor for growth rate as moist matter must dry to their specific dead fuel moisture of extinction before pyrolysis occurs (see section 2.1). Another fuel type property that affects the growth rate is surface area to volume ratio as an increasing surface area relative to fuel type volume allows more pyrolysis. Varying weather affects the moisture content of live and dead matter since the level of moisture content is correlated to precipitation and humidity, and anticorrelated to temperature (Simard 1968; Hansen 2003). Volatile weather also means alternating direction and velocity of the wind. Furthermore, intensive wildfires that cover large areas sometime influence their own behaviour by creating local fire favourable weather in which winds transport fresh air into the wildfire (Hansen 2003).

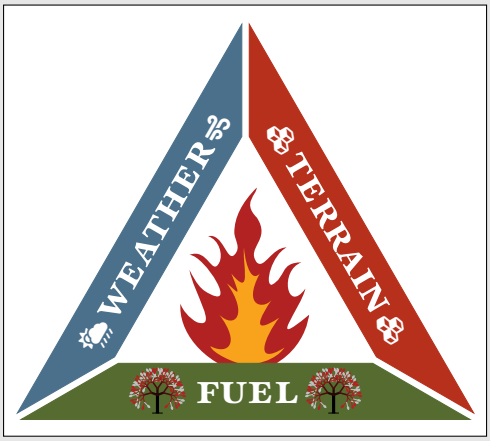

Figure 2.2: Triangle showing the three wildfire behaviour controlling factors.

When a flame tilts forward with the wind its length increases resulting in a more intense heating of matter and a higher rate of propagation in the tilt direction. Similarly, wildfires tend to propagate faster uphill as the steeper terrain source more heating of matter located upslope. In contrast, the rate of propagation decreases in the upwind and downslope directions as matter there experience less heating. Furthermore, wildfire growth is generally more induced by the wind than slope-induced (Davis et al. 1959; Rothermel 1972; Chandler et al. 1983; Hansen 2003) meaning descending winds most likely cause downward propagating wildfires. However, steep slopes and weak winds can influence wildfires equally indicating that the main growth direction is found by summing the slope and wind vectors (Rothermel 1972; Albini 1976b; Anderson et al. 1982; Andrews 2018). Hence, the growth pattern of a wildfire raging in an area with a homogeneous fuel type can be estimated based on the presence of slope and wind. In a scenario with neither slope or wind, the growth rate would be equal in all directions from the ignition point resulting in a circular growth pattern. A more oval shape, stretching uphill or in the wind direction, can be expected if either slope or wind is present. Then, a scenario with slope and wind would result in a wildfire mainly propagating towards the resultant vector of the influencing factors. The lowest rate of propagation is, in that scenario, not necessary found in the direction of the *rear fire*. An oval growth pattern would be the result if both wind and upslope have the same or contrary directions. The latter means slope and wind act as counter forces slowing down the wildfire. In fact, if the influences of slope and wind are equal but in opposite directions the growth pattern would be circular as in the first scenario. Lastly, the growth pattern can be even more complex as most landscapes are mosaics of fuel types with varying characteristics. For example, wetlands and waterbodies are *fire breaks* that limit the growth rate and cause unburnt patches and irregular perimeters such as those seen in Trapper Peak and Sundance (Anderson 1988; Pyne 2015).

2.1.2 How wildfire growth is usually modelled – some concepts described

Wildfire growth is commonly modelled using a gridded representation of reality in which the wildfire grows from a *hotspot* into neighbouring grid cells just like meeples occupy new territories in traditional boardgames such as Risk. New burning pixels are added to the wildfire that, in spite of being part of the same burning perimeter, are treated as individual hotspots meaning the same growth procedure is continuously repeated throughout the simulation. In this procedure, the propagation from a hotspot is often modelled using an elliptical shape stretching in the main growth direction (van Wagner 1969; Albini 1976a,b; Anderson 1983; Tymstra et al. 2010; Andrews 2018). One of the foci of the ellipse is represented by the hotspot, from where propagation occurs, and the length to width ratio is determined based on the growth rate in different directions (van Wagner 1969; Tymstra et al. 2010; Andrews 2018). The ellipse turns circular in a no wind and no slope scenario or when the wind and slope vectors cancel each other out (see section 2.1.1). However, the irregularity of most wildfire perimeters cannot be described using an ellipse (van Wagner 1969; Albini 1976b; Anderson et al. 1982; Anderson 1983, 1988). This can be particularly clear when more than a few hours of real wildfire growth is modelled or when the wind is turbulent (van Wagner 1969; Anderson et al. 1982; Anderson 1983). Moreover, the gridded surface, representing the modelled world, limits wildfire propagation from a hotspot to the eight directions illustrated by figure 2.3. Eight intervals of 45° are used to determine into what grid cells propagation occurs (Tymstra et al. 2010). For example, northeastern propagation towards 25° ignites one grid cell. Similarly, two grid cells (i.e. one in each interval) ignite when the propagation is in between two intervals (i.e. 22.5°, 67.5°, 112.5°, 157.5°, 202.5°, 247.5°, 292.5°or 337.5°).

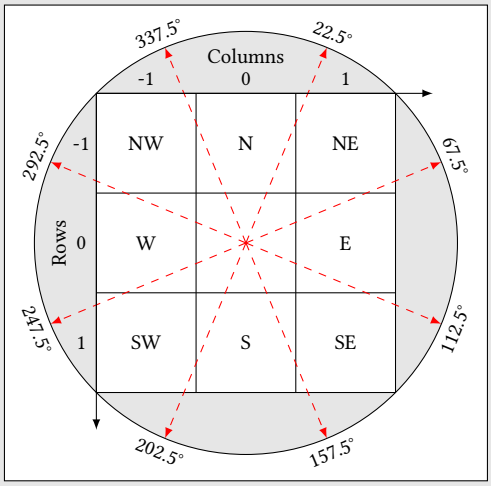

Figure 2.3: Matrix of growth directions from a hotspot into neighbouring cells. The compass degrees indicate direction thresholds and the rows and columns show the pixel coordinates of grid cells relative to the hotspot. Thus, southwards growth (i.e. between 157.5 and 202.5°) means propagation into cell POINT (1 0).

Fuel type moisture content is an important factor affecting growth rate and determines whether ignition can happen (see section 2.1.1). Hence, modelling moisture content is important for a realistic simulation. Several methods describe how moisture content is estimated based on weather readings (Alexander et al. 1984; van Wagner 1987; Nelson Jr 2000). Some of those compute indices of diurnal moisture content (Lawson et al. 1996) while others produce hourly data (van Wagner and Pickett 1985). What method to use depends on the temporal resolution of the available weather information (Tymstra et al. 2010; Andrews 2018). Furthermore, a fuel type is a set of instructions describing wildfire behaviour in a ground cover under certain conditions (e.g. dry; moist; wet; type of understory) meaning the fuel type classification of an area may change with weather and seasonality (Simard 1968; Anderson 1982; Andrews 1989). Consequently, the creation of the fuel type input, needed by wildland fire growth simulation models, is a time consuming and complicated process.

2.2 Brief introduction to simulation model 1 mainly focusing on its input data

Prometheus is the name of the Canadian Wildland Fire Growth Simulation Model. It has been developed since 1999 (Tymstra et al. 2010). The model estimates wildfire growth using the equations by Anderson et al. (1982) and Richards (1990, 1993, 1995, 1999). It supports wildfire growth modelling in heterogeneous ground cover, and varying terrain and weather. Prometheus is built around the Canadian Forest Fire Danger Rating System (i.e. CFFDRS) incorporating the FBP system, from where the model obtains fuel type information (see section 2.2.1), and the FWI system introduced in section 2.2.2. Ignition information (i.e. point, line or polygon features) should be in vector file format (.shp or .gen). Elevation, fuel and weather data, having the same resolution, geographical projection and extent, are supported as regular text files in the Esri ASCII table format (Tymstra et al. 2010). Figure 2.4 displays all parameters going into these ASCII table inputs as well as an example procedure of how the files can be created. The processes shown conform those carried out in this study when creating inputs for Prometheus (see chapter 4).

The weather data input can be represented by one or multiple files serving as weather stations with hourly or diurnal data. One of the weather stations must be chosen as primary if more than one weather input is used. Prometheus should be set up to spatially interpolate weather. The weather information is used by the model to, among others, compute fire danger indices and moisture content of fuel types. Both hourly (van Wagner and Pickett 1985) and diurnal (Lawson et al. 1996) computation of moisture content is supported though only one option can be selected at once. What method to choose when setting up the model depends on the temporal resolution of the weather data input (Tymstra et al. 2010).

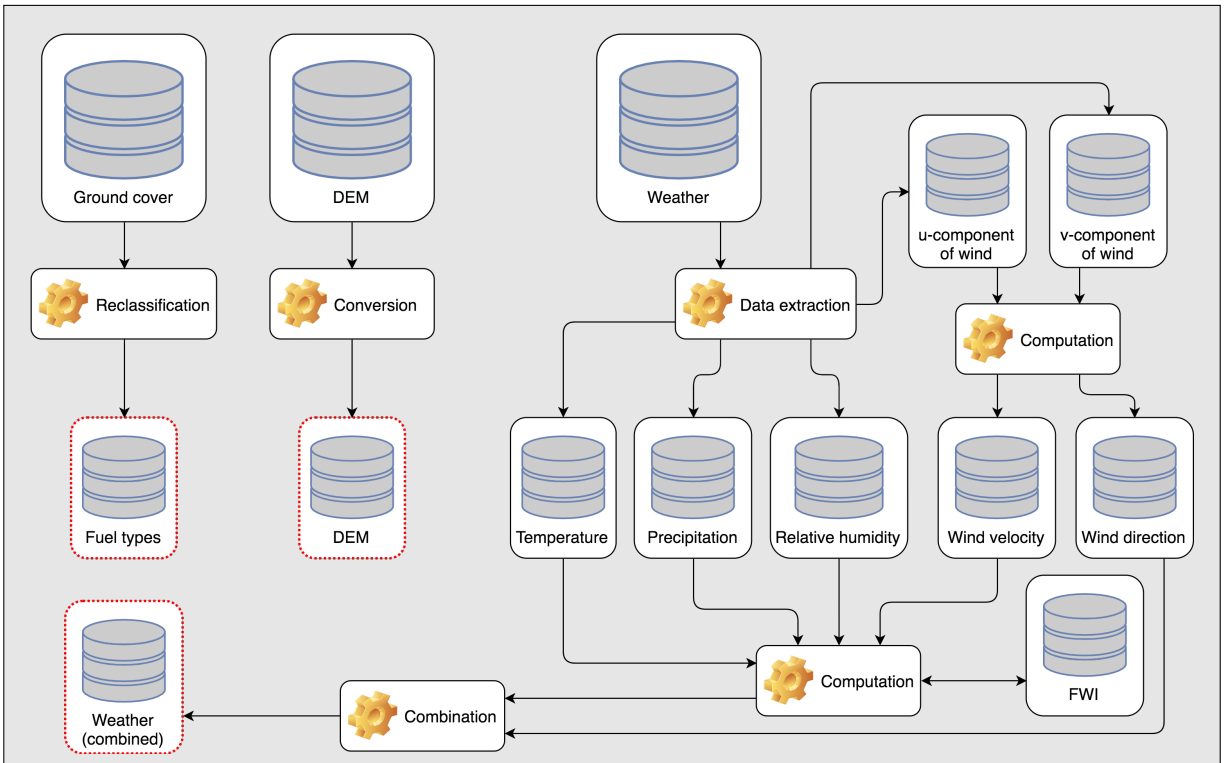

Figure 2.4: Flow diagram showing how the input data for Prometheus were created from the base data sets (i.e. ground cover; topography; weather). Data sets used as model inputs are framed by a red and dotted border. HFFMC, DMC and DC indices are components of the FWI data set.

Furthermore, as shown by figure 2.4, slope and aspect inputs are not required by Prometheus because of the capability of Prometheus to produce those automatically from the elevation data input. Additionally, barriers to wildfire propagation can be included in a simulation. Ground cover representing barriers to wildfire growth (e.g. barelands; recently burned areas; waterbodies) can be classified as incombustible in the fuel type grid input. Prometheus supports multiple barrier input vector files meaning fire breaks being line features (e.g. power lines; railroad tracks; roads; streams) can be imported separately.

2.2.1 The FBP system and its fuel models

The FBP system, a subsystem of the CFFDRS (Forestry Canada Fire Danger Group 1992), constitutes the core of Prometheus (Tymstra et al. 2010). It is used to, among others, estimate rate of spread (ROS), total fuel consumption, head fire intensity, fraction of tree crowns burned, and the type of wildfire (i.e. surface fire, intermittent crown fire or continues crown fire). Currently, its fuel model component incorporates 17 fuel types, including 1 incombustible, that represent ground cover classes (e.g. barelands; dead balsam fir mixedwood-leafless; spruce-lichen woodland; waterbodies) found in Canada (Forestry Canada Fire Danger Group 1992; Natural Resources Canada 2019; NWCG 2019). Each of these fuel types refers to an entry in a database of statistics describing wildfire behaviour of documented experimental, prescribed and wildfires (Forestry Canada Fire Danger Group 1992; Taylor et al. 1996). This indicates a continuously updated database meaning Prometheus has the potential evolving at the rate of wildfire occurrence.

2.2.2 Wildfire behaviour and moisture content estimation using the FWI system

An important component of the FBP system (see section 2.2.1) is its weather subsystem the FWI system. This subsystem describes the influence of moisture content and wind on wildfire behaviour (van Wagner 1987; NWCG 2021; Natural Resources Canada n.d.). Table 2.1 lists six components of the FWI system and briefly describes what the subindices are used for. FFMC, DMC and DC represent moisture content of matter at different soil depths. They indicate the ease of ignition (van Wagner 1987; Forestry Canada Fire Danger Group 1992). ISI, BUI and FWI are indices describing the behaviour of a wildfire (NWCG 2021; Natural Resources Canada n.d.). Both diurnal and hourly indices of FFMC and ISI can be computed while DMC, DC, BUI and FWI are computed diurnally (van Wagner and Pickett 1985; van Wagner 1987).

Table 2.1: Six unitless components of the FWI system (NWCG 2021; Government of Alberta 2022).

Index	Low	Moderate	High	Very high	Extreme	Short description
FFMC*	0-76	77-84	85-88	89-91	92-101	Moisture content of small dead organic matter.
DMC*	0-21	22-27	28-40	41-60	61-∞	Moisture content of decomposed organic matter in upper soil layers.
DC*	0-79	80-189	190-299	300-424	425-1000	Moisture content of organic matter at deeper soil depths.
ISI**	0-1.5	1.5-4.0	4.1-8.0	8.1-15.0	15.1-∞	Relative measure of potential rate of propagation.
BUI**	0-24	25-40	41-60	61-89	90-∞	Relative measure of estimated heat release.
FWI**	0-4	5-10	11-18	19-29	30-∞	Relative measure of fire intensity and an indicator of fire danger.

* Fuel moisture code. ** Fire behaviour index.

2.3 Brief introduction to simulation model 2 mainly focusing on its input data

In 2018, in the aftermath of the two catastrophic wildfire summers of 2014 and 2018, the development of WiSE-FASS (i.e. abbreviation of the Wildfire State Estimator & Fire Attack Support System) began in Sweden to create a modelling system capable of providing forecasts of wildfire growth to the emergency services in the early and most critical phase of a wildfire. WiSE-FASS incorporates the Rothermel (1972) equation extended by Albini (1976a) for computation of wildfire growth. It uses NFDRS fuel types (see section 2.3.1) and aims to support simulation of wildfire growth in Swedish vegetation. WiSE-FASS is based on technologies that support parallel computation on computer clusters. This should increase the forecasting rate while reducing the performance demand of client computers hence enabling model interaction from mobile devices. In contrast to conventional wildland fire growth simulation models (e.g. Prometheus; FARSITE; Wildfire Analyst), WiSE-FASS uses a different approach, such as the example illustrated by figure 2.3, when determining growth direction. However, this novel modelling system is not as capable as a finished software like Prometheus (see section 2.2) because of lacking important functionality (e.g. *fire spotting*; crown fire spread) needed for a proper estimation of wildfire growth.

WiSE-FASS requires the six inputs bordered by red dots in figure 2.5 as HDF5 files before it can initiate a simulation. An example of how these inputs can be compiled, from remotely sensed data, is also illustrated. This example represents the approach used in the present study (see chapter 4). As shown by figure 2.5, WiSE-FASS does not need information about the critical wildfire behaviour influencing parameter wind direction (see section 2.1.1) as an input. Instead, the model computes growth directions from the imported pressure grid data. Furthermore, WiSE-FASS extracts ignition information from the

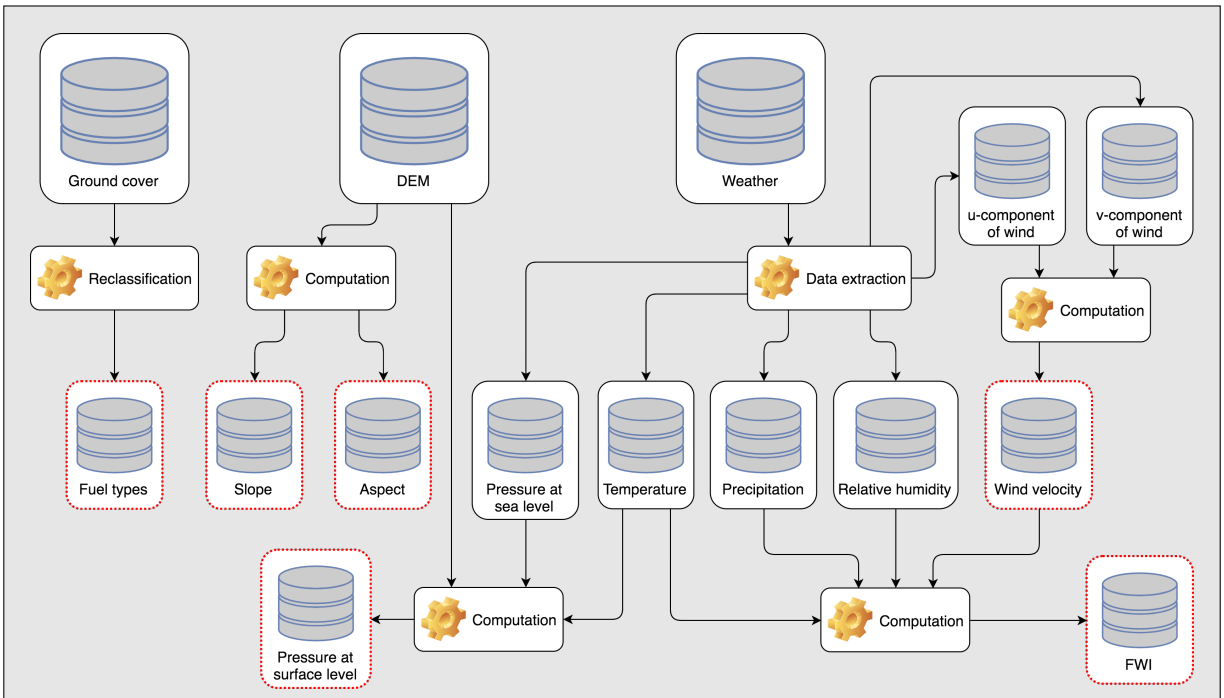

Figure 2.5: Flow diagram showing how the input data for WiSE-FASS were created from the base data sets (i.e. ground cover; topography; weather). Data sets used as model inputs are framed by a red and dotted border. HFFMC and DMC indices are components of the FWI data set.

terminal command, used to initiate a simulation, instead of requiring a separate ignition input file. In addition to the ignition information (i.e. any combination of point, line or polygon features), the terminal command must contain the EPSG code of the provided coordinates. Optional start and end dates of the simulation can be included. If no start and end dates are provided, WiSE-FASS initiates a predefined two hour (i.e. non-realtime) simulation running from the current local time.

Parallel to a simulation, WiSE-FASS is capable of exporting the results (i.e. burned and active fire hotspots) at customizable time intervals. Those are stored in a PostgreSQL/PostGIS database table, as GeoTIFF images or as Esri shapefiles depending on user preference. All three export options can be used simultaneously. The former option requires manual installation and configuration of the database before it can be used. Furthermore, the NFDRS system (see section 2.3.1) incorporates methods to determine the moisture content of NFDRS fuel types (Andrews 1989, 2018). Those are normally used when producing inputs for the Rothermel (1972) equation. However, despite incorporating this equation, WiSE-FASS derives moisture data (see section 2.3.2) using equations designed for the FBP system (see section 2.2.1).

2.3.1 NFDRS fuel models

NFDRS is the abbreviation of the National Fire Danger Rating System developed and used in the USA (Schlobohm and Brain 2002). In 1988, the NFDRS was updated to include 58 fuel types. Five of those are incombustible (i.e. Agricultural or Cropland, Barren, Snow or Ice, Urban or Developed, and Water) and 17 are dynamic (Burgan 1988; Scott and Burgan 2005; Andrews 2018). Dynamic fuel types support curing (i.e. drying). Each of the combustible fuel types specifies a set of parameters, that describes wildfire behaviour (e.g. fuel load; dead fuel moisture of extinction), constituting most of the Rothermel (1972) equation. These parameters were determined empirically in laboratories (Anderson 1982) meaning a custom fuel model can be created if a ground cover class cannot be correctly classified as an existing fuel type (Burgan and Rothermel 1984; Schlobohm and Brain 2002; Andrews 2018).

2.3.2 Moisture content derived from FWI subindices

Swedish authorities rely on the FWI system (see section 2.2.2) for wildfire risk assessment. Therefore, WiSE-FASS implements functionality to estimate moisture content using two FWI subindices. Currently, the model supports estimation of the hourly changing moisture content of fine fuel types (i.e. dead matter) and the slower changing moisture content of live herbaceous fuel types (Burgan 1988; Andrews 2018). Equation 2.1 is used to determine hourly moisture content while the live herbaceous moisture

$$\text{moisture content}_{\text{hourly}} = 147.2 \cdot \frac{101 - \text{hffmc}_{\text{current}}}{59.5 + \text{hffmc}_{\text{current}}} \qquad [\text{moisture content}] = \% \tag{2.1}$$

content is a function of the DMC index (van Wagner 1987; Forestry Canada Fire Danger Group 1992). However, the model lacks a unique method for woody moisture content calculation and it incorrectly updates the moisture contents of both live herbaceous and woody fuel types at rates ten and one hundred times the real update frequency respectively. Live herbaceous moisture content is calculated every ten simulated hours and the value is simultaneously assigned to both live herbaceous and woody fuel types.

Chapter 3

The 2014 Västmanland wildfire

Located roughly 100 km northwest of Stockholm, Sweden, the approximately 13 000 ha large region that was affected by the 2014 Västmanland wildfire is mostly flat at an elevation of 110 ±10 MASL (see figures 3.1 and C.1). It is only in the northernmost part of the real burnt region where the altitude differs and reaches almost 80 m higher (Lantmäteriet 2009). Arable lands stretches along the river valleys and the many lakes that surround most of the study area in the western, northern and eastern directions (see figure 4.1). Roughly 73 % of the region was covered by forests (see table 3.1) that could provide a wildfire with more than 1 260 000 m^3 of potential fuel. Further preconditions for wildfire ignition and growth in the study area are described in section 3.1. A more profound summary of the weather situation during the 2014 Västmanland wildfire, when it was actively growing, is found in section 3.2. The latter is based on archived weather information by SMHI (2014a) (see appendix A.1.5; plotted in figures C.2 to C.15) and emergency service incident reports summarised by the Swedish Civil Contingencies Agency.

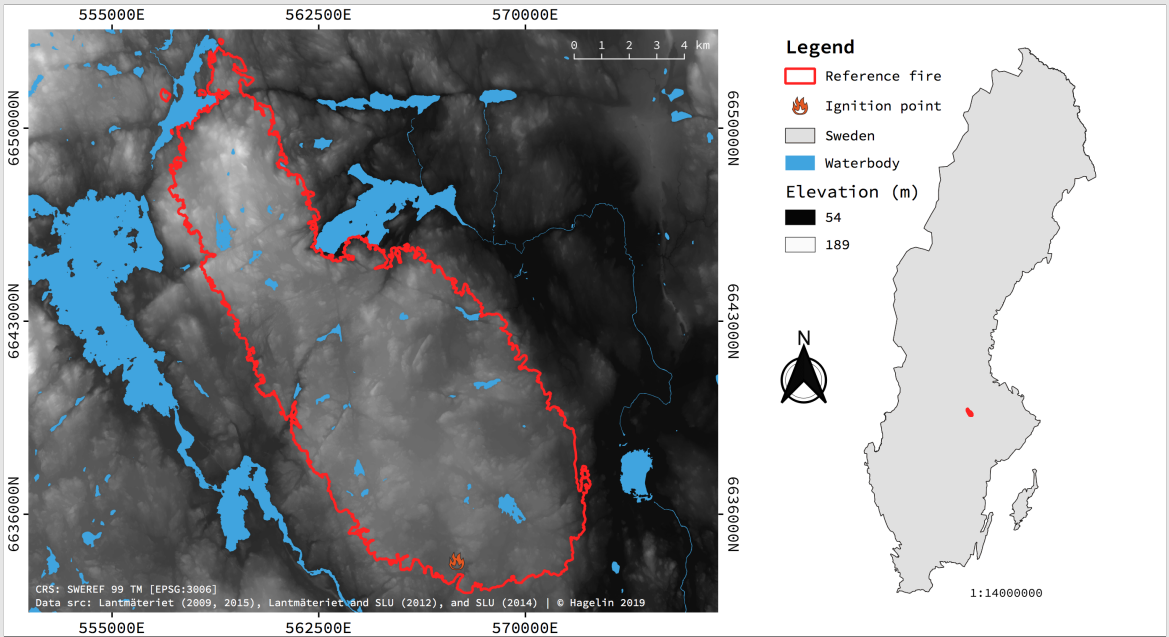

Figure 3.1: The study area relative to Sweden, its surrounding waterbodies and regional elevation.

3.1 Preconditions for wildfire ignition and growth in the study area

Understory vegetation in Swedish coniferous forests is commonly composed by a mixture of dead branches, coniferous needle litter and low grown finely divided matter such as ferns, blueberry and lingonberry bushes, lichens and mosses (MSB 2012). Therefore, the majority of the forest floors within the region that was affected by the 2014 Västmanland wildfire (see figure 3.1) were likely covered by such vegetation. Only 3 % of the study area was covered by deciduous forests (see table 3.1). Deciduous forests typically allow more sunlight to pass through their canopies, compared to the sunlight reaching the forest floor in coniferous forests, meaning the lower continuity levels in deciduous forests often consist of dense broadleaved vegetation. Furthermore, figure 4.1 and appendix B show patches of grass and wetlands scattered across the forest dominated landscape. These two ground cover classes influence wildfire behaviour differently (Taylor et al. 1996; Scott and Burgan 2005; Andrews 2018). Because of the large surface area to volume ratio of many grass species, the rate of propagation usually increases when a wildfire reaches grasslands. In contrast, because of their high level of moisture content, wetlands often reduce the rate of wildfire propagation.

Most of the finely divided matter in the study area was very dry and fire prone as a result of recent weather (MSB 2015). The area had experienced two heatwaves (i.e. defined by Persson and Wern (2011) as at least five consecutive days with temperatures above 25 ℃) and less than 20 mm of precipitation in the past month (SMHI 2014a). In early July, the daytime temperature was almost 30 ℃ throughout the region. By the end of the month it had risen to just above 30 ℃ which caused a lowering of the daytime relative humidity from about 55 ±5 % to 35 ±5 % (SMHI 2014a; MSB 2015). It means the fire risk level in the study area was extreme on 31 July when the 2014 Västmanland wildfire was ignited.

Table 3.1: Almost three fourths of the region burnt by the 2014 Västmanland wildfire were covered by forests. The region contained roughly 1 200 000 m^3 of woody matter. Coniferous trees made up 63.2 % of the woody species out of which 65 % was pine. Data source: Nilsson et al. (2014).

Forest type	Total extent (ha)	Extent study area (%)	Volume (m^3)
Pine forest	5 364	41.0	673 676
Spruce forest	945	7.2	220 899
Mixed coniferous forest	1 962	15.0	276 538
Deciduous forest	396	3.0	31 185
Mixed forest	729	5.6	59 178
Recently planted forest	180	1.4	0
Total	9 576	73.2	1 261 476

3.2 The weather situation during the 2014 Västmanland wildfire

Slope and wind are the two main controlling factors of wildfire growth in homogeneous fuels (see section 2.1.1). It means a rather circular growth pattern, revolving the ignition point, could be expected in the overall flat and coniferous forest dominated study area (see figure 3.1 and appendix B) if no wind was present. The propagation would deviate slightly uphill towards the northwest and circulate the wetlands and waterbodies present in the area. However, the final extent of the 2014 Västmanland wildfire does not have a circular shape. Also, the ignition point is located at the southern border of the reference fire perimeter indicating a wildfire propagation greatly influenced by wind of alternating direction. Furthermore, the final growth pattern is partly a result of firefighting measures such as the construction of fire breaks that limited wildfire propagation (MSB 2015). For example, on 1 August wildfire propagation was successfully interrupted about 3 km to the northeast of the ignition point. The next day, northward propagation was limited by another fire break located an additional 3 km away in the same direction. Fire breaks constructed during 3 to 5 August had little to no effect meaning the majority of the final growth pattern had natural causes.

The following sections 3.2.1 to 3.2.5 summarise the weather situation in the study area from the time of ignition, on 31 July, until the end of 4 August when most of the total area affected by the 2014 Västmanland wildfire had been burnt. Almost no additional growth occurred on 5 August onwards due to considerably less fire favourable weather (see figures C.2 to C.15). The 2014 Västmanland wildfire was declared as under control by the Swedish emergency services about a week after 5 August (MSB 2015).

3.2.1 Day one: Favourable weather for wildfire ignition on 31 July

Daytime relative humidity was 40 ±5 %, no precipitation occurred and the temperature ranged between 20 and 25℃ (see appendix C). Winds were peaking at 10 to 12 m/s, just after noon, and the average wind velocity was a third of that. The temperature declined to 12℃ during the night resulting in a high relative humidity of about 90 %. Average wind velocity was slightly lower (i.e. 2-3 m/s) with no noticeable wind peaks. Wind direction was 45° that day and it shifted northwards at night. This weather resulted in an approximately 3 km long burning area that pointed towards the northeast (MSB 2015). Wildfire growth rate during the night was very low as a response to the high relative humidity and low wind velocity.

3.2.2 Day two: The easternmost part of the final perimeter was reached on 1 August

This day experienced almost the same weather as the previous day (see appendix C). The temperature between ten in the morning and seven in the afternoon was 20 to 25℃ resulting in a rather high relative humidity ranging from 60 to 40 %. Maximum wind velocity was 10 to 12 m/s in the afternoon while the daily average was 4 m/s. The gentle morning breeze allowed for a rather even wildfire propagation in all directions while the increasing wind velocity in the afternoon made the 2014 Västmanland wildfire propagate mainly towards the northeast (MSB 2015). By the end of the day, the wildfire had reached the eastern part of the reference fire perimeter. During the night the temperature fell to 10℃, the relative humidity rose to 100 % and there was almost no wind. Thus, no wildfire growth could occur that night.

3.2.3 Day three: Wildfire propagation towards the northwest on 2 August

Slightly warmer, compared to the previous days, daily temperatures of 25 to 28℃ and an average relative humidity of 35 ±5 % indicate a more favourable weather situation for wildfire growth. However, the wind velocity was low (2 m/s) with moderate 4 m/s maximum winds locally in the region (see appendix C). Because of this, the 2014 Västmanland wildfire did not experience any significant growth until after noon when the highest temperature was reached (MSB 2015). The direction of propagation was mainly towards the northwest as the wind direction had shifted from about 35 to 340° during the morning. This shifting wind direction resulted in a 5 to 6 km wide *fire front* as the left flank of the reference fire now became the foremost part of the wildfire (MSB 2015). Moreover, the nighttime temperatures was 10℃ lower than those experienced during the day and the relative humidity increased to 90 %. The wind velocity was unchanged but, after midnight, its direction turned southwards for a couple of hours.

3.2.4 Day four: A somewhat unclear weather situation on 3 August

Wildfire growth rate on 3 August was reported by MSB (2015) as low due to a relative humidity of almost 60 % most of the day. The only exception was between three and five in the afternoon when it was 10 % lower (see appendix C). Daytime temperature averaged around 25℃ and the wind blew towards the northwest with a velocity of about 3 m/s. According to the authority, local thunderstorms caused 5 mm of precipitation. This cannot be verified in the downloaded weather data (see figures C.2 to C.15). However, the maximum wind velocities that ranged between 7 and 12 m/s in different parts of the region indicate an unstable weather situation. Also, regional wildfire propagation towards the northeast occurred in the afternoon as a result of winds generated by the suction force from the intense wildfire (MSB 2015). This behaviour cannot be deduced from the weather data set either. Furthermore, the night between 3 and 4 August experienced light, 1 to 2 m/s, alternating winds towards the west and southwest. Local temperatures ranged between 15 and 18℃ and the relative humidity rose to 100 %.

3.2.5 Day five: A raging and rapidly propagating conflagration on 4 August

The weather on 4 August was extremely favourable for wildfire growth. Daytime temperatures ranged between 30 and 35℃, and the relative humidity was just below 30 % all day except in the early afternoon when it fell to 24 % (see appendix C) as a response to the rapidly increasing fire intensity (MSB 2015). Mean wind velocity was around 3 m/s while peaking winds were four times faster. The strongest wind gusts were experienced in the western parts of the region (see points 4, 8, 11 and 14 in appendix C). However, a reported rate of wildfire propagation of about 1.3 m/s, winds that fell healthy trees and fire spotting occurring 2 km ahead of the main wildfire (MSB 2015) indicate stronger winds than what is shown by the downloaded weather data (see appendices A.1.5 and C). Furthermore, three fourths (i.e. almost 10 000 ha) of the area, affected by the 2014 Västmanland wildfire, was burnt this afternoon. By the end of the day, the wildfire had grown to the northernmost border of the reference fire perimeter (see figure 3.1) and most of the area was burnt. According to MSB (2015), almost no growth occurred the following night because the temperature fell below 20℃ causing a relative humidity of almost 100 %. Also, the wind became gentle to moderate (i.e. 1-2 m/s) weakly peaking at 3.5 m/s in parts of the region.

Chapter 4

Methodology

The first section (4.1) of this chapter describes the processes involved when producing the many data inputs needed by Prometheus and WiSE-FASS (see figures 2.4 and 2.5). Open source technologies were used for this task because the processes involved relied on custom algorithms. Meta information of the resulting data sets is found in appendix A.2. The subsequent section (4.2) details how Prometheus and WiSE-FASS were setup, before the simulations, and how the modelled wildfire growths were managed. Furthermore, Prometheus 6.1.0 and an unpublished version of WiSE-FASS were applied to model the reference fire. GIS application (e.g. transformations; area comparisons) was performed in Python 3.6.8 while QGIS 3.6.2 was used for visual inspection of the simulated wildfire growths and map generation. Image manipulation and vector rendering were made in Gimp 2.10.10 and the LaTeX library Ti*k*Z 3.1.3.

4.1 Description and processing of data sets

Data sets describing the elevation, ground cover and weather of the study area are considered as base information in the present study because they were needed when creating all input data sets introduced in sections 2.2 and 2.3. Retrieval of the base data was made from Swedish governmental authorities (see appendices A.1.2, A.1.3 and A.1.5 for meta information). These base data sets were then processed in Python 3.6.8. Table 4.1 shows the most important open source Python libraries used in this process.

Table 4.1: Important Python libraries when creating the input data sets detailed in appendix A.2.

Name	Used for	Source
Affine 2.2.2	Pixel to world coordinate transformations	Gillies (2018a)
Fiona 1.8.4	Reading and writing of shapefiles	Gillies (2018b)
Matplotlib 3.0.4	Data filtering	Hunter (2007)
Numba 0.42.0	Code optimization	Anaconda, Inc (2018)
NumPy 1.15.4	Matrix manipulations	van der Walt et al. (2011); Oliphant (2015)
Pandas 0.24.1	Data analyses and statistics	McKinney (2010, 2011)
PyGrib 2.0.2	Reading of GRIB files	Whitaker (2016a)
PyProj 1.9.5.1	Geographical coordinate transformations	Whitaker (2016b)
Rasterio 1.0.18	Reading and writing of raster files	Gillies (2019)
Shapely 1.6.4	Manipulation of vector features	Gillies (2018c)
Tables 3.4.3	Reading and writing of HDF5 files	Alted et al. (2018)

Sections 2.2 and 2.3 show that the simulation models need similar, but differently formatted, inputs. Prometheus loads most data from text files (.asc; .csv) while WiSE-FASS reads data from the scientific data format HDF5 (.hdf5). Producing the many input files (see appendix A.2) required several processing steps. First the projections of the DEM and ground cover data sets were verified to be SWEREF 99 TM (i.e. ESPG:3006; national coordinate reference system in Sweden). The DEM was then clipped to the extent of the study area (see figure 3.1). This extent was set to be a minimum of 5 km outside the final perimeter of the 2014 Västmanland wildfire (see appendix A.1.4) and matches the extent used by Hagelin and Cluzel (2016). It allows for some overestimated modelled wildfire propagation before the simulations are terminated as a result of intersecting this perimeter. The ground cover feature data was rasterized to match the resolution and extent of the elevation data. Finally, both these data sets were converted to ASCII tables for use in Prometheus and saved as two HDF5 files, with a related CSV file containing the affine transformation information, for WiSE-FASS. The continued processing of base data, including extraction of weather data from the MESAN data set, and creation of the various inputs are described in sections 4.1.1 to 4.1.4. The final section (4.1.5) concerns the selection of four virtual weather stations for Prometheus and how these specific inputs were created.

4.1.1 CompSA: An algorithm to compute slope and aspect

As described in section 2.3, WiSE-FASS requires slope and aspect indices as inputs. Those were created by executing an algorithm (i.e. CompSA) that incorporates the planar methods shown by equations 4.1 and 4.2 (Esri 2017a,b). CompSA computes slope and aspect from the elevation data stored in the HDF5 files and appends values to new subindices in the same HDF5 files. This algorithm was chosen for this process, instead of conventional GIS, because of its support for both reading and writing HDF5 files.

$$\text{slope} = \arctan\left(\sqrt{\left(\frac{\Delta z}{\Delta x}\right)^2 + \left(\frac{\Delta z}{\Delta y}\right)^2}\right) \cdot \frac{180}{\pi} \tag{4.1}$$

$$\text{aspect} = \frac{180}{\pi} \cdot \arctan_2\left(\left(\frac{\Delta z}{\Delta y}\right)^2, \left(\frac{\Delta z}{\Delta x}\right)^2\right), \qquad \text{aspect} = \begin{cases} \text{-1}, & \text{if slope} = 0 \\ 450 - \text{aspect}, & \text{if aspect} > 90 \\ 90 - \text{aspect}, & \text{otherwise} \end{cases} \tag{4.2}$$

4.1.2 Classification of ground cover data as fuel types

Figure 4.1 shows the ground cover within the region that was affected by the 2014 Västmanland wildfire. Coniferous forests dominated the area (i.e. ground cover classes 610 to 642; see appendix B for a complete list of ground cover names in Swedish) and patches of wetlands are easily seen across the region. Before this base data could be used as an input in Prometheus and WiSE-FASS, it had to be reclassified as

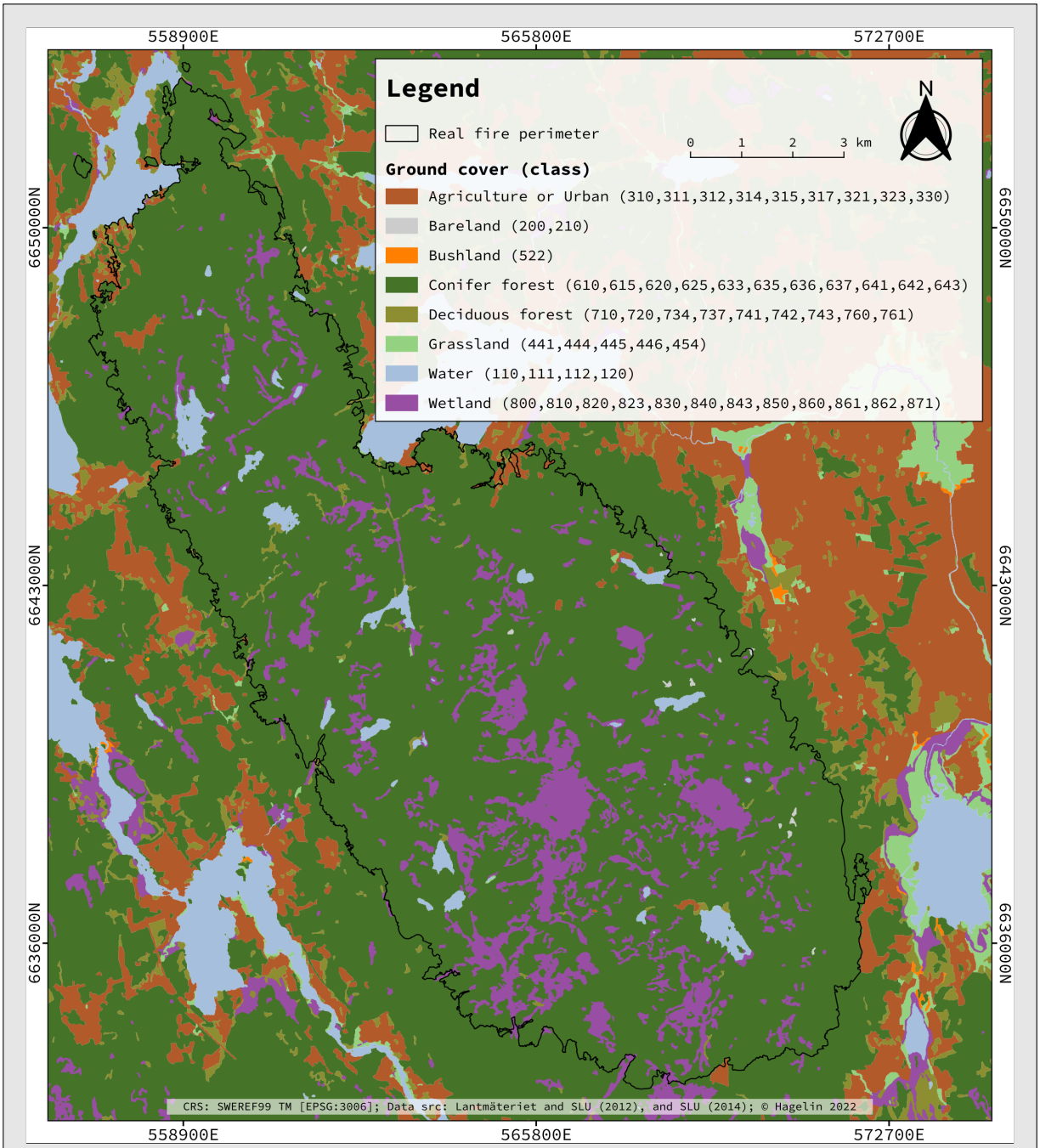

Figure 4.1: Ground cover in the area that was affected by the 2014 Västmanland wildfire. This base data was used to create the fuel type inputs for both Prometheus and WiSE-FASS. A full fuel type classification scheme with class names is found in appendix B.

fuel types. Sections 2.2 and 2.3 describe that the simulation models simulate wildfire growth based on different fuel type systems; Prometheus uses fuel types from the Canadian FBP system and WiSE-FASS gets combustion information from the national fire danger rating system (NFDRS) used in the USA. The classification scheme by Hagelin and Cluzel (2016) was used when reclassifying the ground cover data in figure 4.1 as FBP fuel types. This was to allow for the assessment of the weather data (see objective 3). Figure 4.2 displays an area mostly classified as the FBP fuel type classes 3, 6 and 32 (i.e. Mature Jack or Lodgepole Pine; Conifer Plantation; Standing Grass). The majority of the wetlands seen in figure 4.1 are

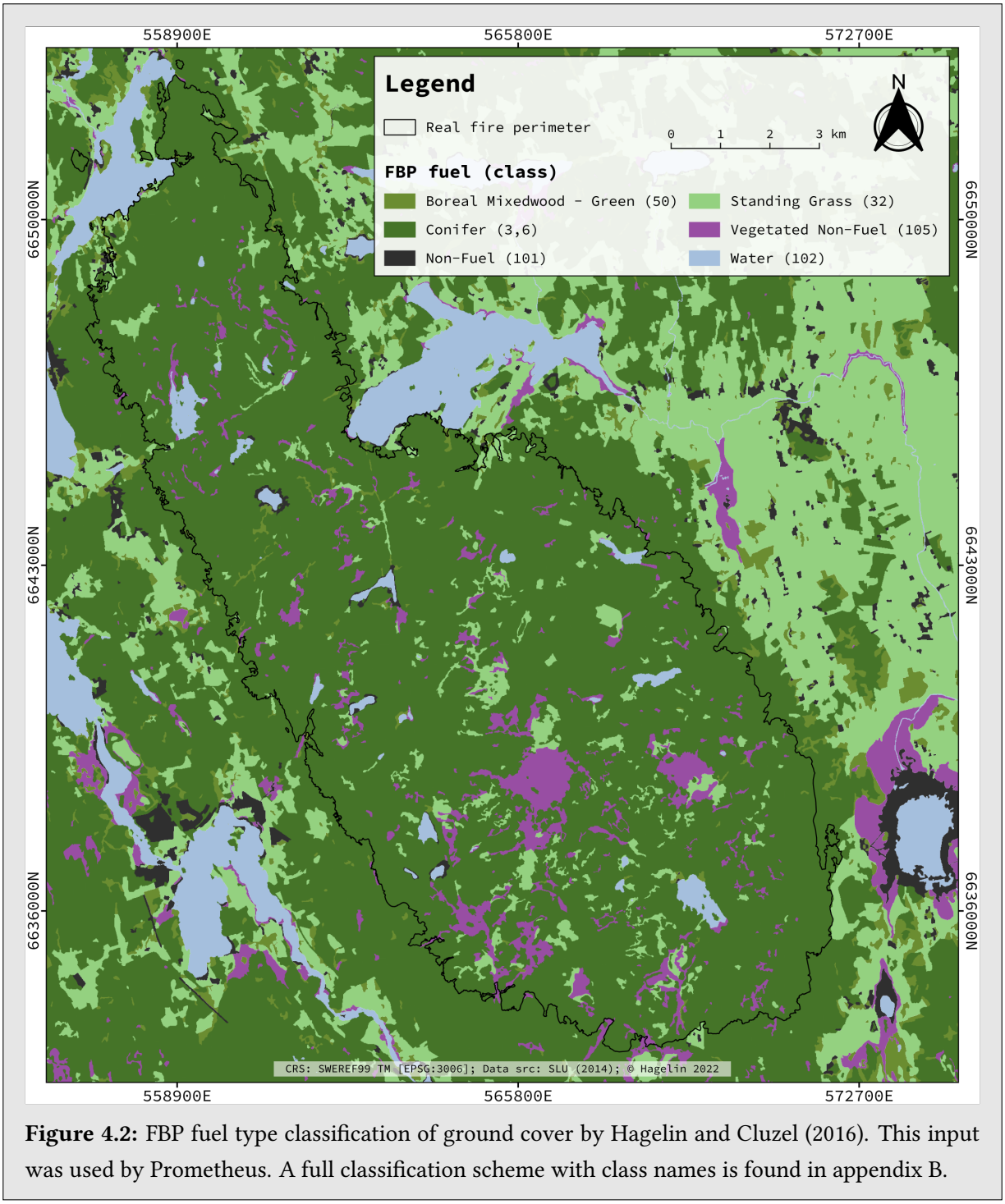

Figure 4.2: FBP fuel type classification of ground cover by Hagelin and Cluzel (2016). This input was used by Prometheus. A full classification scheme with class names is found in appendix B.

classified as non-fuels. Furthermore, the NFDRS fuel type grid shown by figure 4.3 was created using information by Scott and Burgan (2005). Long-needle litter (i.e. class 188; dissolved as Conifer-litter) dominates the area. Patches of the NFDRS fuel types 122, 141, 161 and 165 are spread across the region.

Reclassifications were carried out using conditional statements describing the key in appendix B. This key shows the full classification scheme of both fuel type systems and includes all fuel type class names. One ASCII table containing FBP fuel type data was saved for Prometheus. NFDRS fuel type information was appended as a new subdirectory in the ground cover HDF5 file for use by WiSE-FASS.

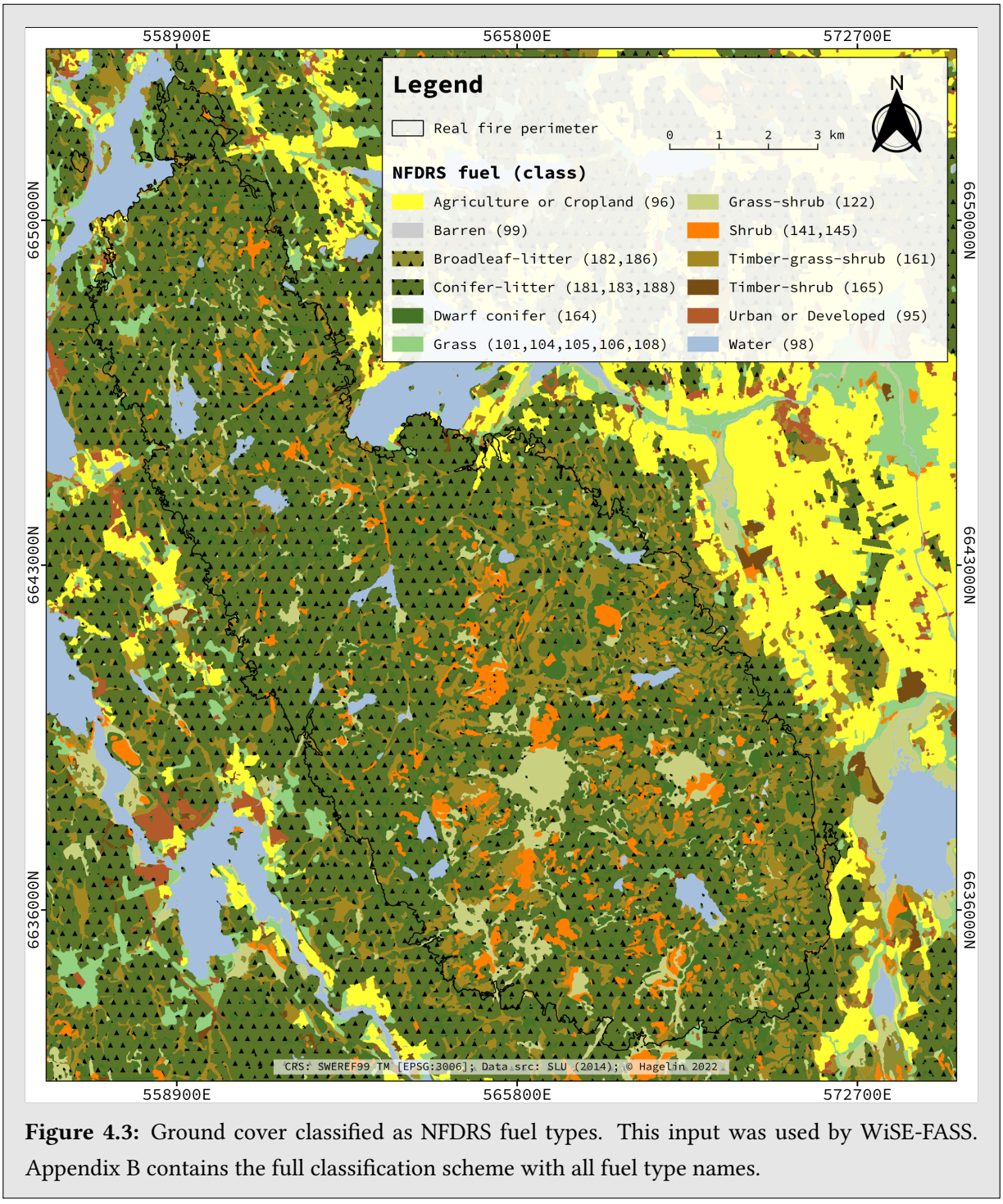

Figure 4.3: Ground cover classified as NFDRS fuel types. This input was used by WiSE-FASS. Appendix B contains the full classification scheme with all fuel type names.

4.1.3 Data selection and extraction from the weather data set

The MESAN data set (see appendix A.1.5) is provided by the Swedish Meteorological and Hydrological Institute (SMHI) in the multidimensional binary data file format GRIB (.grb). A total of 130 GRIB files were acquired from SMHI (2014a) to cover the period when the 2014 Västmanland wildfire was actively growing (i.e. 31 July 2014 at 13:00 to 5 August 2014 at 23:00). Each file holds hourly point data and covers roughly 725 000 km^2 in northern Europe (see insert map in figure 4.4). It contains 65 928 data points on a grid with an unknown degree of rotation. Information about the affine transformation was not available but the GRIB meta header contained world coordinates for all data points which allowed for continued processing. Furthermore, out of the 65 928 data points only those representing the study area were of interest. Figure 4.5 illustrates how a buffer distance was chosen to filter the 14 points of interest, shown as yellow and red dots in figure 4.4, from the MESAN data set. The Pythagorean theorem was used to compute the maximum extent covered by a single MESAN data point. As illustrated by figure 4.5, a spatial resolution of 11 km meant a buffer zone of about 7.8 km outside the study area. In total, seven weather parameters were exported from the MESAN data set. Precipitation, temperature, relative humidity, sea surface pressure, and u and v components of wind were required to create the needed inputs. Also, wind gust data, used when reviewing the modelled wildfire growths, was extracted.

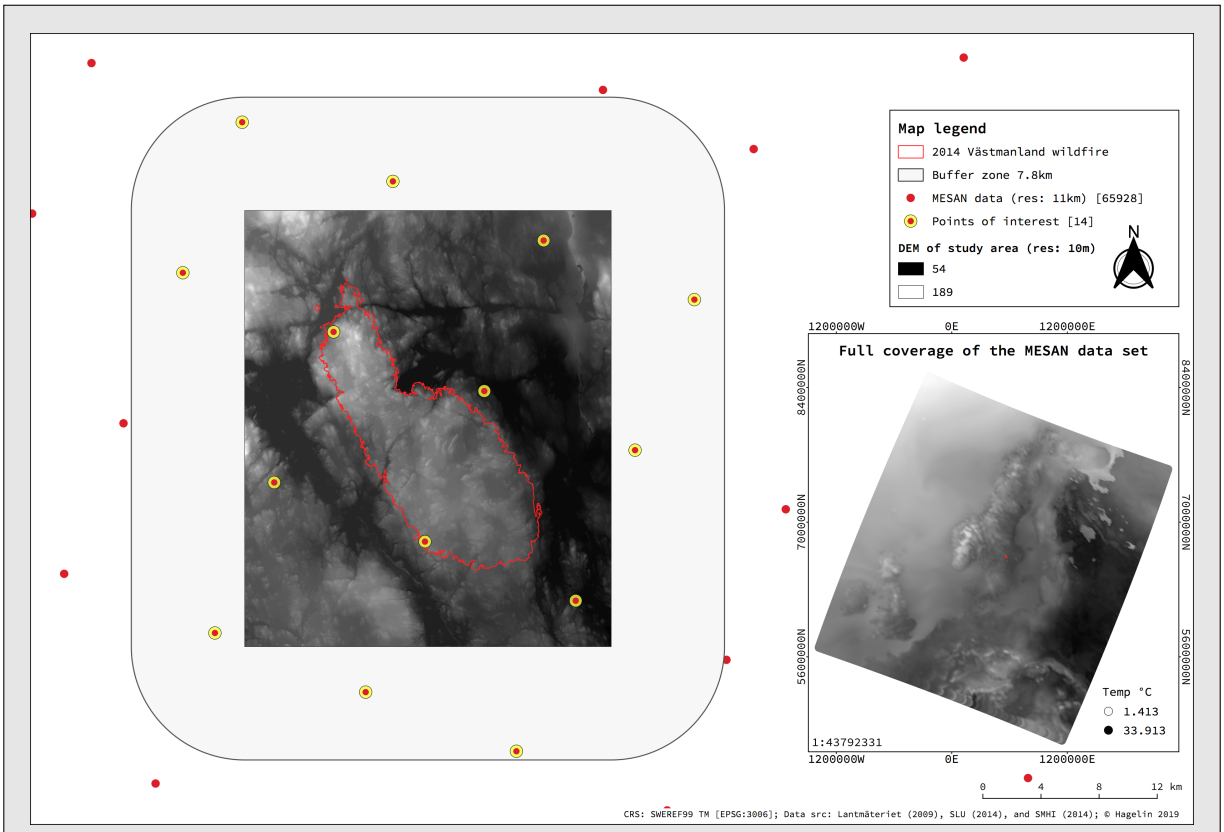

Figure 4.4: Data points of weather information (i.e. points of interest) were filtered from the MESAN data set (see appendix A.1.5) using a buffer zone of 7.8 km around the study area. The insert map shows the full coverage and geographical location of the data set consisting of 65 928 data points evenly distributed over 268 rows. The DEM represents the study area.

Weather data having a spatial resolution of 11 km are too sparse for use in wildfire growth modelling (see section 2.1.2). Prometheus can cope with this as the model has functionality to interpolate wind (see section 2.2). WiSE-FASS lacks equivalent functionality meaning that grids having the same resolution as the other data inputs (i.e. 10 m) were needed. This was achieved by first creating empty containers (i.e. one per exported weather parameter) as subdirectories in a new HDF5 file. Those had the same spatial resolution and extent as the DEM base data. Every pixel coordinate (i.e. [row,col]) of this container was transformed, using the affinity of the downloaded DEM base data, to its world coordinate representation. Then, the nearest point of interest, of the 14 filtered data points in the MESAN data (see figure 4.4), was determined by computing the distance between each pixel, in the container, and those 14 points. Finally, the values of the nearest point were assigned to the corresponding cell in the containers. Figure 4.6 shows a computed grid of pixelated uniform surfaces.

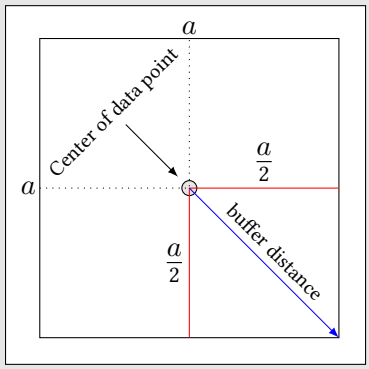

Figure 4.5: Illustration shows how the buffer distance, used to filter points to use in the MESAN data set, was chosen. The spatial resolution of the weather data set (i.e. 11 km) is symbolised as variable a.

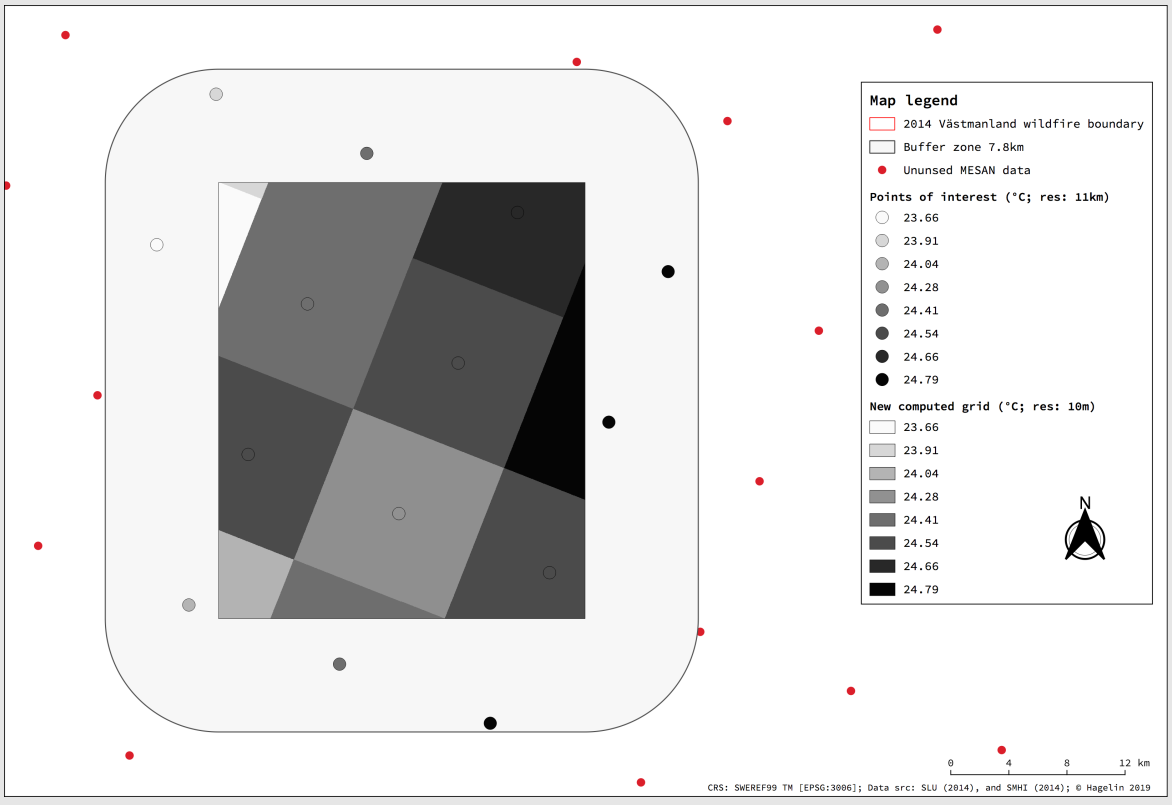

Figure 4.6: 10 m resolution grids, one per needed weather variable in the MESAN data set (see appendix A.1.5), were created from the filtered points of interest. Each pixel of these rasters was given the value of its nearest point of interest. A computed grid consists of fields of 10 m resolution pixels. Every field represents a uniform surface covered by an 11 km resolution weather data point.

4.1.4 Wind, pressure and FWI subindices

Wind direction and wind velocity are two important data inputs that influence wildfire behaviour (see section 2.1.1). Those two parameters were not contained in the MESAN data set (see appendix A.1.5) meaning they had to be created. This was achieved by using equations 4.3 and 4.4. The indices of u and v components of wind, exported in section 4.1.3 from the weather base data, were equation variables.

$$\text{wd} = 270 - \arctan_2(v, u) \cdot \frac{180}{\pi}, \qquad \text{wd} = \begin{cases} \text{wd} - 360, & \text{if wd} > 360 \\ \text{wd}, & \text{otherwise} \end{cases} \tag{4.3}$$

$$\text{wv} = \sqrt{u^2 + v^2} \tag{4.4}$$

WiSE-FASS does not use a wind direction input. Instead, the model computes growth directions from a grid of surface pressure at 2 m above the ground. This index was not part of the MESAN data set either. Instead, it was created using equation 4.5 (Barani Design n.d.). Sea level pressure, extracted from the MESAN data set, and the elevation base data were used in the equation. Three additional subdirectories were created in the weather HDF5 file for the wind direction, wind velocity and surface pressure indices.

$$\text{pres}_{\text{at elev}} = \text{pres}_{\text{sea level}} \cdot \left(1 - \frac{0.0065 \cdot \text{elev}}{\text{temp}_{\text{Kelvin}} + 0.0065 \cdot \text{elev}}\right)^{\text{-5.257}} \tag{4.5}$$

Furthermore, three additional indices had to be created. FFMC and DMC are needed by both Prometheus and WiSE-FASS whilst DC is used only by Prometheus. Those are subindices of the FWI system (see section 2.2.2 and table 2.1) and were computed using equations by van Wagner (1987). Hourly FFMC and daily DMC and DC indices were stored in separate subdirectories in a new HDF5 file.

4.1.5 Ignition information, virtual weather stations and barrier inputs

Prometheus requires an ignition input as a vector feature (.shp or .gen). Therefore, a shapefile was created containing the ignition point of the 2014 Västmanland wildfire (i.e. lon 16.20446, lat 59.84088; see chapter 3). This ignition input was not used by WiSE-FASS. WiSE-FASS obtains its ignition information from the command initiating the simulation (see section 2.3). Moreover, Prometheus needs weather data represented as virtual weather stations (i.e. point data). Because no actual weather station was located within the study area (Hagelin and Cluzel 2016), four virtual weather stations (see appendix A.2.12) were generated from the weather and FWI HDF5 files (see sections 4.1.3 and 4.1.4). Positions of these virtual weather stations were chosen based on the MESAN data points; the two MESAN data points within the perimeter of the reference fire and the two closest neighbouring points were chosen as virtual weather stations (i.e. points 6, 7, 9 and 10 in figure C.1). Weather values at those locations were extracted from the same HDF5 files. Lastly, a barrier input (see appendix A.2.3) was created for use in a second Prometheus simulation (see objective 4). This barrier input contains seven digitised polyline features representing fire breaks (i.e. six constructed fire breaks and one natural barrier). Their geospatial locations were interpreted from observations (MSB 2015) and the estimates by Hagelin and Cluzel (2016).

4.2 Model configurations and management of the modelled wildfire growths

Sections 2.2 and 2.3 picture two simulation models with structural differences implying differing set up processes. However, some of the settings were the same. Both Prometheus and WiSE-FASS can export their simulated wildfire perimeters, at customizable time intervals, as vector features. Also, the simulation models can be set up to terminate the simulation when the modelled wildfire growth reaches the outer extent of the data inputs (see chapter 2). This option was chosen because the modelled surface would not be representative after that moment, and because the simulation had reached more than 5 km outside the real burnt region. Furthermore, details about how the simulation models were prepared prior to simulation start are described in sections 4.2.1 and 4.2.2 respectively. Prometheus was set up using the same settings in both simulations except for an additional input layer used to assess the influence of barriers. Lastly, section 4.2.3 briefly describes how the modelled wildfire growths were processed.

4.2.1 Setting up Prometheus

The ASCII tables describing the elevation and fuel type distribution (see appendices A.2.4 and A.2.5) were imported as *topography* and *fuel type grid*. A foliar moisture content of 120 % was chosen because of the time of the year when the 2014 Västmanland wildfire occurred (Hirsch 1996; Alexander 2010). Spatial weather modelling was turned on to enable usage of the four files containing hourly weather information (see appendix A.2.12). The virtual weather station closest to the ignition point (i.e. MESAN data point 10 in figure C.1) was chosen as the primary weather station. Initial FFMC, DMC and DC (see table 2.1) values were assigned 90, 55 and 453 respectively in accordance with the prevailing fire risk assessment on 31 July (Malmeström and Millbourn 2015). The distance and perimeter resolutions were set to five grid cells (i.e. 50 m since 1 grid cell equals the spatial resolution of the fuel type grid; a high value). These settings affect the size of the modelled wildfire. A low value may cause an underestimated wildfire distribution when the fuel type grid is heterogeneous like it is in figure 4.3 (Tymstra et al. 2010). Furthermore, the display was set to refresh every simulated 24 hours, breaching of barriers (i.e. both barrier inputs and non-fuel type grid cells) was enabled to allow for barrier breaching if the modelled wildfire intensity pass a barrier specific threshold, and the options *Buildup*, *Green-up* and *Terrain* were enabled to instruct Prometheus to account for fuel losses caused by weak winds, to simulate the effect of leaf production, and to combine slope factors and wind factors into a net wind speed and direction.

4.2.2 Setting up WiSE-FASS

The four HDF5 files detailed in sections 4.1.1 to 4.1.4, storing terrain, fuel and weather information as well as the FWI subindices FFMC and DMC, were arranged in designated directories called *Terrain*, *Fuel* and *Weather*. Two HDF5 files, named *Weather* and *FWI*, were placed in the last directory. Also, the CSV file containing the affine transformation of the gridded data had its own designated directory. WiSE-FASS requires the following naming of its HDF5 inputs and their [subdirectories]: *Fuel [fuel]*, *FWI [hffmc, dmc]*, *Terrain [aspect, slope]* and *Weather [prec, pressure, relhum, temp, windvel]*. These names were accounted for in the creation process. Furthermore, burnt cells and activate hotspots were set to be automatically exported at the end of every simulated hour. Shapefile was set as export format.

4.2.3 Export and processing of the modelled wildfire perimeters

Prometheus does not support data export during ongoing simulations. Instead, its forecasted wildfire growth was manually and sequentially exported when a simulation had completed. For consistency with the export settings chosen when preparing WiSE-FASS (see section 4.2.2), 130 shapefiles were exported. Most of the contained polygons had topological errors that were corrected in QGIS before they could be assessed. In contrast, WiSE-FASS automatically exported point data parallel to its simulation. Thus, its modelled wildfire growth could be assessed immediately after simulation completion. Furthermore, area measurements contrasting simulated extents to the reference fire perimeter were computed using Python libraries in table 4.1. These were used to aid the suitability assessment of available spatial data in Sweden for wildfire growth modelling. Also, figure 4.7 shows the simulation by Hagelin and Cluzel (2016) that were used as comparative simulation when evaluating the weather data used in this study.

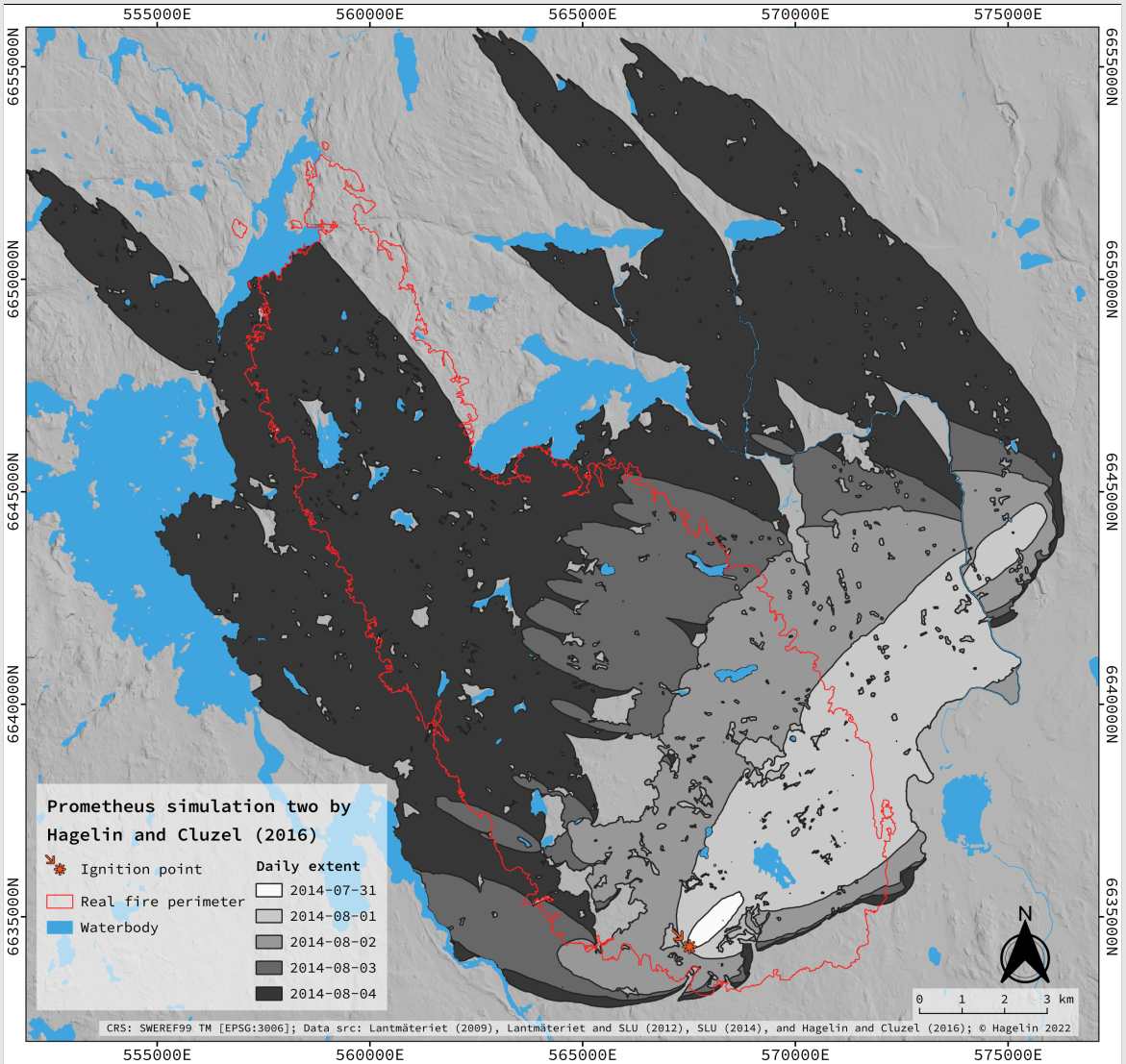

Figure 4.7: Simulation of the 2014 Västmanland wildfire. Constitutes a basis in the evaluation of the weather data used in the present study. Daily extents retrieved from Hagelin and Cluzel (2016).

Chapter 5

Intermediate results: Modelled wildfire growths

Prometheus was used in two out of three simulations. The second Prometheus simulation included a barrier input representing one presumed natural barrier (i.e. young healthy spruce tree line) and six constructed barriers. All other inputs were the same between these simulations. The second Prometheus simulation was performed to study the influence of barriers on wildfire growth modelling. WiSE-FASS does not support barriers in a simulation meaning only one simulation was performed using that model.

An area summary of the simulations is found in table 5.1. WiSE-FASS modelled a small 228 ha burnt surface located within the real fire perimeter. In comparison, the first Prometheus simulation is almost 90 times larger, it covers roughly 80 % of the real burnt region and it breached the real fire perimeter on day two. Furthermore, in the second Prometheus simulation, overestimation was delayed until the 3 August. The total modelled burnt surface was almost 21 % smaller compared to the surface modelled in first Prometheus simulation but, as the "Extent within VF" increased to 63.8 %, the conformity with the real fire perimeter was higher. Maps of the simulations are found in the subsequent sections 5.1 and 5.2.

Table 5.1: Simulated areas summarised and compared to the region that was burnt by the 2014 Västmanland wildfire (see chapter 3). Daily extents over the period 31 July 2014 to 5 August 2014 are displayed at 23.59. WiSE-FASS produced a simulation that overlaps almost 2 % of the real burnt region. Prometheus modelled a surface that overlaps the real burnt region by 81.5 % when excluding the barrier input. The overlap was reduced to 77.2 % when the barrier input was included.

	Reference fire (VF)	**Prometheus* simulation**						**WiSE-FASS** simulation**					
	total area: 13 096 ha	31/7	1/8	2/8	3/8	4/8	5/8	31/7	1/8	2/8	3/8	4/8	5/8
w/o barrier	Area simulated (ha)	393	2 333	5 973	8 412	18 444	19 997	11	12	61	110	195	228
	Extent within VF (%)	100	80.5	66.6	64.9	56.0	53.4	100	100	100	100	100	100
	Fraction of VF (%)	3.0	14.3	30.4	41.7	78.8	81.5	0.08	0.09	0.5	0.8	1.5	1.7
w. barrier***	Area simulated (ha)	311	1 055	2 570	3 709	14 255	15 848	—	—	—	—	—	—
	Extent within VF (%)	100	100	100	99.2	68.8	63.8	—	—	—	—	—	—
	Fraction of VF (%)	2.4	8.1	19.6	28.1	74.9	77.2	—	—	—	—	—	—

* Simulation model 1. ** Simulation model 2. *** Barrier implementation is not supported by WiSE-FASS**.

5.1 Simulation model 1: Maps of wildfire growths and an emphasis on barriers

About 80 % of the area affected by the reference fire was burnt during the first simulation by Prometheus (shown by figure 5.1). In the first two days, an elliptical growth pattern stretched from the ignition point towards the northeast. By the end of 1 August, the simulation had propagated almost 2 km to the east outside the real fire perimeter. Then, on the 2 August, the simulation turned to the northwest and caused western overestimation. In total, roughly 50 % of the simulated surface is within the real fire perimeter.

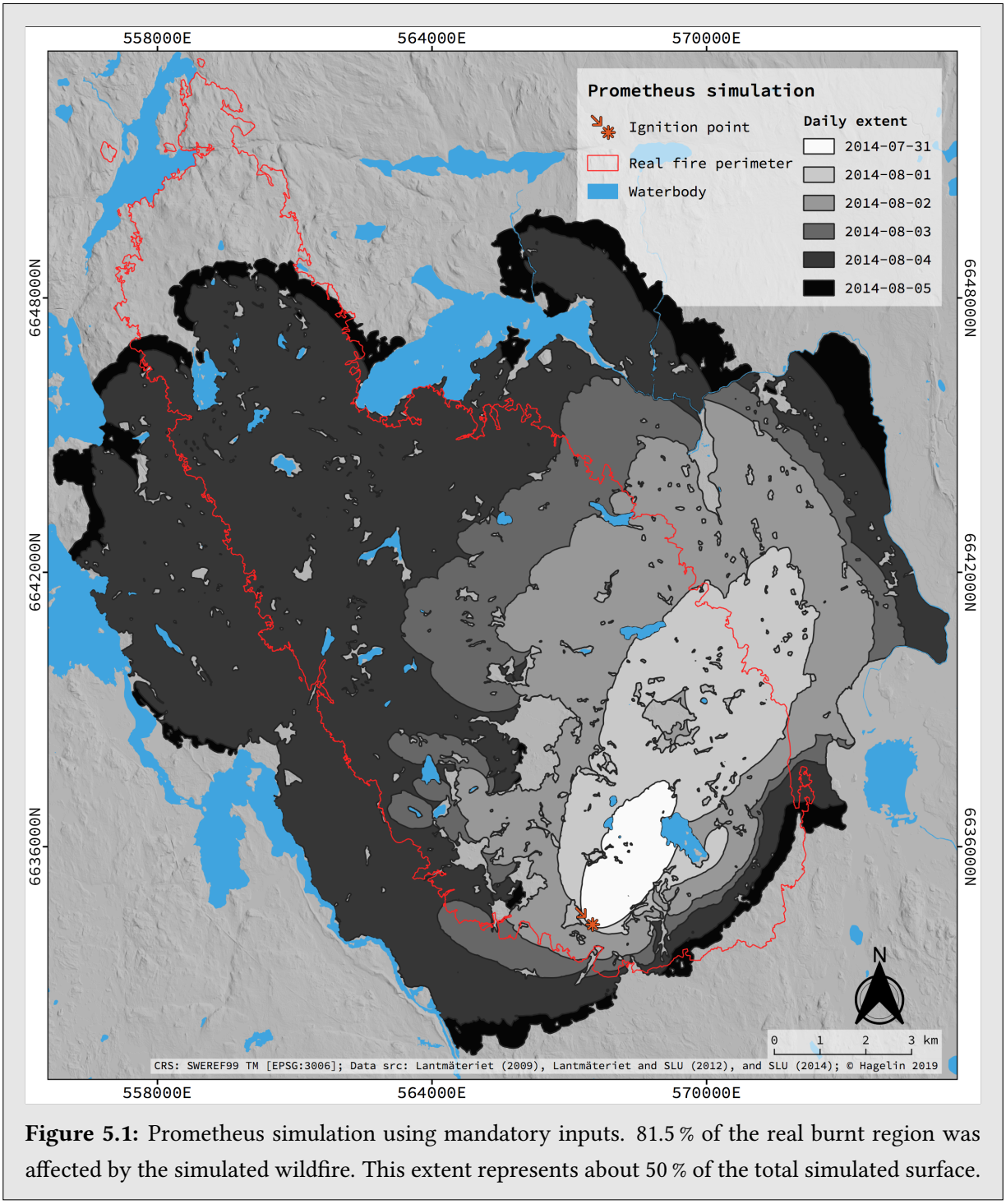

Figure 5.1: Prometheus simulation using mandatory inputs. 81.5 % of the real burnt region was affected by the simulated wildfire. This extent represents about 50 % of the total simulated surface.

Figure 5.2 shows the elliptically shaped and northwestward stretching area produced by Prometheus when the model was set up to use the barrier input (see appendix A.2.3). Almost 64 % of the simulated area overlaps the real burnt region. This constitutes roughly 77 % of the same region (see table 5.1). It is clearly seen that constructed barriers limited wildfire propagation to the northeast on 31 July and 1 August. Overestimation is seen both to the east and west of the real fire perimeter and the modelled wildfire had reached about 2.5 to 3 km outside this perimeter in both directions by the end of 5 August.

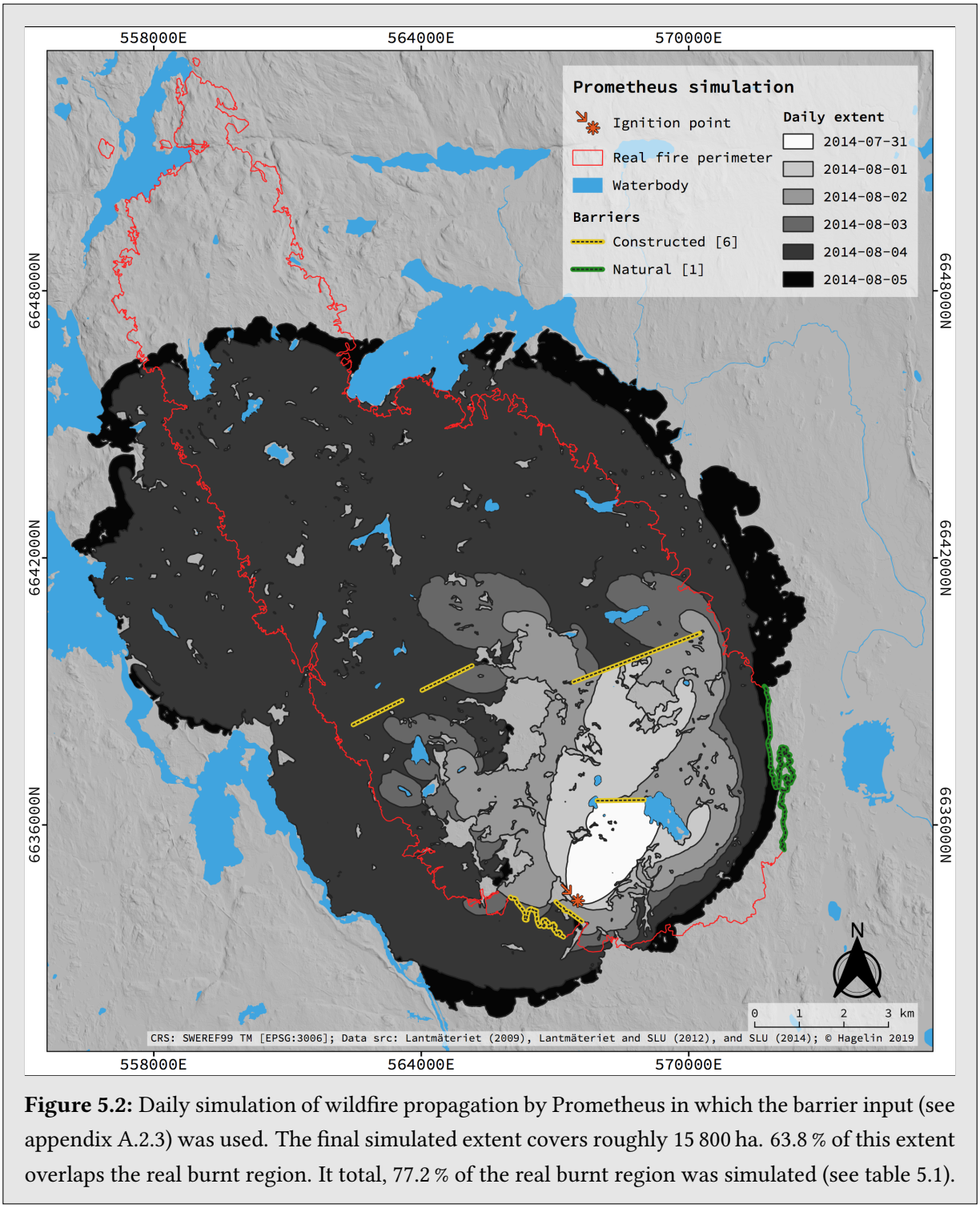

Figure 5.2: Daily simulation of wildfire propagation by Prometheus in which the barrier input (see appendix A.2.3) was used. The final simulated extent covers roughly 15 800 ha. 63.8 % of this extent overlaps the real burnt region. It total, 77.2 % of the real burnt region was simulated (see table 5.1).

5.2 Simulation model 2: A poor simulation visually displayed

The 228 ha simulated extent by WiSE-FASS is displayed in figure 5.3. This represents 1.7 % of the real burnt region. During the first three days, the main direction of simulated wildfire propagation was northeasterly. On 1 August, only one hectare was burnt (see table 5.1) meaning almost no wildfire growth occurred. Simulated propagation on 3 to 5 August were mainly towards the north northwest. The flame symbols in figure 5.3 indicate that roughly 17 ha was still burning when the simulation ended.

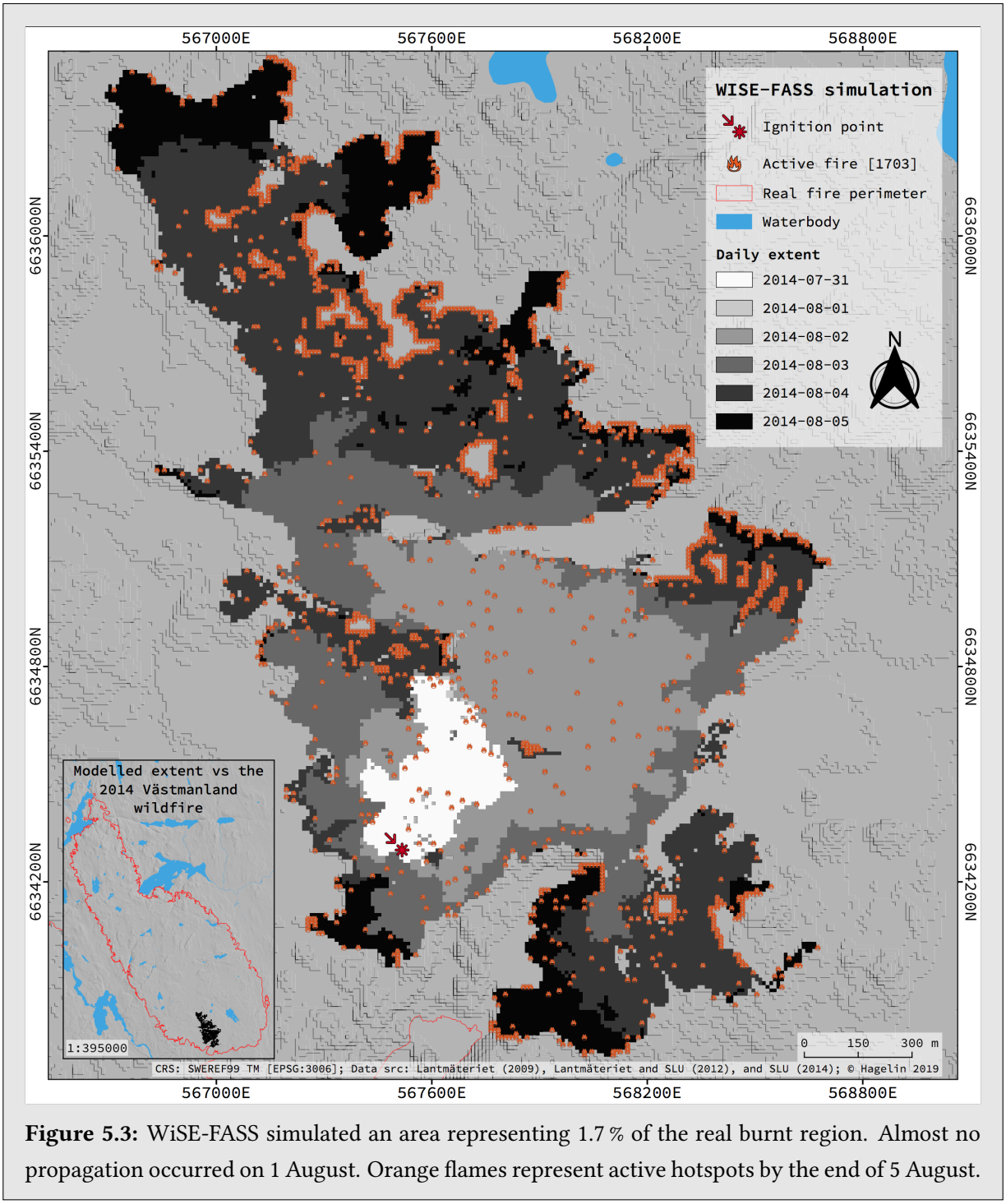

Figure 5.3: WiSE-FASS simulated an area representing 1.7 % of the real burnt region. Almost no propagation occurred on 1 August. Orange flames represent active hotspots by the end of 5 August.

Chapter 6

Results & discussion

Beginning with section 6.1, this chapter first presents the findings when attempting to fulfil objectives 3 to 5. Then, focusing on objective 6, section 6.2 contains a suitability assessment of the, in Sweden, available base data concerning its applicability for wildfire growth modelling. The evaluation is based on an assumed forecasting preciseness need of emergency services trying to suppress a wildfire. An usually very challenging and physically demanding task because of many reasons. For example, according to MSB (2015), several barriers were constructed during the 2014 Västmanland wildfire attempting to interrupt the wildfire propagation. However, despite some of the barriers being longer than a kilometre, parts of the fire front were missed. Perhaps these attempts had been more successful if locations where the fire front was going to pass had been known. This implies a precision need of a few tens of metres.

6.1 The influence of data inputs on wildfire growth modelling

The two Prometheus simulations performed in this study used the mandatory model specific inputs described in section 2.2. One of these simulations used an additional barrier input (see appendix A.2.3) meaning it was possible reviewing whether any existing barriers beneficially should be included when modelling the growth of a wildfire. The extents modelled in the Prometheus simulation excluding the barrier input was compared to the extents modelled in a Prometheus simulation by Hagelin and Cluzel (2016). Except for the weather data input, this compared simulation used the same settings and inputs as the Prometheus simulation performed in the present study. Hence, simulated differences caused by the weather data could be identified. The weather and barrier data assessments are found in sections 6.1.1 and 6.1.2 respectively. Furthermore, the final section (6.1.3) contains a discussion of potential data related reasons to the poor simulation performance of WiSE-FASS. Model specific weaknesses (see section 2.3) are emphasised. Despite greatly underestimating the rate of wildfire propagation, WiSE-FASS modelled a similarly shaped, but scaled down, surface as the one that was burnt by the 2014 Västmanland wildfire.

6.1.1 Weather related differences between two simulations of Prometheus

Table 6.1 and figure 6.1 were added to this section to facilitate the assessment, according to objective 3, of differences between two comparable simulations of the 2014 Västmanland wildfire. The table shows all wind direction and velocity values used in the compared Prometheus simulation (see figure 4.7) by Hagelin and Cluzel (2016), it summarises area measurements from the compared simulation, and it lists daily differences between these area measurements and the extents modelled in the first Prometheus simulation (see figure 5.1 and table 5.1) in the present study. Figure 6.1 shows the modelled daily extents of these simulations side by side. Because of the simulated growth reaching the outer extent of the input data in the compared simulation, it was terminated on 4 August. Thus, the map to the right in this figure, showing daily extents from the present study, excludes the extent modelled on 5 August. On 4 August, the first Prometheus simulation performed in this study modelled a 7 653 ha smaller surface than the total surface (i.e. 26 097 ha) modelled by the compared simulation. The modelled surface outside the real fire perimeter and the surface overlapping the real burnt region are 7 047 and 606 ha smaller respectively. It means the Prometheus simulation performed in this study has a higher, compared to the simulation by Hagelin and Cluzel (2016), conformity with the real burnt region. Hence, as the weather data input is the only difference between the two simulations, the weather base data (see appendix A.1.5) used in this study contains information seemingly more representative of the real weather situation during the 2014 Västmanland wildfire than the weather data input used in the compared simulation. Furthermore, when visually comparing the simulations shown in figure 6.1, it is seen that the daily rates of propagation differs. The wind velocities used in the compared simulation (see table 6.1) are higher than those used in the present study (see figures C.2 to C.15), meaning a higher growth rate all days is expected. Despite this, on 31 July, the compared simulation modelled the smallest shape inconsistently with the wind data. Yet, conformity is shown by the length to width ratio. Thus, the seemingly inhibited wildfire modelled that day cannot be explained by wind velocity. This cannot be explained by the differing wind directions either, as the fuel type grid in that area being relatively homogeneous (see figure 4.2). Different relative humidities or a faulty weather interpolation by Prometheus are two other unconfirmed potential causes.

Table 6.1: Wind data used as input in the compared simulation by Hagelin and Cluzel (2016). Daily area measurements of simulated wildfire growth are summarised. The summary is compared with the area measurements from the Prometheus simulation excluding barriers found in table 5.1.

Reference fire (VF)	Prometheus* simulation**				
total area: 13 096 ha	31 July	1 August	2 August	3 August	4 August
Wind direction (°)	45	45	270	293	315
Wind velocity (m/s)	11.1	11.9	6.1	11.9	11.9
Area simulated (ha)	73	3 050	6 787	10 180	26 097
Extent within VF (%)	100	53.0	54.2	54.3	41.9
Fraction of VF (%)	0.6	12.6	28.1	42.2	83.5
Area simulated (ha)***	−320	717	814	1 768	7 653
Extent within VF (ha)***	−320	−262	−299	68	606

* Simulation model 1. ** By Hagelin and Cluzel (2016). *** Difference to the Prometheus* simulation w/o barrier in table 5.1.

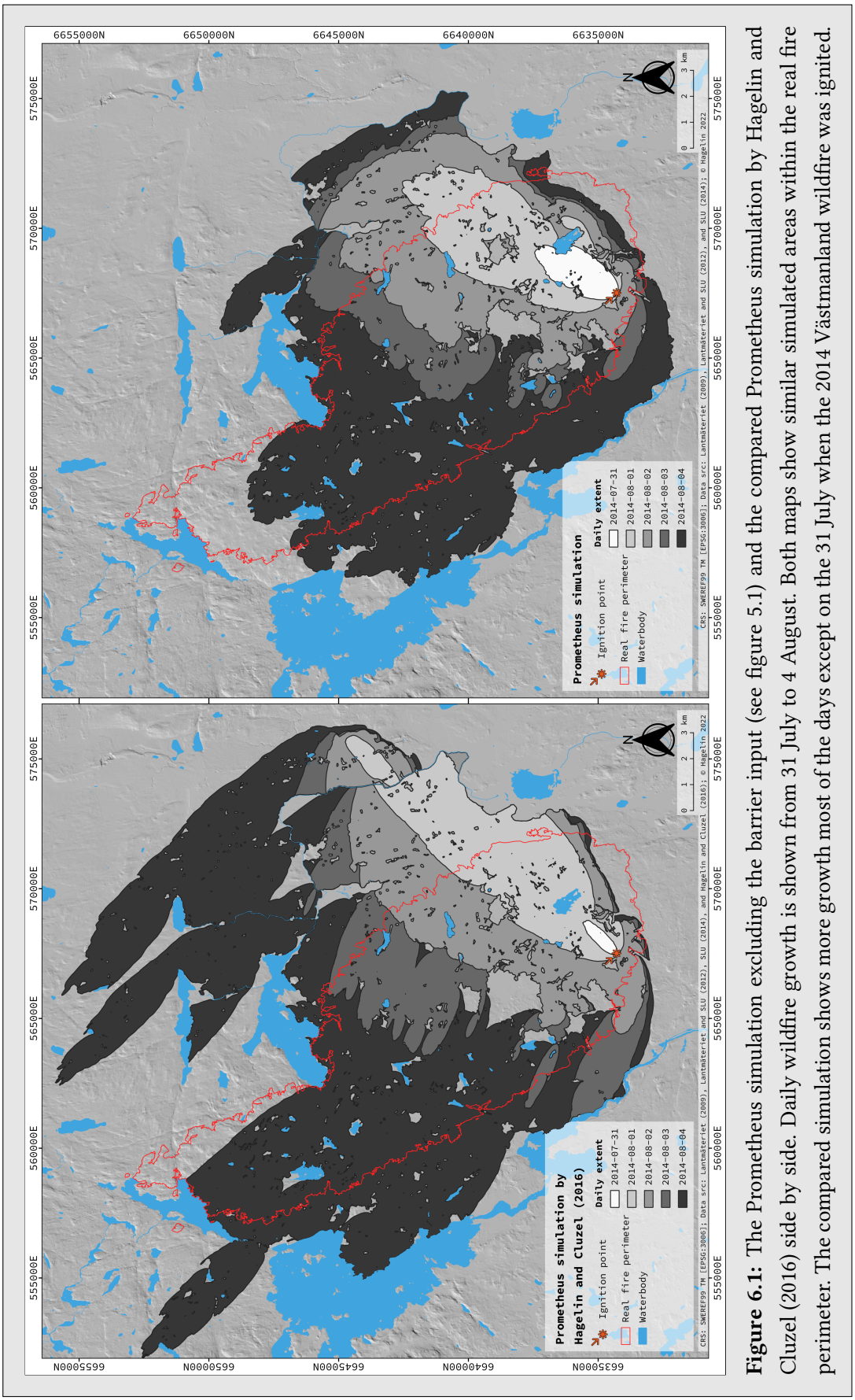

Figure 6.1: The Prometheus simulation excluding the barrier input (see figure 5.1) and the compared Prometheus simulation by Hagelin and Cluzel (2016) side by side. Daily wildfire growth is shown from 31 July to 4 August. Both maps show similar simulated areas within the real fire perimeter. The compared simulation shows more growth most of the days except on the 31 July when the 2014 Västmanland wildfire was ignited.

6.1.2 The importance of barriers when modelling the growth of a wildfire

A barrier input (see appendix A.2.3) was included in the second Prometheus simulation, performed in this study, to test the influence of barriers on wildfire growth modelling (see objective 4). The input contains six, by the emergency services, constructed (i.e. modification of the fuel type grid, e.g. removal of vegetation from the surface; soaking the surface with water) barriers that are distributed across the lower half of the real burnt region, and one natural barrier located at the easternmost part of the real fire perimeter. All barriers were digitised based on information summarised by MSB (2015). Their lengths, widths and spatial locations have not been validated in field. Unfortunately, it was a mistake to include the natural barrier in the barrier input. Because of having a natural origin (i.e. it was a young healthy spruce tree line), it should already be reflected in the fuel type grid input. Providing this barrier as part of the barrier input, instructed Prometheus to limit (i.e. not to prevent; the barrier breaching option was enabled as described in section 4.2.1) simulated wildfire propagation past this tree line. Consequently, the natural barrier could have impacted the simulation, hence the evaluation of the influence of barriers on wildfire growth modelling would have been prevented. Fortunately, as seen in figure 5.2, the natural barrier was not reached until 5 August. Thus, its impact, if any, on the simulation was low. In contrast, the two barriers constructed on 1 and 2 August (see section 3.2) impacted the simulation significantly. This is seen when visually comparing the simulated extents shown by figures 5.1 and 5.2. However, as the barrier, constructed on 1 August, interrupted the northeasterly simulated wildfire growth already on 31 July, it is clear that the barrier functionality in Prometheus has pronounced limitations. For instance, there is no option to assign an appearance date to an imported barrier. Also, new inputs cannot be added to Prometheus during a simulation because of the limitation, found in most wildland fire growth simulation models, preventing adjustments of the virtual representation in which the growing wildfire is modelled. There seems to be no apparent approach to circumvent this issue. Adjusting the distance and perimeter resolution settings (see section 4.2.1) would affect all simulated extents equally (i.e. both over and underestimated extents would either grow or reduce in size synchronous), not only the extent modelled on a particular day. If instead reviewing potential causes to the seemingly overestimated rate of wildfire propagation, it becomes evident that the FBP fuel type classification does not reflect the real ground cover in this particular region of the study area. *Map 1* in figure 6.2 shows a rather heterogeneous area covered by patches of coniferous forests and wetlands while *Map 2*, shown in the

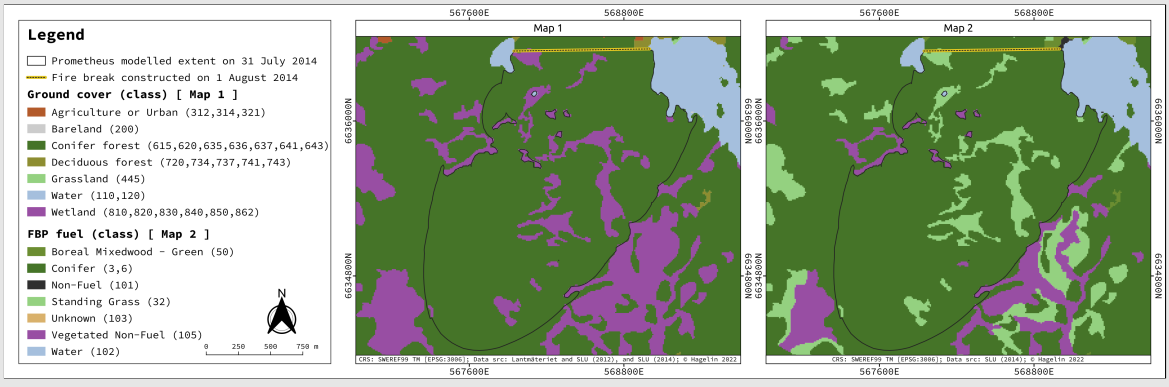

Figure 6.2: Ground cover and FBP fuel types in the perimeter modelled by Prometheus on 31 July.

same figure, shows a more homogenous region classified as coniferous and grass fuel types. Wetlands are barriers to wildfire growth while grasslands combusts rapidly implying that Prometheus modelled an exaggerated rate of propagation on 31 July. Reclassifying the ground cover data is not an easy task as the FBP fuel type system does not contain any fuel types representing the wetlands found in the study area (see figure 4.1 and table B.2). Regardless of this barrier related limitation and the inaccurately simulated rate of wildfire propagation on 31 July, figures 5.1 and 5.2 display two differently sized simulated total extents. The inclusion of the barrier input, made Prometheus model a 4 149 ha smaller total surface than the total surface modelled when the input was omitted (see table 5.1). Also, the total modelled surface overlapping the real burnt region increased from 53.4 to 63.8 %, and simulated overestimation occurred two days later. It means the barrier input improved the simulation conformity with the real burnt region. Hence, the importance to consider barriers when modelling wildfire growth is denoted.

6.1.3 Capabilities of WiSE-FASS and potential causes to its poor performance

In total, WiSE-FASS modelled a 228 ha small surface (see table 5.1) that overlaps the real burnt region by about 1.7 %. Most of the simulated wildfire propagation took place on 4 August, in consistency with reality (see section 3.2), and the simulation model did not overestimate any wildfire growth. Not much else is worthwhile to describe concerning the modelled extent except that only one hectare was burnt on 1 August, possibly because of several reasons in addition to the missing functionality described in section 2.3. For example, the fuel type grid input may have been inaccurately classified because of being created based on assumptions (see section 4.1.2). A proper fuel type classification scheme was not available but should preferably be used when creating this input. The majority of the fuel types in the fuel type input is represented by coniferous species (see figure 4.1 and tables B.1 and B.2) meaning it conforms with the information in table 3.1 showing that roughly 63 % of the real burnt region was covered by coniferous forests. However, the NFDRS fuel type system contains many different coniferous fuel types. Those fuel types affect the rate of wildfire propagation differently because of having varying fuel type characteristics (e.g. fuel load; dead fuel moisture of extinction; surface area to volume ratio). It is likely that some of the classes in the ground cover base data (see appendix A.1.3) were incorrectly classified. As WiSE-FASS lacks a proper methodology for estimation of the moisture content in woody fuel types (see section 2.3.2), the majority of the fuel types in the fuel type grid input may have experienced an exaggerated daily variation of their moisture content. Consequently, WiSE-FASS may underpredict the rate of wildfire propagation when simulating wildfire growth in a grid containing slow burning woody fuel types. Likewise, the rather high relative humidity of 60 to 40 % on 1 August (see section 3.2.2 and appendix C), rising to 100 % during the night, could cause a reduced rate of wildfire propagation because of the same reason. Furthermore, when reviewing the final extent modelled by WiSE-FASS (see figure 5.3) it becomes clear that this surface is reminiscent of the insert map, showing the real fire perimeter, because both areas are wide in the south and taper towards the northwest. Also, except for the almost non-existent modelled wildfire propagation on 1 August, the overall simulated daily growth directions are rather consistent with the information reported by MSB (2015). For example, it is easily seen that the main simulated wildfire growth was northeasterly the first days before turning towards the northwest on 2 August onwards, and days experiencing stronger winds are distinguishable.

6.2 Applicability of available data for wildfire modelling as fire suppression support

As seen in section 2.1.1, wildfires are greatly influenced by parameters obtained from weather readings. They mainly grow in the wind direction and their rate of combustion is controlled by the moisture content of matter and by the wind velocity. Also, their rate of propagation is influenced by aspect and degree of upslope as the rising heat from the flame accelerates the drying of uphill fuels. Therefore, the base data, used to create model inputs, should be of a reasonably high spatial and temporal resolution to account for changes in the weather and terrain. This is particularly important when modelling wildfire growth in a landscape with varying topography and ground cover. Another factor affecting the required base data resolution is the intended use case of the forecasted wildfire growth. For example, barrier construction and fire suppression in field may require more detailed predictions of expected wildfire propagation than the level of detail needed for the decision making process planning the evacuation of urban areas as a result of a nearby conflagration. Furthermore, the spatial resolution of all input data sets must be the same to allow for a simulation whilst the temporal resolution can differ. Frequent updating of elevation data is not needed unless disturbances (e.g. urban development; mining; natural disasters) transform the topography. The ground cover changes more frequently thus requires weekly or monthly review and following sudden changes (e.g. harvest; natural disasters) needed to be reflected by the fuel type grid. Weather changes constantly meaning the shorter the update interval the better those variations will be reflected by the weather data set.

The temporal resolution of the downloaded weather base data set (see appendix A.1.5) is one hour. It is a resolution often considered as adequate when modelling the growth of a wildfire (Tymstra et al. 2010). However, it cannot account for momentarily wind peaks, such as those causing fire spotting two kilometres ahead of the main wildfire on 4 August during the 2014 Västmanland wildfire (MSB 2015), meaning a higher temporal resolution is required when detailed forecasts of wildfire growth is desired. The spatial resolution of 11 km is needless to assess because of more recent weather data having a resolution of 2.5 km (SMHI 2012). That is a welcomed improvement though the weather data still cannot reflect local varying winds. As the spatial resolution must increase further before the weather data can be used in wildfire growth modelling, the need to apply a non trivial data interpolation is indicated. However, such an extreme interpolation (e.g. 2.5 km to 10 m) risks introducing unrealistic wind values. A better approach is to apply a multidimensional wind model such as WindNinja (Forthofer et al. n.d.). Alternatively, the approach used in this study (see section 4.1.3) is easier to implement. It increases the pixel density, preserves the two-dimensional representation of the data and does not alter the original information. Furthermore, a data set containing ground cover information is available as a 10 m resolution raster (Olsson 2019). It is unsuitable for wildfire growth modelling because of its planned update interval (i.e. temporal resolution) of five years. The elevation data is available as 1, 10 and 50 m resolution grids whereas only the latter is freely available (Lantmäteriet n.d.). A 50 m resolution data set requires preprocessing before it can be used in wildfire growth modelling. This is especially true if the map of forecasted wildfire propagation is intended to support those combating a wildfire in the field. A minimum margin of forecasting error of 50 m (i.e. spatial resolution of one grid cell) is twice the length of a typical manoeuvre hose used by firefighters in Sweden (Särdqvist 2006). If instead the resolution is 10 m, an error of two grid cells is covered by one manoeuvre hose instead of three as in the 50 m case.

Chapter 7

Conclusions & recommendations for future studies

The majority of the time spent on this thesis project was consumed by the preprocessing of spatial base data. Because most of the input data, required by the simulation models, was expected in formats not supported by common GIS, custom scripts was adapted, tested and applied. This is reflected by the methodology chapter (4). A limited availability of sufficiently documented wildfires (i.e. only the final perimeter of the 2014 Västmanland wildfire was available) prevented a thorough statistical evaluation of the modelled wildfire growths. Instead, theoretical evaluations, relying on the background information obtained from literature reviews, were conducted. Five conclusions were drawn in the data assessment. Those are presented in section 7.1. The final section (7.2) introduces six recommendations, mostly based on the study conclusions, attempting to encourage others to venture into this developing field of science.

7.1 Conclusions

Three data sets (i.e. terrain; ground cover; weather), considered as base data when preparing data inputs for wildland fire growth simulation models, are available in Sweden. Their resolutions are sufficient to allow for the initiation of a wildfire growth simulation. However, their contained information do not meet the requirements for the temporal resolution needed to allow for any practical use of the modelled wildfire growth. Sections 7.1.1 to 7.1.5 clarify this while presenting the conclusions of the present study.

7.1.1 Hourly weather data allowed for the most conforming simulation

Prometheus set up to use hourly weather data modelled an extent having a higher, compared to an analogous simulation using diurnal weather data, conformity with the region devastated by the 2014 Västmanland wildfire. The higher conformity was mainly because of a reduced (i.e. by roughly 7 000 ha) modelled overestimation. Hence, hourly weather data should be used when modelling wildfire growth rather than relying on the interpolation functionality built into wildland fire growth simulation models.

7.1.2 Fire breaks ought to be included when modelling wildfire growth

Including a barrier input, containing fire breaks, in one of the simulations, performed in the present study, resulted in a 4 149 ha smaller modelled extent, compared to the extent modelled in the simulation excluding the input, while the surface overlapping the total area burnt by the 2014 Västmanland wildfire

(i.e. reference fire) increased from 53.4 to 63.8 %. It means the barrier input improved the simulation conformity with the reference fire. Therefore, this study concludes that all types of barriers limiting wildfire growth ought to be considered, and included, when preparing to model the growth of a wildfire.

7.1.3 Sweden is lacking a fuel type classification scheme

Many fuel types describe similar ground cover despite having varying characteristics that greatly, and differently, influence the wildfire growth rate. Their similarities make them difficult to differentiate, especially for someone untrained in fuel type classification, unless a developed classification scheme is available. However, no complete fuel type classification scheme, detailing how Swedish ground cover should be classified as fuel types, currently exists in Sweden. Consequently, the deviating growth rate, modelled by both simulation models, is likely partly a consequence of a faulty fuel type classification.

7.1.4 The creation of wind indices is a non-trivial process

The velocity and direction of wind are the two environmental factors having the greatest influence on wildfire behaviour. Indices of this information can be difficult to create because of its correlation with other physical geographical features. Common interpolation techniques, found in GIS, are unsuitable for the task. Instead, a wind model, designed for the purpose, ought to be used when creating these inputs. However, application of a dedicated wind model is not always feasible, for instance, because of time constraints or the lack of computational resources. Therefore, the present study emphasises the use of methods that increase the pixel density of the data without altering the original information.

7.1.5 Unreliable ground cover data because of its inadequate temporal resolution

The spatial resolution of the, in Sweden, available base data sets is sufficient to allow for wildfire growth modelling either as it is or after a resolution increasing process. The DEM and weather data sets have feasible temporal resolutions. In contrast, the planned update frequency of the ground cover data is five years meaning this information risks being unreliable. Hence, the already complex task to correctly classify ground cover as fuel types becomes impossible. Consequently, the temporal resolution of the ground cover data set must increase in order to, at least, make the information reflect natural variations in the vegetation. This is needed before the forecasted wildfire growth may be suitable for use at all.

7.2 Recommendations for future studies

Wildfire growth modelling has the potential constituting a useful measure to limit the consequences of wildfires. However, more research is needed before a wildland fire growth simulation model can be introduced in Sweden as a measure to increase the societal preparedness to wildfires. Hence, the recommendations, formulated as objectives, in sections 7.2.1 to 7.2.6 define what future studies can do.

7.2.1 Model high resolution wind data using a dedicated wind model

Incorporate a wind model, such as WindNinja, when preprocessing the base data. The application of a wind model allows for the creation of two data collections, containing information of wind velocity and direction, whose spatial variability matches the spatial resolution of the terrain and ground cover data sets. Hence, as long as the temporal resolution of the wind information is at least 1 h, it is likely that the modelled wind data would enable a more realistic simulation than what was seen in the present study.

7.2.2 Draft a workflow for barrier documentation

Design a workflow that defines the process of documenting fire breaks. It is important that the workflow includes the collection of the precise geographical coordinates of a barrier and, if relevant, the local time of its appearance. Another important, but rarely documented information, is the intelligence of where, when and to what extent a wildfire is fought by the emergency services. This information is relevant as wildfire suppression involves activities attempting to change the moisture content of the ground cover.

7.2.3 Develop a Swedish fuel type classification scheme

Create a fuel type classification scheme that describes how the Swedish ground cover information should be classified as fuel types. The scheme ought to be based on the fuel types found in either of, or if possible both, the FBP and NFDRS fuel type systems to make it compatible with any of the most commonly used wildland fire growth simulation models. Consequently, the classification scheme may not be suitable to use when preparing the fuel type input prior to a simulation if none of those fuel types are represented.

7.2.4 Generate new wind data sets accounting for wind gust

Develop a methodology that describes the generation of two new data sets comprising information of wind velocity and direction. The spatial and temporal resolution of these data sets should be reasonably high to account for local and momentarily winds. Such high quality data sets would most probably greatly increase the accuracy of the forecasts produced by any of the most commonly used wildland fire growth simulation models. That is due to the incapability of those models to account for wind gusts.

7.2.5 Discover methods to increase the update frequency of the ground cover data

Identify and investigate methods to increase the temporal resolution of the ground cover information. The update frequency should reflect natural variations during the growing season. Otherwise, the data

set cannot be trusted to be true to reality. However, it is preferred to have an update frequency reflecting abrupt changes (e.g. harvesting; urban development; droughts; storms; wildfires) in the ground cover.

7.2.6 Outline a process of ground truthing that documents the growth of wildfires

Form a framework outlining the ground truth collection in field post a wildfire. In addition to the base data sets, needed when preparing the different data inputs required by wildland fire growth simulation models, it is important to document the wildfire propagation at various time intervals as well as the final perimeter. Hourly and daily documentation of wildfire growth is recommended because it allows for evaluation of hourly and daily modelled wildfire growth. Also, this ground truth data set would facilitate the parametrisation and calibration of a forthcoming Swedish wildland fire growth simulation model.

Bibliography

Albini, F. A. 1976a. COMPUTER-BASED MODELS OF WILDLAND FIRE BEHAVIOR: A USERS' MANUAL. U.S. Department of Agriculture, Forest Service, Intermountain Forest and Range Experiment Station, Manual Ogden, UT, USA, 74 pp.

Albini, F. A. 1976b. Estimating Wildfire Behavior and Effects. USDA Forest Service, Intermountain Forest and Range Experiment Station, General Technical Report INT-30, Ogden, UT, USA, 92 pp.

Alexander, M. E., B. S. Lee, and C. Y. Lee. 1984. Hourly Calculation of the Fine Fuel Moisture Code, Initial Spread Index, and Fire Weather Index with the Texas Instruments Model 59 Hand-Held Calculator. Department of Agriculture, Ministry of State for Forestry, Canadian Forestry Service, Northern Forest Research Centre, Study NOR-5-191, File Report 7, Edmonton, AB, Canada, 18 pp.

Alexander, M. E. 2010. Foliar Moisture Content Input in the Canadian Forest Fire Behavior Prediction System for Areas Outside of Canada. In *Proceedings of the 6th International Conference on Forest Fire Research*. Ed. D. X. Viegas, 13. Coimbra, Portugal: University of Coimbra.

Alted, F., I. Vilata, S. Prater, V. Mas, T. Hedley, A. Valentino, J. Whitaker, J. Moore, et al. 2018. Tables 3.4.3: Hierarchical datasets for Python. Retrieved 12 May, 2022, from https://pypi.org/project/tables/3.4.3/.

Anaconda, Inc. 2018. Numba: A High Performance Python Compiler. Retrieved 12 May, 2022, from https://numba.pydata.org/.

Anderson, D. H., E. A. Catchpole, N. J. De Mestre, and T. Parkes. 1982. Modelling the Spread of Grass Fires. *The Journal of the Australian Mathematical Society. Series B. Applied Mathematics* 23: 451. doi: 10.1017/S0334270000000394

Anderson, H. E. 1982. Aids to Determining Fuel Models For Estimating Fire Behavior. U.S. Department of Agriculture, Forest Service, Rocky Mountain Research Station, General Technical Report INT-122, Ogden, UT, 22 pp.

Anderson, H. E. 1983. Predicting Wind- Driven Wild Land Fire Size and Shape. U.S. Department of Agriculture, Forest Service, Intermountain Forest and Range Experiment Station, Research Paper INT-305, Ogden, UT, USA, 32 pp.

Anderson, H. E. 1988. Sundance Fire: An Analysis of Fire Phenomena. U.S. Department of Agriculture, Forest Service, Intermountain Forest and Range Experiment Station, Research Paper INT-56, Ogden, UT, USA, 48 pp.

Andrews, P. L. 1989. BEHAVE: Fire Behavior Prediction and Fuel Modeling System–BURN Subsystem, Part 1. U.S. Department of Agriculture, Forest Service, lntermountain Research Station, General Technical Report INT-194, Ogden, UT, USA, 134 pp.

Andrews, P. L. 2018. The Rothermel Surface Fire Spread Model and Associated Developments: A Comprehensive Explanation. U.S. Department of Agriculture, Forest Service, Rocky Mountain Research Station, General Technical Report RMRS-GTR-371, Fort Collins, CO, USA, 132 pp.

Barani Design. n.d. Mean Sea Level Pressure Calculator (Converter). Retrieved 15 May, 2022, from https://barani.biz/apps/sea-level-pressure/.

Bengtsson, L.-G. 2001. *Enclosure Fires*. Karlstad: Swedish Rescue Services Agency.

Burgan, R. E. 1988. 1988 Revisions to the 1978 National Fire-Danger Rating System. U.S. Department of Agriculture, Forest Service, Southeastern Forest Experiment Station, Research Paper SE-273, Asheville, NC, USA, 44 pp. doi: 10.2737/SE-RP-273

Burgan, R. E., and R. C. Rothermel. 1984. BEHAVE: Fire Behavior Prediction and Fuel Modeling System–FUEL Subsystem. U.S. Department of Agriculture, Forest Service, Intermountain Forest and Range Experiment Station, INT-GTR-167, Ogden, UT, USA, 132 pp. doi: 10.2737/INT-GTR-167

Burman, J., A. Granström, I. Bohlin, P.-Å. Gradmark, and C. Lejon. 2016. Kartläggning av spridningsmodeller för brand i vegetation: Test av modeller lämpliga för svenska förhållanden. Swedish University of Agricultural Sciences (SLU), Swedish Defence Research Agency (FOI) and Swedish Civil Contingencies Agency (MSB), Studierapport MSB1037 - december 2016, Karlstad, Sweden, 53 pp. [in Swedish].

Chandler, C. C., P. Cheney, P. Thomas, L. Trabaud, and D. Williams. 1983. *Fire in Forestry. Volume 1, Forest Fire Behavior and Effects*. Vol. 1. New York: John Wiley & Sons, Inc.

Davis, K. P., G. M. Byram, and W. R. Krumm. 1959. *FOREST FIRE: Control and Use*. Ed. H. J. Vaux, New York: McGraw-Hill Book Company, inc.

Esri. 2017a. How Aspect Works. Retrieved 12 May, 2022, from https://desktop.arcgis.com/en/arcmap/10.5/tools/spatial-analyst-toolbox/how-aspect-works.htm.

Esri. 2017b. How Slope Works. Retrieved 12 May, 2022, from https://desktop.arcgis.com/en/arcmap/10.5/tools/spatial-analyst-toolbox/how-slope-works.htm.

Finney, M. A. 2004. FARSITE: Fire Area Simulator–Model Development and Evaluation. U.S. Department of Agriculture, Forest Service, Rocky Mountain Research Station, Research Paper RMRS-RP-4, Ogden, UT, 47 pp.

Forestry Canada Fire Danger Group. 1992. Development and Structure of the Canadian Forest Fire Behavior Prediction System. Forestry Canada, Fire Danger Group and Science and Sustainable Development Directorate, Information Report ST-X-3, Ottawa, ON, Canada, 66 pp.

Forthofer, J., B. Butler, and N. Wagenbrenner. n.d. WindNinja. Retrieved 8 May, 2022, from https://www.firelab.org/project/windninja.

Gillies, S. 2018a. Affine 2.2.2: Matrices describing affine transformation of the plane. Retrieved 12 May, 2022, from https://pypi.org/project/affine/2.2.2/.

Gillies, S. 2018b. Fiona 1.8.4: Fiona reads and writes geographic data files. Retrieved 12 May, 2022, from https://pypi.org/project/Fiona/1.8.4/.

Gillies, S. 2018c. Shapely 1.6.4:Geometric objects, predicates, and operations. Retrieved 12 May, 2022, from https://pypi.org/project/Shapely/1.6.4/.

Gillies, S. 2019. Rasterio 1.0.18: Fast and direct raster I/O for use with Numpy and SciPy. Retrieved 10 May, 2022, from https://pypi.org/project/rasterio/1.0.18/.

Government of Alberta. 2022. Understanding Fire Weather. Retrieved 15 November, 2022, from https://wildfire.alberta.ca/wildfire-status/fire-weather/understanding-fire-weather.aspx.

Hagelin, H., and M. Cluzel. 2016. Applying FARSITE and Prometheus on the Västmanland Fire, Sweden (2014): Fire Growth Simulation as a Measure against Forest Fire Spread – A Model Suitability Study. *Student thesis series INES* 375: 1–56.

Hansen, R. 2003. *Skogsbrandsläckning*. Karlstad: Räddningsverket. [in Swedish].

Hansen, R. 2008. Pilot Study: Modeling of Wildfires. *BTH DIVA* 1236: 1–79.

Hirsch, K. G. 1996. Canadian Forest Fire Behavior Prediction (FBP) System: User's Guide. Natural Resources Canada, Canadian Forest Service, Northern Forestry Centre, Special Report 7, Edmonton, AB, Canada, 134 pp.

Hunter, J. D. 2007. Matplotlib: A 2D Graphics Environment. *Computing in Science Engineering* 9: 90–95. doi: 10.1109/MCSE.2007.55

IPCC. 2014. *Climate Change 2014: Impacts, Adaptation, and Vulnerability - Part A: Global and Sectoral Aspects*. Ed. C. B. Field, V. R. Barros, D. J. Dokken, K. J. Mach, M. D. Mastrandrea, T. E. Bilir, M. Chatterjee, K. L. Ebi, et al., New York, NY: Cambridge University Press.

IPCC. 2018. Summary for Policymakers. In *Global Warming of 1.5°C. An IPCC Special Report on the Impacts of Global Warming of 1.5°C above Pre-Industrial Levels and Related Global Greenhouse Gas Emission Pathways, in the Context of Strengthening the Global Response to the Threat of Climate Change, Sustainable Development, and Efforts to Eradicate Poverty*, ed. M.-D. Valérie, P. Zhai, H.-O. Pörtner, D. Roberts, J. Skea, P. R. Shukla, A. Pirani, W. Moufouma-Okia, et al., 1–26. Geneva: World Meteorological Organization.

Krivtsov, V., O. Vigy, C. Legg, T. Curt, E. Rigolot, I. Lecomte, M. Jappiot, C. Lampin-Maillet, et al. 2009. Fuel Modelling in Terrestrial Ecosystems: An Overview in the Context of the Development of an Object-Orientated Database for Wild Fire Analysis. *Ecological Modelling* 220: 2915–2926. doi: 10.1016/j.ecolmodel.2009.08.019

Lam, S., A. Hay, S. Gorman, L. Shumaker, and S. Cameron-Moore. 2018. 'Everything Destroyed' as wildfire scorches Paradise, California. Retrieved 23 April, 2022, from https://www.reuters.com/article/us-california-wildfires-idUSKCN1ND34V.

Lantmäteriet. 2009. Höjddata 10m raster. Data set. Lantmäteriet (Land Survey of Sweden), Gävle, Sweden. Retrieved 8 May, 2016, from https://atlas.slu.se/get/. [in Swedish].

Lantmäteriet. 2015. GSD-Sverigekartor, vektor. Data set. Lantmäteriet (Land Survey of Sweden), Gävle, Sweden. Retrieved 20 May, 2019, from https://www.lantmateriet.se/sv/Kartor-och-geografisk-information/geodataprodukter/sverigekartor/?steg=1. [in Swedish].

Lantmäteriet. n.d. Markhöjdmodell Nedladdning, grid 50+. Retrieved 4 June, 2022, from https://www.lantmateriet.se/sv/Kartor-och-geografisk-information/geodataprodukter/produktlista/markhojdmodell-nedladdning-grid-50/. [in Swedish].

Lantmäteriet, and SLU. 2012. Vegetation Västmanland vektor. Data set. Lantmäteriet (Land Survey of Sweden), Gävle, Sweden. Retrieved 8 May, 2016, from https://atlas.slu.se/get/. [in Swedish].

Lawson, B. D., O. B. Armitage, and W. D. Hoskins. 1996. Diurnal Variation in the Fine Fuel Moisture Code: Tables and Computer Source Code. Canada-British Columbia Partnership Agreement on Forest Resource Development: FRDA II, Natural Resources Canada, Canadian Forest Service, Pacific Forestry Centre, FRDA Report 245, Victoria, BC, Canada, 20 pp.

López, N., K. Frid, S. Frisk, F. Renman, M. Klintevall, and G. Hamidi-Nia. 2018. Här är bränderna som härjar i Sverige just nu. Retrieved 19 April, 2022, from https://www.svt.se/nyheter/inrikes/har-ar-branderna-som-harjar-i-sverige-just-nu. [in Swedish].

Länsstyrelsen i Västmanlands län. 2014. Skogsbranden i Västmanland 2014 - En Dokumentation Utgiven av Länsstyrelsen i Västmanlands Län. Länsstyrelsen i Västmanlands län, Dokumentation Västerås, Sweden, 32 pp. [in Swedish].

Malmeström, A., and N.-K. Millbourn. 2015. En studie av skogsbrandshantering – Med fokus på skogsbranden i Västmanland. Department of Fire Safety Engineering, Technical Report 5494, Lund University, Sweden, 108 pp. [in Swedish].

Malmstedt, M., and M. Hedlund. 2018. Så stor yta täckte sommarens skogsbränder. Retrieved 19 April, 2022, from https://www.svt.se/special/karta-skogsbrander-2018/. [in Swedish].

McKinney, W. 2010. Data Structures for Statistical Computing in Python. In *Proceedings of the 9th Python in Science Conference (SciPy 2010)*. Ed. S. van der Walt, and J. Millman, 51–56. Austin, TX, USA: SciPy.org.

McKinney, W. 2011. Pandas: A Foundational Python Library for Data Analysis and Statistics. In *Proceedings of the 10th Python in Science Conference (SciPy 2011)*. Ed. S. van der Walt, and J. Millman, 9. Austin, TX, USA: SciPy.org.

MSB. 2012. *Tumregler vid skogsbrand*. Vol. 2. Karlstad: Swedish Civil Contingencies Agency (MSB). [in Swedish].

MSB. 2015. Skogsbranden i Västmanland 2014. Swedish Civil Contingencies Agency (MSB), Observatörsrapport MSB798 - februari 2015, Karlstad, Sweden, 68 pp. [in Swedish].

MSB. 2016. Ansvar, samverkan, handling. Åtgärder för stärkt krisberedskap utifrån erfarenheterna från skogsbranden i Västmanland 2014 (Ju2015/1400/SSK). Swedish Civil Contingencies Agency (MSB), Report MSB989 - Mars 2016, Karlstad, Sweden, 82 pp. [in Swedish].

MSB. 2018. Nationell riskbedömning 2018 som underlag till Sveriges rapportering till Europeiska kommissionen - Svar på uppdrag 8 i MSB:s regleringsbrev 2018. Swedish Civil Contingencies Agency (MSB), Avrapportering Diarienummer 2018-01094, Karlstad, Sweden, 237 pp. [in Swedish].

Natural Resources Canada. 2019. FBP Fuel Type Descriptions. Retrieved 30 May, 2022, from https://cwfis.cfs.nrcan.gc.ca/background/fueltypes/c1.

Natural Resources Canada. n.d. Canadian Forest Fire Weather Index (FWI) System. Retrieved 30 May, 2022, from https://cwfis.cfs.nrcan.gc.ca/background/summary/fwi.

Nelson Jr, R. M. 2000. Prediction of Diurnal Change in 10-h Fuel Stick Moisture Content. *Canadian Journal of Forest Research* 30: 1071–1087. doi: 10.1139/x00-032

Nilsson, B., M. Tyboni, A. Pettersson, A. Granström, and H. Olsson. 2014. Punktgittertolkning av brandområdet i Västmanland. Institutionen för skoglig resurshushållning, Swedish University of Agricultural Sciences (SLU), Arbetsrapport 433 2014, Umeå, Sweden, 17 pp. [in Swedish].

NWCG. 2019. Fire Behavior Prediction (FBP) System. Retrieved 30 May, 2019, from https://www.nwcg.gov/publications/pms437/cffdrs/fire-behavior-prediction-system.

NWCG. 2021. Fire Weather Index (FWI) System. Retrieved 30 May, 2022, from https://www.nwcg.gov/publications/pms437/cffdrs/fire-weather-index-system.

Oliphant, T. E. 2015. *A Guide to NumPy*. Austin, TX, USA: Texas Continuum Press.

Olsson, B. 2019. Nationella Marktäckedata (NMD). Retrieved 4 June, 2022, from https://www.naturvardsverket.se/verktyg-och-tjanster/kartor-och-karttjanster/nationella-marktackedata/. [in Swedish].

Ondrus, J., and L. Gylldorff. 1996. *Brandteori*. Karlstad: Statens räddningsverk. [in Swedish].

Opperman, T., J. Gould, M. Finney, and C. Tymstra. 2006. Applying Fire Spread Simulators in New Zealand and Australia: Results from an International Seminar. In *Fuels Management - How to Measure Success: Conference Proceedings. Proceedings RMRS-P-41. 28-30 March 2006*. Ed. P. L. Andrews, and B. W. Butler, 12. Fort Collins, CO: U.S. Department of Agriculture, Forest Service, Rocky Mountain Research Station.

Persson, G., and L. Wern. 2011. Värmeböljor i Sverige. Swedish Meteorological and Hydrological Institute (SMHI), Faktablad nr 49 – 2011, Norrköping, Sweden, 12 pp. [in Swedish].

Pyne, S. J. 2015. *Between Two Fires: A Fire History of Contemporary America.* Tucson, AZ: The University of Arizona Press.

Ramirez, J., S. Monedero, and D. Buckley. 2011. New Approaches in Fire Simulations Analysis with Wildfire Analyst. In *Proceedings of the 5th International Wildland Fire Conference, Sun City, South Africa, 9–13 May 2011*, 15. Missoula, MT, USA: The International Association of Wildland Fire (IAWF). doi: 10.13140/2.1.2045.7766

Reinhardt, E. D., and M. B. Dickinson. 2010. First-Order Fire Effects Models for Land Management: Overview and Issues. *Fire Ecology* 6: 131–142. doi: 10.4996/fireecology.0601131

Richards, G. D. 1990. An Elliptical Growth Model of Forest Fire Fronts and Its Numerical Solution. *International Journal for Numerical Methods in Engineering* 30: 1163–1179. doi: 10.1002/nme.1620300606

Richards, G. D. 1993. The Properties of Elliptical Wildfire Growth for Time Dependent Fuel and Meteorological Conditions. *Combustion Science and Technology* 95: 357–383. doi: 10.1080/00102209408935341

Richards, G. D. 1995. A General Mathematical Framework for Modeling Two-Dimensional Wildland Fire Spread. *International Journal of Wildland Fire* 5: 63–72. doi: 10.1071/WF9950063

Richards, G. D. 1999. The Mathematical Modelling and Computer Simulation of Wildland Fire Perimeter Growth over a 3-Dimensional Surface. *International Journal of Wildland Fire* 9: 213–221. doi: 10.1071/WF00019

Rothermel, R. C. 1972. A Mathematical Model for Predicting Fire Spread in Wildland Fuels. U.S. Department of Agriculture, Forest Service, Intermountain Forest and Range Experiment Station, Research Paper INT-115, Ogden, UT, USA, 40 pp.

Schlobohm, P., and J. Brain. 2002. Gaining an Understanding of the National Fire Danger Rating System. NWCG Fire Danger Working Team, Report PMS 932/NFES 2665, Boise, ID, USA, 82 pp.

Scott, J. H., and R. E. Burgan. 2005. Standard Fire Behavior Fuel Models: A Comprehensive Set for Use with Rothermel's Surface Fire Spread Model. U.S. Department of Agriculture, Forest Service, Rocky Mountain Research Station, General Technical Report RMRS-GTR-153, Ft. Collins, CO, USA, 80 pp. doi: 10.2737/RMRS-GTR-153

Simard, A. J. 1968. The Moisture Content of Forest Fuels - I: A Review of the Basic Concepts. Government of Canada, Department of Forestry and Rural Development, Forest Fire Research Institute, Information Report FF-X-14, Ottawa, ON, Canada, 47 pp.

SLU. 2014. Brandkartan. Swedish University of Agricultural Sciences (SLU), Uppsala, Sweden. [in Swedish].

SMHI. 2012. Observation eller beräknat värde? Retrieved 4 June, 2022, from https://www.smhi.se/kunskapsbanken/observation-modellberaknat-varde-1.21115. [in Swedish].

SMHI. 2014a. Meteorologisk analysmodell MESAN (HIRLAM) - historiska analysdata. Data set. Swedish Meteorological and Hydrological Institute (SMHI), Norrköping, Sweden. Retrieved 15 March, 2019, from http://opendata-download-grid-archive.smhi.se/explore/?modeltype=4. [in Swedish].

SMHI. 2014b. Meteorologiska modeller. Retrieved 6 June, 2022, from https://www.smhi.se/kunskapsbanken/meteorologi/meteorologiska-modeller-1.5932. [in Swedish].

Song, M., K. Chen, Z. He, and Z. X. 2013. Wind resource assessment on complex terrain based on observations of a single anemometer. *Journal of Wind Engineering and Industrial Aerodynamics* 125: 22–29. doi: 10.1016/j.jweia.2013.11.011

Särdqvist, S. 2006. *Vatten och andra släckmedel.* Vol. 2. Karlstad: Räddningsverket. [in Swedish].

Taylor, S. W., R. G. Pike, and M. E. Alexander. 1996. *Field Guide to the Canadian Forest Fire Behaviour Prediction (FBP) System.* FRDA Handbook, 012 11. Edmonton, AB: Pacific Forestry Centre.

Tymstra, C., R. Bryce, B. Wotton, S. Taylor, and O. Armitage. 2010. Development and Structure of Prometheus: The Canadian Wildland Fire Growth Simulation Model. Natural Resources Canada, Canadian Forest Service, Northern Forestry Centre, Information Report NOR-X-417_2010, Edmonton, AB, Canada, 88 pp.

Vakalis, D., H. Sarimveis, C. Kiranoudis, A. Alexandridis, and G. Bafas. 2004. A GIS Based Operational System for Wildland Fire Crisis Management I. Mathematical Modelling and Simulation. *Applied Mathematical Modelling* 28: 389–410. doi: 10.1016/j.apm.2003.10.005

van Wagner, C. E. 1969. A Simple Fire-Growth Model. *The Forestry Chronicle* 45: 103–104. doi: 10.5558/tfc45103-2

van Wagner, C. E. 1987. Development and Structure of the Canadian Forest Fire Weather Index System. Government of Canada, Canadian Forestry Service, Forestry Technical Report 35, Ottawa, ON, Canada, 48 pp.

van Wagner, C. E., and T. L. Pickett. 1985. Equations and FORTRAN Program for the Canadian Forest Fire Weather Index System. Canadian Forestry Service, Petawawa National Forestry Institute, Forestry Technical Report 33, Chalk River, ON, Canada, 25 pp.

van der Walt, S., S. C. Colbert, and G. Varoquaux. 2011. The NumPy Array: A Structure for Efficient Numerical Computation. *Computing in Science Engineering* 13: 22–30. doi: 10.1109/MCSE.2011.37

Whitaker, J. 2016a. PyGrib 2.0.2: Python module for reading/writing GRIB files. Retrieved 10 May, 2022, from https://pypi.org/project/pygrib/2.0.2/.

Whitaker, J. 2016b. PyProj 1.9.5.1: Python interface to PROJ (cartographic projections and coordinate transformations library). Retrieved 10 May, 2022, from https://pypi.org/project/pyproj/1.9.5.1/.

Appendix A

Meta information of data sets

A total of five base data sets were downloaded for this study. Three of those were used when producing the ten data inputs (see figures 2.4 and 2.5) required by the simulation models. The remaining two were used either as a reference or to improve the visualisation of maps. Meta information of the base data sets is found in appendix A.1 while appendix A.2 lists similar information of the created data inputs.

A.1 Downloaded base data and data sets used for map generation

Three data sets, considered as base data (see appendices A.1.2, A.1.3 and A.1.5), were retrieved for the creation of the data inputs (see appendix A.2) required by the simulation models (see sections 2.2 and 2.3). Also, two vector files, representing districts of Sweden and the final perimeter of the 2014 Västmanland wildfire (see appendices A.1.1 and A.1.4), were retrieved. The feature data were used to visualise Sweden in produced maps and as the reference when evaluating the modelled wildfire growths respectively.

A.1.1 Boundary of Sweden

Type (file format): Polygon feature (.shp).
Date of creation: 2015.
Reference system: SWEREF 99 TM [EPSG:3006].
Description: Vector feature of Swedish districts used to create a polygon representation of Sweden.
Source: Lantmäteriet (2015).

A.1.2 Digital Elevation Model (DEM)

Type (file format): GeoTIFF (.tif).
Date of creation: 2009.
Spatial resolution: 10 m.
Temporal resolution: Unknown.
Reference system: SWEREF 99 TM [EPSG:3006].
Unit: Metres above sea level (MASL).
Description: Laser scanned digital representation of the elevation in the study area. This particular data set requires a license in order to access. A 50 m resolution grid (Lantmäteriet n.d.) is publicly available.
Source: Lantmäteriet (2009).

A.1.3 Ground cover (Nationella Marktäckedata)

Type (file format): GeoTIFF (.tif).
Date of creation: 2010.
Spatial resolution: 10 m.
Temporal resolution: 5 years.
Reference system: SWEREF 99 TM [EPSG:3006].
Description: The ground cover in the study area used for creating fuel type grid inputs. Its ground cover classes are listed in table B.2. An updated ground cover data set of Sweden is freely available as a 10 m resolution grid (Olsson 2019).
Source: Lantmäteriet and SLU (2012).

A.1.4 Outer fire perimeter of the 2014 Västmanland wildfire

Type (file format): Polygon feature (.shp).
Date of creation: 2014.
Reference system: SWEREF 99 TM [EPSG:3006].
Description: Final perimeter of the 2014 Västmanland wildfire.
Source: SLU (2014).

A.1.5 Weather data (MESAN)

Type (file format): GRIB file archive (.grb).
Date of creation: 2014.
Spatial resolution: 11 km.
Temporal resolution: Hourly.
Reference system: SWEREF 99 TM [EPSG:3006].
Description: This data set contains weather information produced by a mesoscale analysis model (i.e. MESAN) used by SMHI. Its contained information is, according to SMHI (2014b), based on weather forecasts, observations and remotely sensed data. Air pressure at sea level, precipitation, relative humidity, temperature, u and v components of wind, and wind gust data were exported, at 14 evenly distributed locations (see figure C.1), for use in this study (see section 4.1.3 for extraction methodology). The data set is publicly available.
Source: SMHI (2014a).

A.2 Meta information on the created data inputs

Meta data of all inputs, created for the simulation models, are detailed in appendices A.2.1 to A.2.13. All coordinates of vector features are presented, as WKT geometries, in SWEREF 99 TM [EPSG:3006]. Each grid (i.e. 3 003 rows and 2 522 columns) covers the surface framed by the bounding box [551920, 6627872 : 577140, 6657902]. Table A.1 lists information on which data input was used by each simulation model.

A.2.1 Air pressure

Type (file format): Scientific data format (.hdf5).
Date of creation: 2019.
Spatial resolution: 10 m.
Temporal resolution: Hourly between 31 July 2014 13:00 and 5 August 2014 23:00.
Reference system: SWEREF 99 TM [EPSG:3006].
Unit: Hectopascal (hPa).
Description: Hourly mean air pressure data at 2 MASL.
Created from: MESAN weather data set (see appendix A.1.5).

A.2.2 Aspect

Type (file format): Scientific data format (.hdf5).
Date of creation: 2019.
Spatial resolution: 10 m.
Reference system: SWEREF 99 TM [EPSG:3006].
Unit: Compass degrees (0–360°).
Description: Direction of downslope.
Created from: Digital Elevation Model (see appendix A.1.2).

Table A.1: Checklist showing what input data were used by which simulation model.

Data input	Prometheus	WiSE-FASS
Air pressure	–	✓
Aspect	–	✓
Barriers*	✓	–
DEM (converted)	✓	–
Fire Weather Index (FWI)	–	✓
Fuel types	✓	✓
Ignition point**	✓	✓
Precipitation***	–	–
Relative humidity***	–	–
Slope	–	✓
Temperature***	–	–
Weather (combined)	✓	–
Wind velocity	–	✓

* Not a mandatory input. Used by Prometheus in the second simulation (see table 5.1 and figure 5.2).
** Only the coordinate of the ignition point was used as input for WiSE-FASS. Prometheus used the vector file.
*** Temporary data set used for creation of other data sets.

A.2.3 Barriers

Type (file format): LineString feature (.shp).
Date of creation: 2019.
Reference system: SWEREF 99 TM [EPSG:3006].
Description: Barriers to wildfire growth at the estimated locations show by figure 5.2. Contains six constructed and one natural fire break (i.e. a young healthy spruce trees). Not a mandatory input.
Created from: Interpretation of information in MSB (2015).

A.2.4 DEM (converted)

Type (file format): ASCII table (.asc).
Date of creation: 2019.
Spatial resolution: 10 m.
Reference system: SWEREF 99 TM [EPSG:3006].
Unit: Metre (m).
Description: Converted version of the elevation base data. Used by Prometheus to compute aspect and slope.
Created from: Digital Elevation Model (see appendix A.1.2).

A.2.5 Fuel types

Type (file format): ASCII table (.asc) for Prometheus; Scientific data format (.hdf5) for WiSE-FASS.
Date of creation: 2019.
Spatial resolution: 10 m.
Reference system: SWEREF 99 TM [EPSG:3006].
Unit: Unitless.
Description: FBP fuel type grid for Prometheus whereas WiSE-FASS uses a grid of NFDRS fuel types. Classification schemes shown by tables B.1 and B.2.
Created from: Ground cover data set (see appendix A.1.3).

A.2.6 Fire Weather Index (FWI)

Type (file format): Scientific data format (.hdf5).
Date of creation: 2019.
Spatial resolution: 10 m.
Reference system: SWEREF 99 TM [EPSG:3006].
Unit: Rating (n/a).
Description: Data set containing the FWI subindices FFMC (hourly), DMC (diurnally) and DC (diurnally). HFFMC and DMC values are used by both simulation models while the DC values are used only by Prometheus. The data for this wildland fire growth simulation model is stored in the combined weather data set (i.e. appendix A.2.12).
Created from: Precipitation (see appendix A.2.8), previous FFMC, DMC and DC values from Malmeström and Millbourn (2015), relative humidity (see appendix A.2.9), temperature (see appendix A.2.11) and wind velocity (see appendix A.2.13).

A.2.7 Ignition point

Type (file format): Point feature (.shp).
Date of creation: 2019.
Temporal resolution: 31 July 2014 13:29.
Reference system: SWEREF 99 TM [EPSG:3006].
WKT representation: POINT (16.204462150170738 59.8408793554774)
Description: Location of where the 2014 Västmanland wildfire was ignited. The feature point data was used as input for Prometheus while WiSE-FASS obtained the coordinate as part of the terminal command initiating the simulation. WKT coordinate in WGS 84 [EPSG:4328] according to the WKT standard.
Created from: Derived from MSB (2015).

A.2.8 Precipitation

Type (file format): Scientific data format (.hdf5).
Date of creation: 2019.
Spatial resolution: 10 m.
Temporal resolution: Hourly between 31 July 2014 13:00 and 5 August 2014 23:00.
Reference system: SWEREF 99 TM [EPSG:3006].
Unit: Millimetre per hour (mm/h).
Description: Accumulated hourly value.
Created from: MESAN weather data set (see appendix A.1.5).

A.2.9 Relative humidity

Type (file format): Scientific data format (.hdf5).
Date of creation: 2019.
Spatial resolution: 10 m.
Temporal resolution: Hourly between 31 July 2014 13:00 and 5 August 2014 23:00.
Reference system: SWEREF 99 TM [EPSG:3006].
Unit: Percent (%).
Description: Mean hourly value at 2 m above the ground surface.
Created from: MESAN weather data set (see appendix A.1.5).

A.2.10 Slope

Type (file format): Scientific data format (.hdf5).
Date of creation: 2019.
Reference system: SWEREF 99 TM [EPSG:3006].
Unit: Degrees (°).
Description: Mean hourly value at 2 m above the ground surface.
Created from: MESAN weather data set (see appendix A.1.5).

A.2.11 Temperature

Type (file format): Scientific data format (.hdf5).
Date of creation: 2019.
Spatial resolution: 10 m.
Temporal resolution: Hourly between 31 July 2014 13:00 and 5 August 2014 23:00.
Reference system: SWEREF 99 TM [EPSG:3006].
Unit: Degrees Celsius (℃).
Description: Mean hourly value at 2 m above the ground surface.
Created from: MESAN weather data set (see appendix A.1.5).

A.2.12 Weather (combined)

Type (file format): Comma separated values table (.csv).
Date of creation: 2019.
Spatial resolution: 11 km.
Temporal resolution: Hourly between 31 July 2014 13:00 and 5 August 2014 23:00.
Reference system: SWEREF 99 TM [EPSG:3006].
WKT representations: MULTIPOINT ((16.039909 59.979140), (16.224360 59.940996), (16.148099 59.848600), (16.331721 59.810312))
Units: FFMC (rating), DMC (rating), DC (rating); precipitation (mm); relative humidity (%); temperature (℃); wind direction (0–360°); wind velocity (kph).
Description: Four data points (i.e. 6, 7, 9, 10 in figure C.1) near or within the reference fire perimeter representing virtual weather stations for Prometheus. Structure according to Tymstra et al. (2010). WKT coordinates provided as WGS 84 [EPSG:4328] according to the WKT standard.
Created from: FWI subindices (i.e. FFMC, DMC, DC; see appendix A.2.6), precipitation (see appendix A.2.8), relative humidity (see appendix A.2.9), temperature (see appendix A.2.11), wind direction (see appendix A.1.5), wind velocity (see appendix A.2.13).

A.2.13 Wind velocity

Type (file format): Scientific data format (.hdf5).
Date of creation: 2019.
Spatial resolution: 10 m.
Temporal resolution: Hourly between 31 July 2014 13:00 and 5 August 2014 23:00.
Reference system: SWEREF 99 TM [EPSG:3006].
Unit: Metre per second (m/s).
Description: Mean hourly value at 2 m above the ground surface.
Created from: MESAN weather data set (see appendix A.1.5).

Appendix B

Interpretation and classification keys

The classes of the FBP and NFDRS fuel types chosen to represent the ground cover (see appendix A.1.3) in the study area are listed by the translation key in table B.1. Their distribution in the fuel type inputs (see appendix A.2.5 and figures 4.2 and 4.3) was determined by reclassifying the ground cover classes in figure 4.1 using the classification key shown by table B.2. Also, table B.2 contains an interpretation key showing how the ground cover classes in figure 4.1 are named by the Swedish governmental authorities.

Table B.1: Translation key showing the FBP and NFDRS fuel type classes, and their corresponding names, chosen when classifying the ground cover, within the study area, as fuel types for the simulation models. A full classification key, used when reclassifying the ground cover to these fuel types, is listed in table B.2. Figures 4.2 and 4.3 show the two reclassified surfaces respectively.

FBP fuel type class and name		NFDRS fuel type class and name	
3	Mature Jack or Lodgepole Pine	95	Urban or Developed
6	Conifer Plantation	96	Agricultural or Cropland
32	Standing Grass	98	Water
50	Boreal Mixedwood - Green	99	Barren
101	Non-fuel	101	Grass - short & sparse - dry climate
102	Water	104	Grass - dry climate (moderate load)
103	Unknown	105	Grass - humid climate (low load)
105	Vegetated Non-Fuel	106	Grass - humid climate (moderate load)
		108	Grass - very coarse - humid climate (high load)
		122	Grass-shrub - dry climate (moderate load)
		141	Shrub - dry climate (low load)
		144	Timber-shrub - humid climate (low load)
		145	Shrub - dry climate (high load)
		161	Timber-grass-shrub - dry climate (light load)
		164	Dwarf conifer with understory
		165	Timber-shrub - dry climate (very high load)
		181	Conifer-litter - compact (low load)
		182	Broadleaf-litter (low load)
		183	Conifer-litter (moderate load)
		186	Broadleaf-litter (high load)
		188	Long-needle-litter

Table B.2: Classification key used when classifying the ground cover base data (see appendix A.1.3), documented by Lantmäteriet and SLU (2012), as FBP* and NFDRS fuel types.

Swedish ground cover class and name		FBP class*	NFDRS class	Swedish ground cover class and name		FBP class*	NFDRS class
110	Öppet vatten	102	98	635	Frisk barrskog (ej lavrik)	3	188
111	Grunda bottnar	102	98	636	Frisk-fuktig barrskog	6	161
112	Periodisk vattensamling	102	98	637	Fuktig barrskog	6	161
120	Vattenvegetation (ospec)	101	98	641	Våt barrskog	6	164
200	Öppen substratdominerad mark	101	99	642	Våt barrskog och myrbarrskog	6	164
210	Hällmark	32	99	643	Barrskogsmyr	6	164
310	Kulturmark	32	99	710	Lövskog (ospec)	50	165
311	Åker/vall	32	96	720	Lövskog på tunt jordtäcke	50	161
312	Kultiverad gräsmark	32	101	734	Torr-frisk lövskog	50	161
314	Igenväxt och planterad kulturmark	32	106	737	Fuktig lövskog	50	165
315	Skogsplanterad f.d. öppen mark	6	144	741	Våt lövskog	50	182
317	Odlad busk- och trädmark	103	144	742	Våt lövskog och lövskogsmyr	50	182
321	Bebyggelse/tomtmark	101	95	743	Lövskogsmyr	50	182
323	Gräsmatte-, park- och tomtmark	32	101	760	Blandad ädellövskog (ospec)	50	186
330	Exploaterad mark	101	95	761	Ekskog	50	186
441	Torr gräs-örtveg	32	105	800	Öppen myrvegetation (ej skogsbevuxen)	105	141
444	Frisk gräs-örtveg	32	104	810	Ristuvemyr	32	141
445	Fuktig gräs-örtveg	32	108	820	Fastmattemyr	32	141
446	Fuktig-våt gräs-örtveg	32	105	823	Fastmattekärr (högstarrvariant)	105	122
454	Sötvattensstrandäng (nordlig; sedimentationsbetingad)	105	122	830	Mjukmattemyr	105	122
				840	Lösbottenmyr	105	122
522	Videbuskveg	32	145	843	Lösbottenkärr (brunmossvariant)	105	122
610	Barrskog (ospec)	6	183	850	Mjuk-fastmattemyr	105	122
615	Hällmarksbarrskog	6	161	860	Högstarr-sumpkärr	105	122
620	Barrskog på tunt jordtäcke	6	181	861	Högstarrkärr	105	122
625	Lavmarksbarrskog	6	164	862	Sumpkärr	105	122
633	Torr barrskog	6	181	871	Videkärr	105	122

* FBP fuel type classification by Hagelin and Cluzel (2016).

Appendix C

The weather during the 2014 Västmanland wildfire

The data points extracted from the MESAN data set (see section 4.1.3 and appendix A.1.5) are numbered in figure C.1 to simplify referencing. Their hourly values, for the entire studied period, are plotted in figures C.2 to C.15. Also, figure C.1 shows the in general flat terrain within the reference fire perimeter.

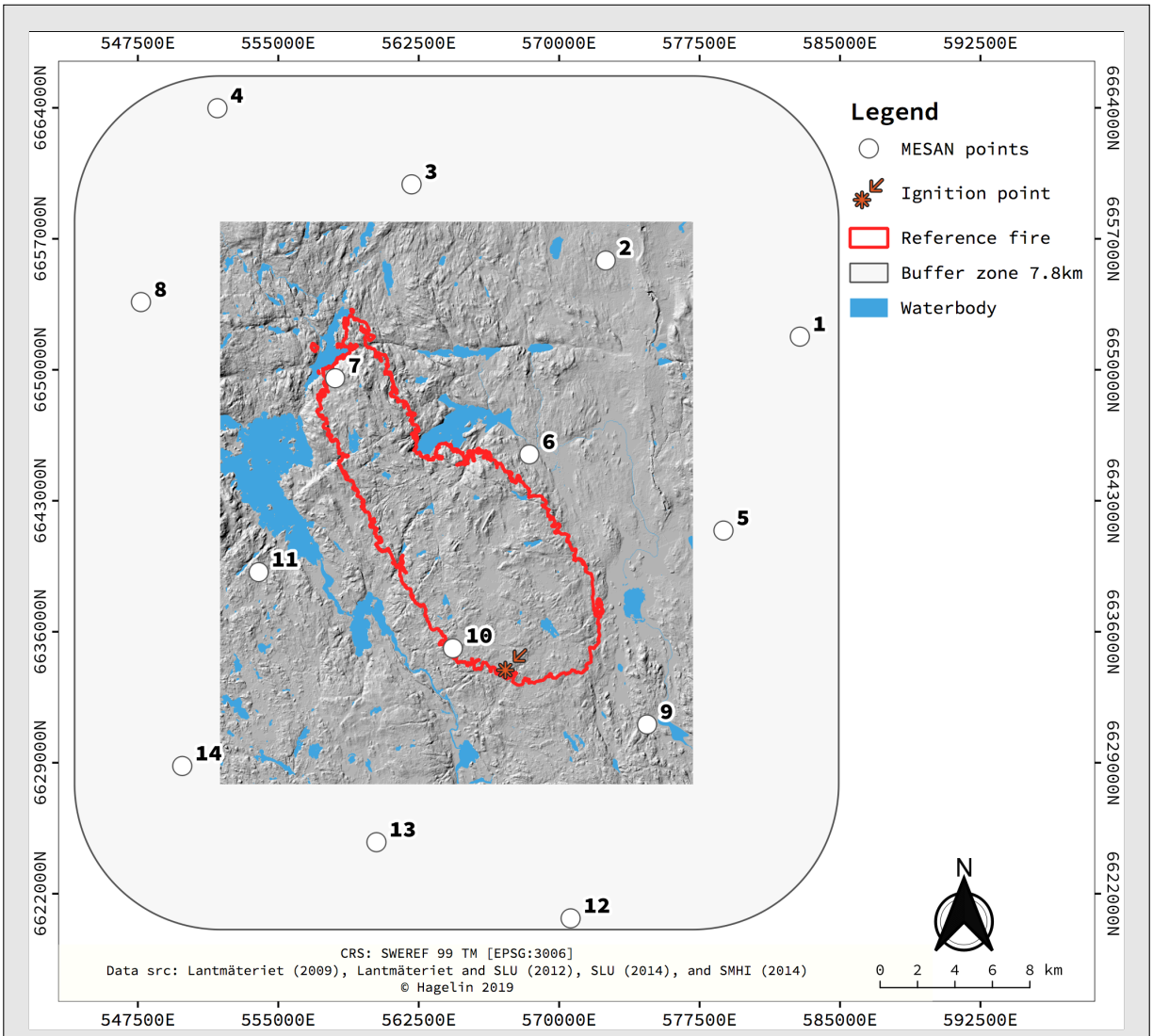

Figure C.1: The 14 MESAN data points, used in this study, numbered in accordance with extraction order for simpler referencing. Hillshaded background map illustrates the terrain in the study area.

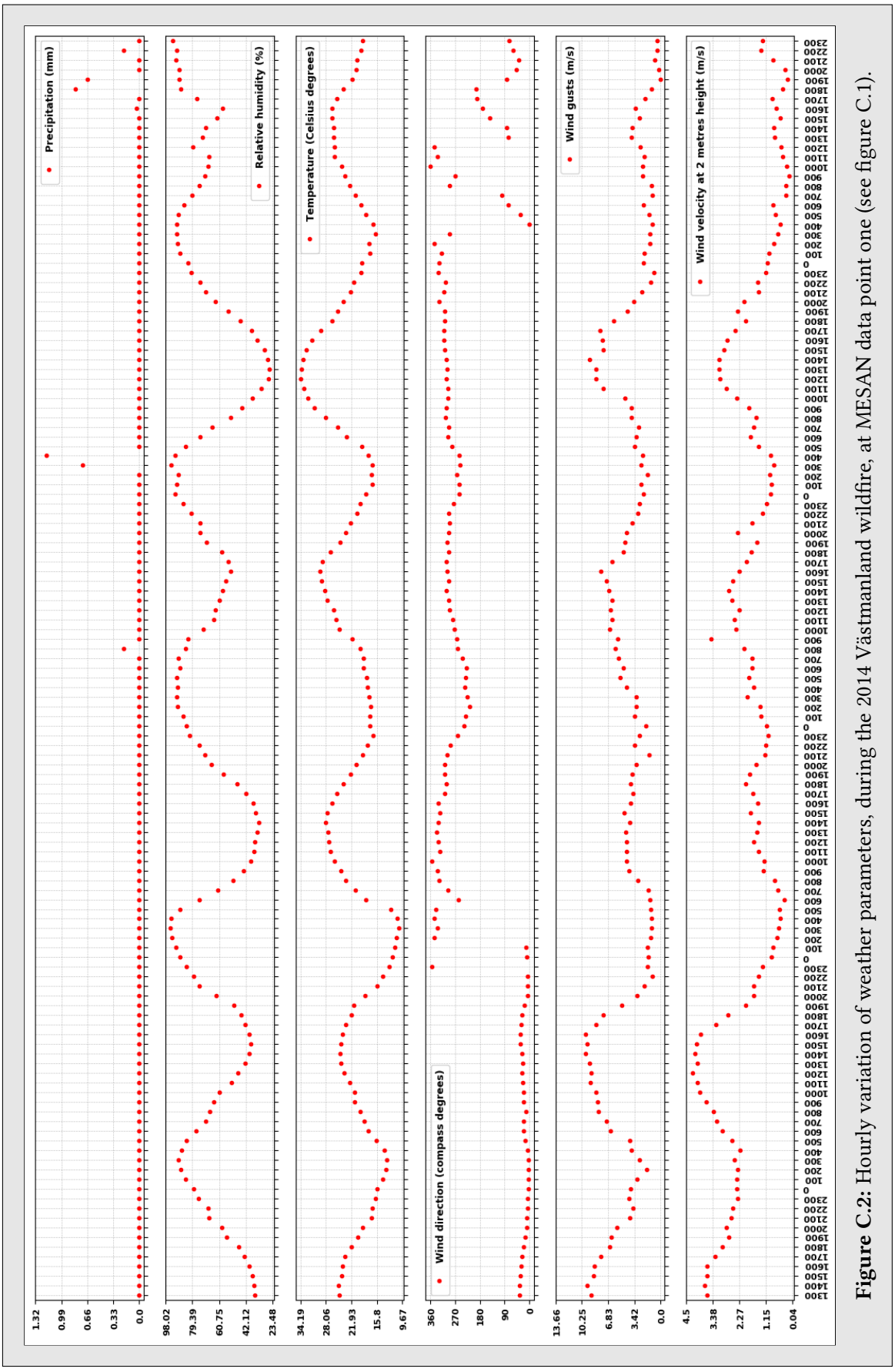

Figure C.2: Hourly variation of weather parameters, during the 2014 Västmanland wildfire, at MESAN data point one (see figure C.1).

MESAN data point two

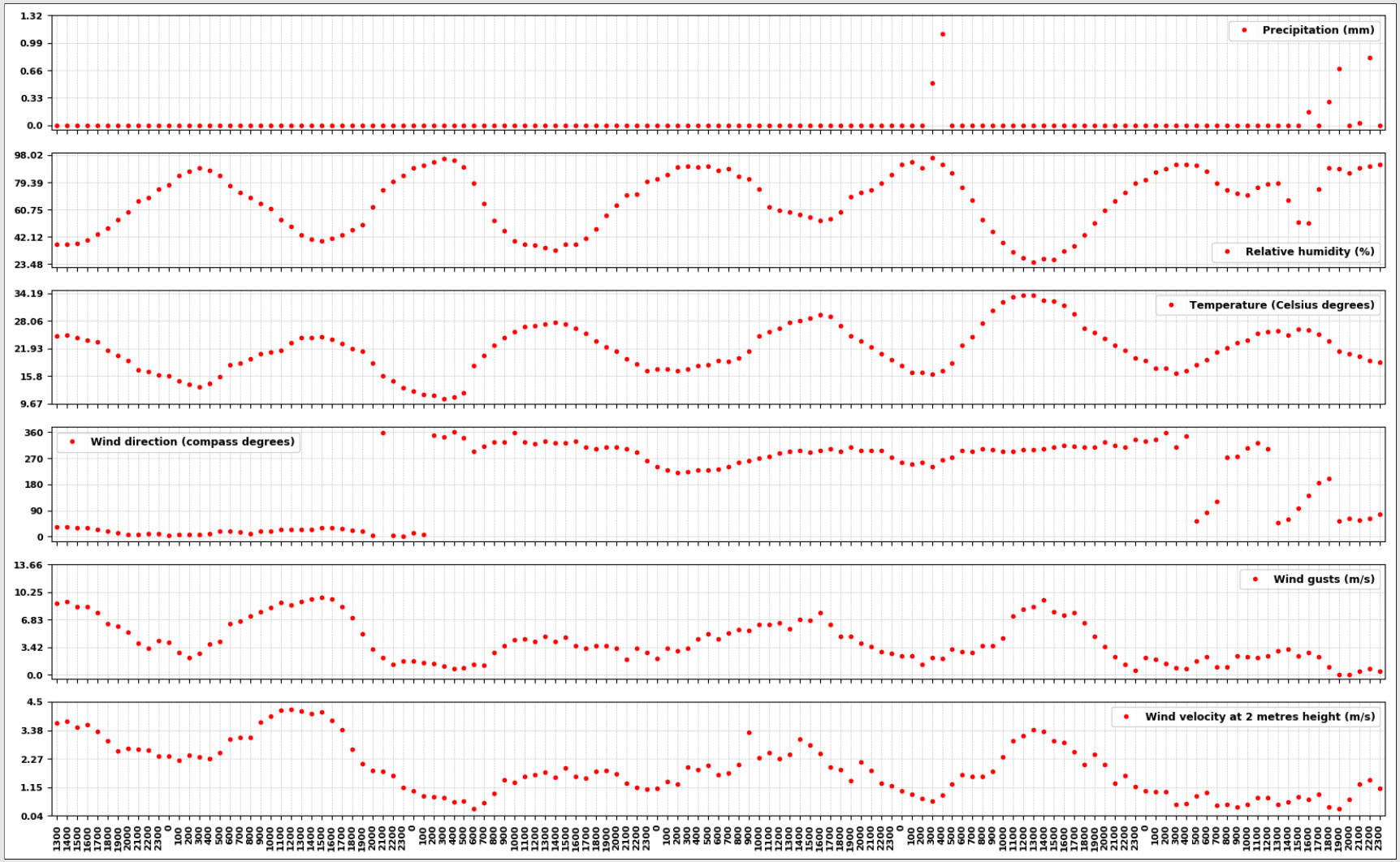

Figure C.3: Hourly variation of weather parameters, during the 2014 Västmanland wildfire, at MESAN data point two (see figure C.1).

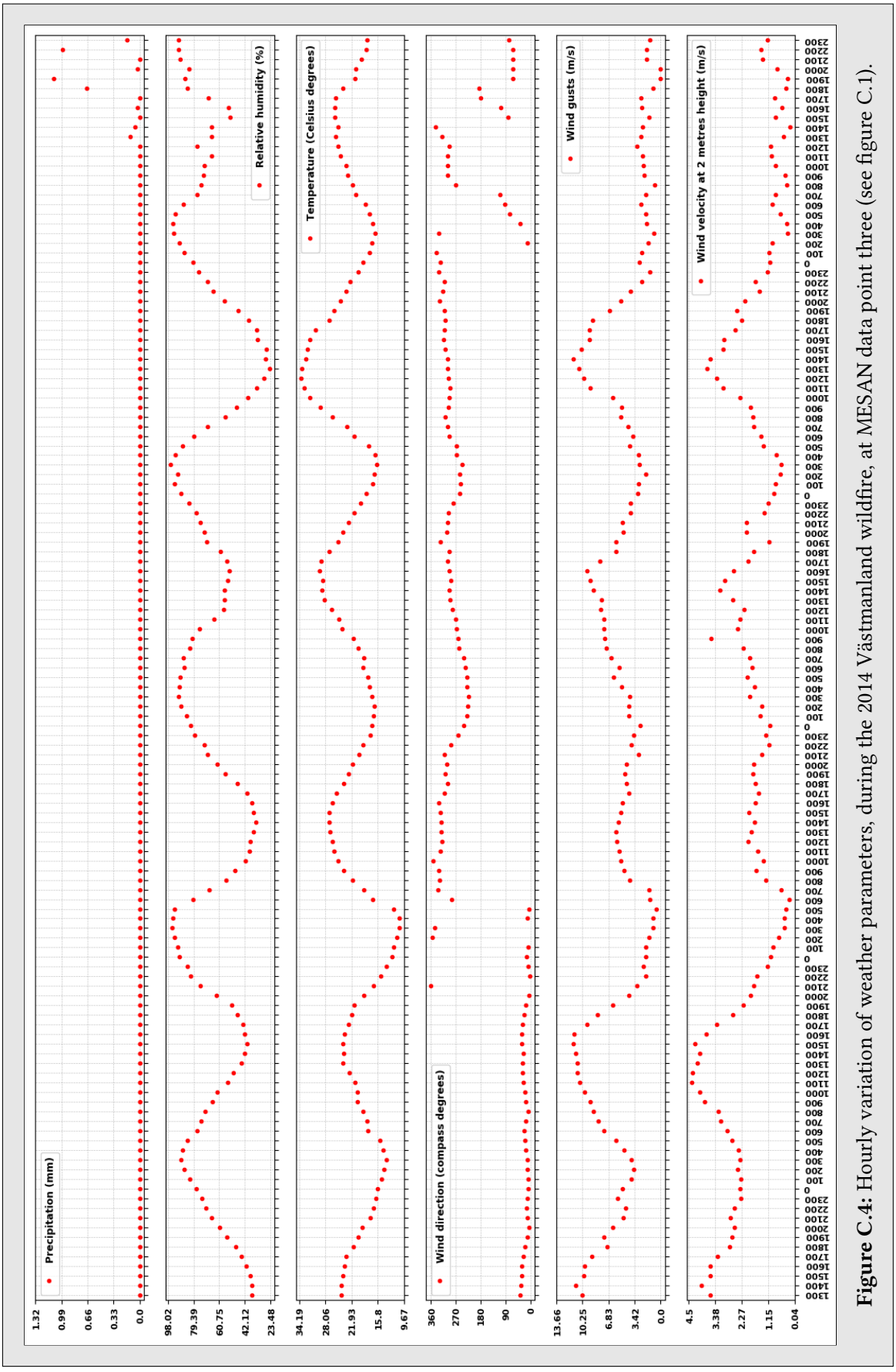

Figure C.4: Hourly variation of weather parameters, during the 2014 Västmanland wildfire, at MESAN data point three (see figure C.1).

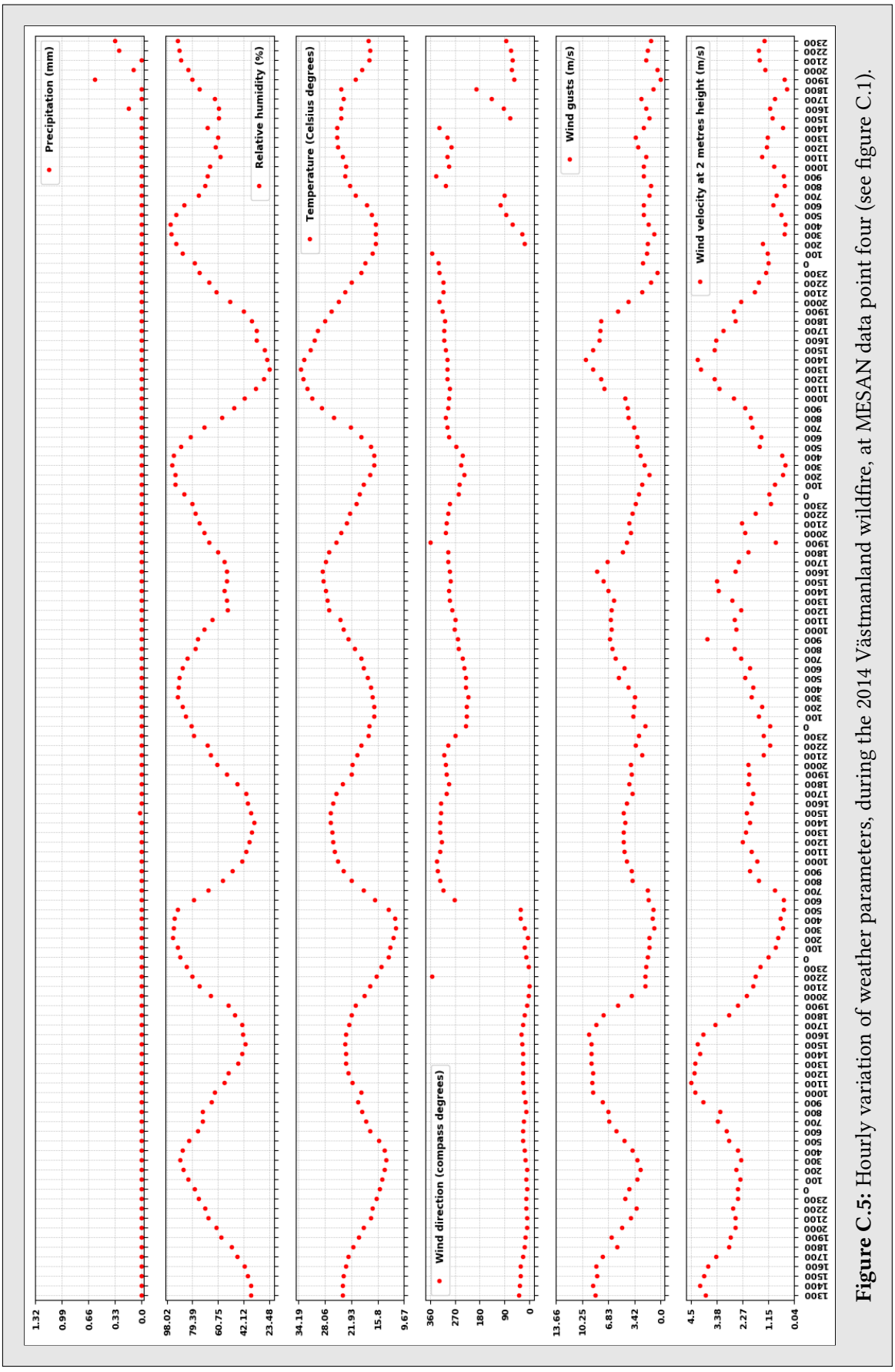

Figure C.5: Hourly variation of weather parameters, during the 2014 Västmanland wildfire, at MESAN data point four (see figure C.1).

MESAN data point five

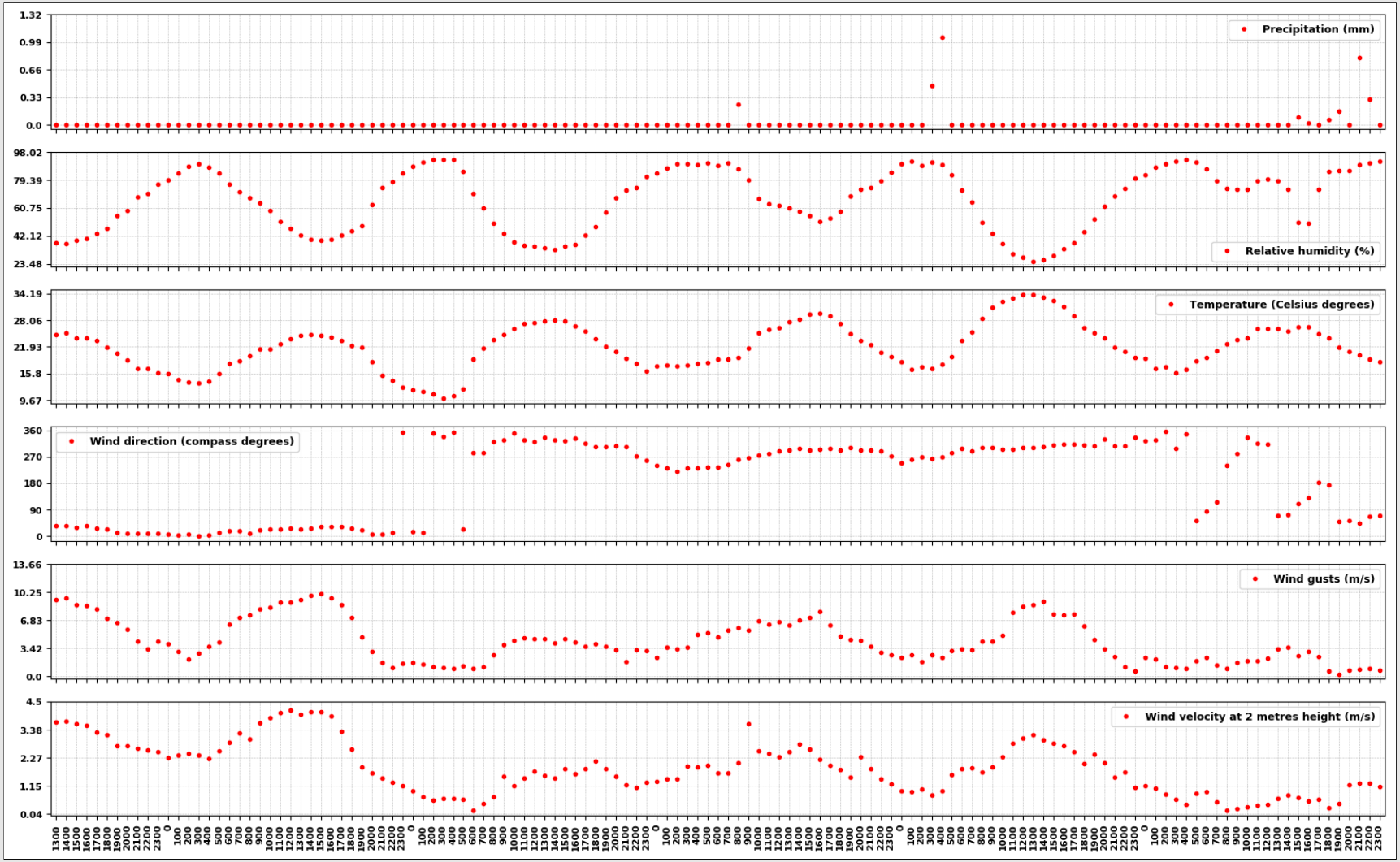

Figure C.6: Hourly variation of weather parameters, during the 2014 Västmanland wildfire, at MESAN data point five (see figure C.1).

MESAN data point six

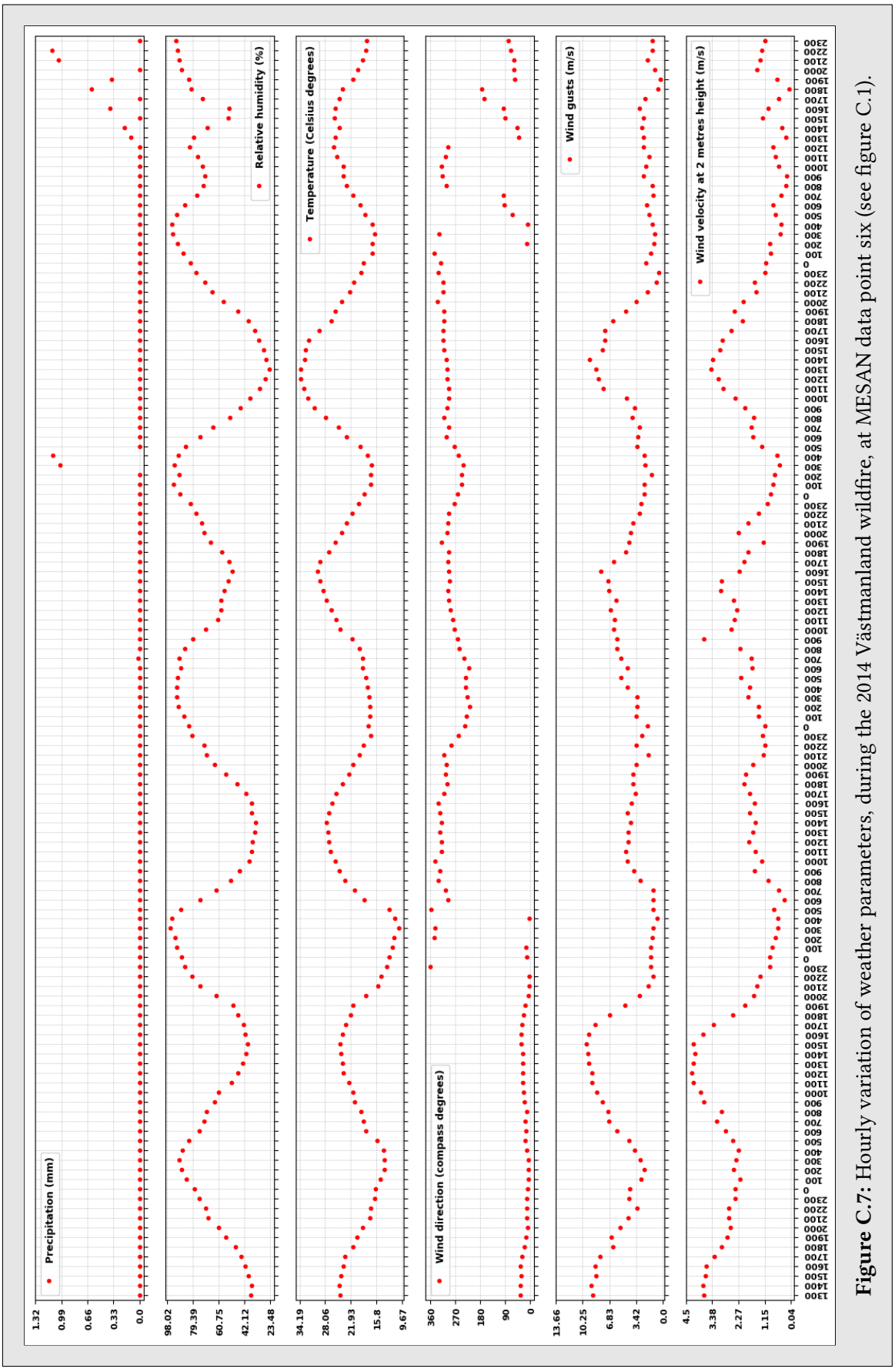

Figure C.7: Hourly variation of weather parameters, during the 2014 Västmanland wildfire, at MESAN data point six (see figure C.1).

MESAN data point seven

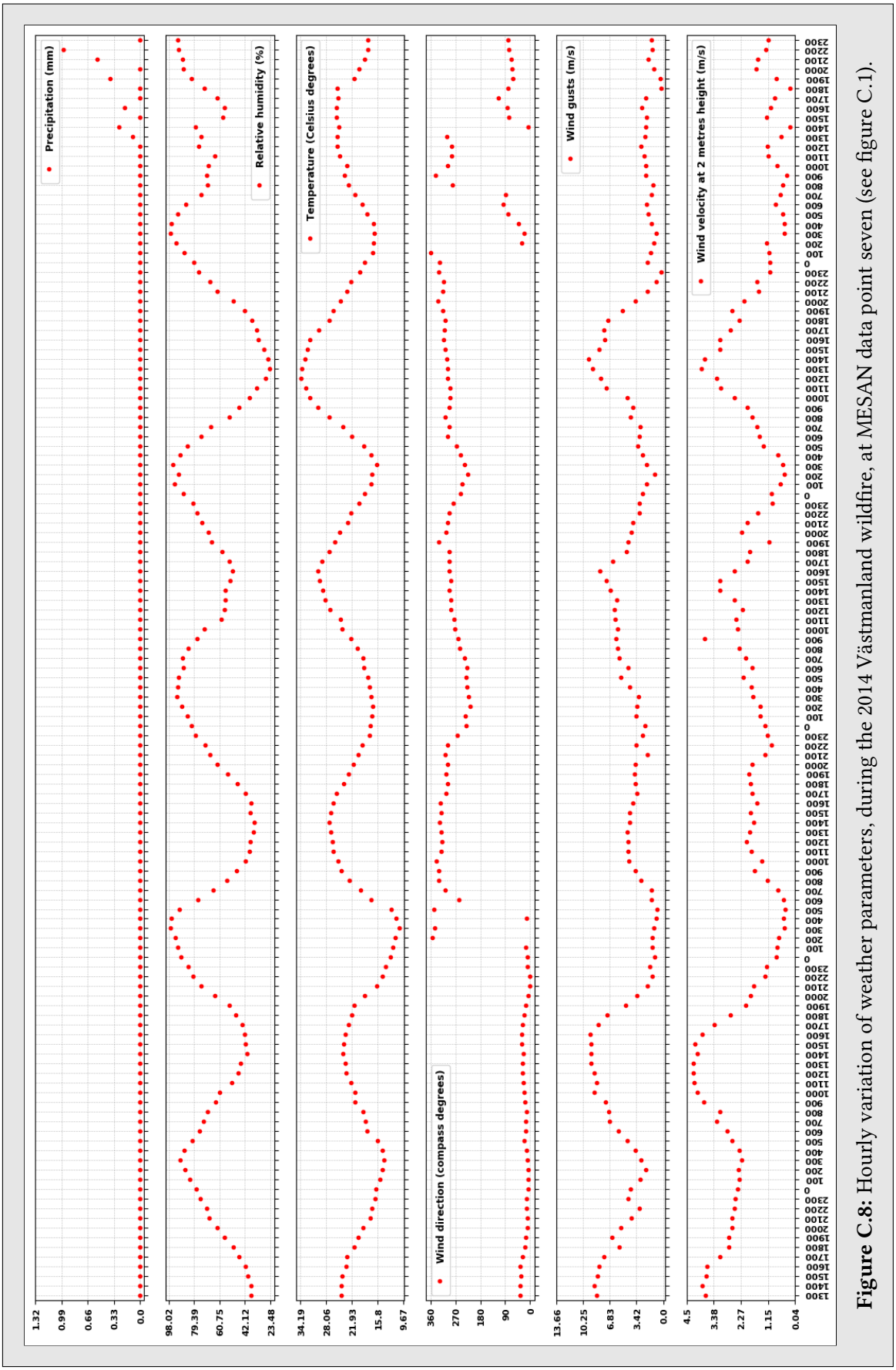

Figure C.8: Hourly variation of weather parameters, during the 2014 Västmanland wildfire, at MESAN data point seven (see figure C.1).

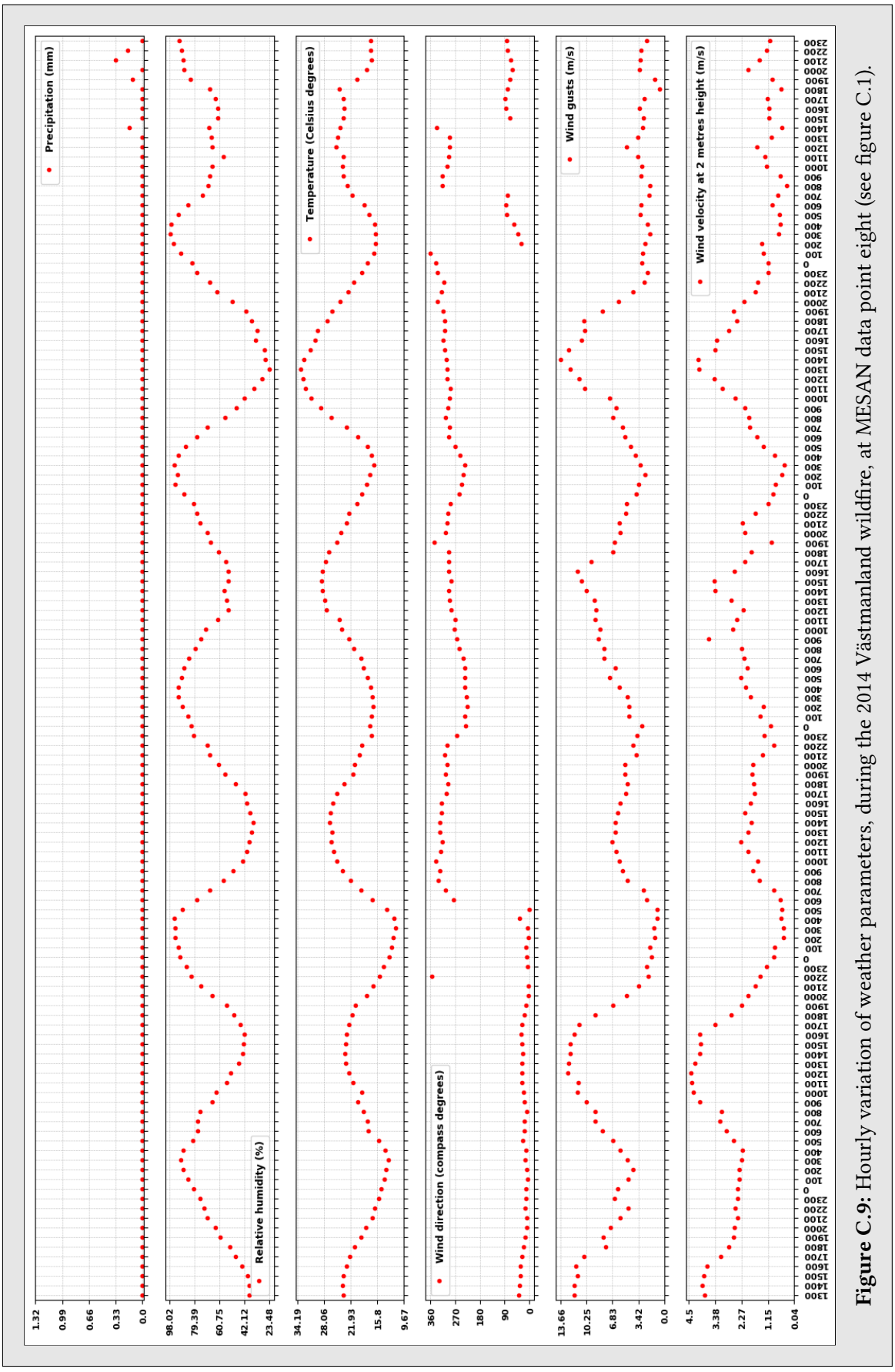

Figure C.9: Hourly variation of weather parameters, during the 2014 Västmanland wildfire, at MESAN data point eight (see figure C.1).

MESAN data point nine

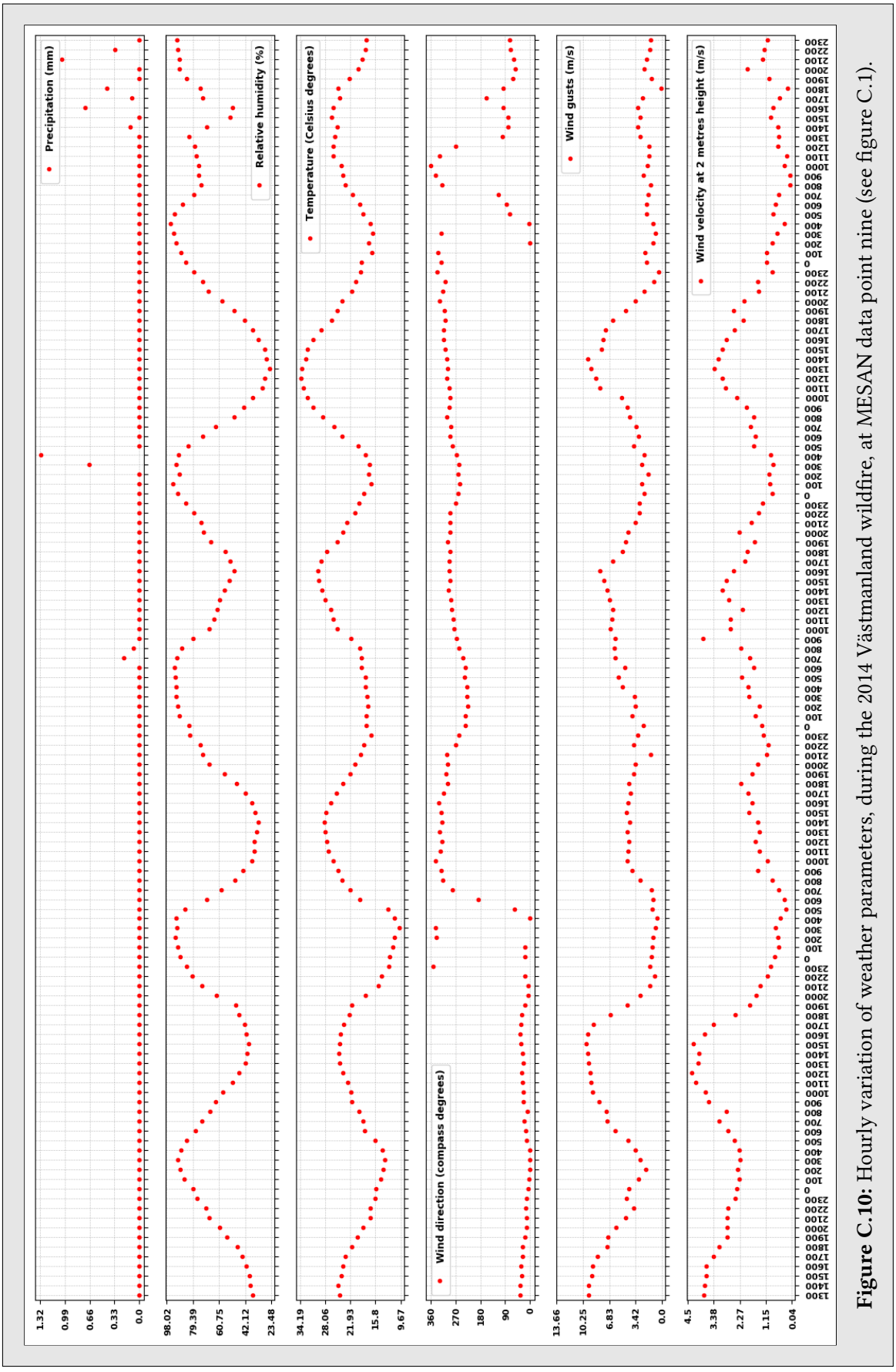

Figure C.10: Hourly variation of weather parameters, during the 2014 Västmanland wildfire, at MESAN data point nine (see figure C.1).

MESAN data point ten

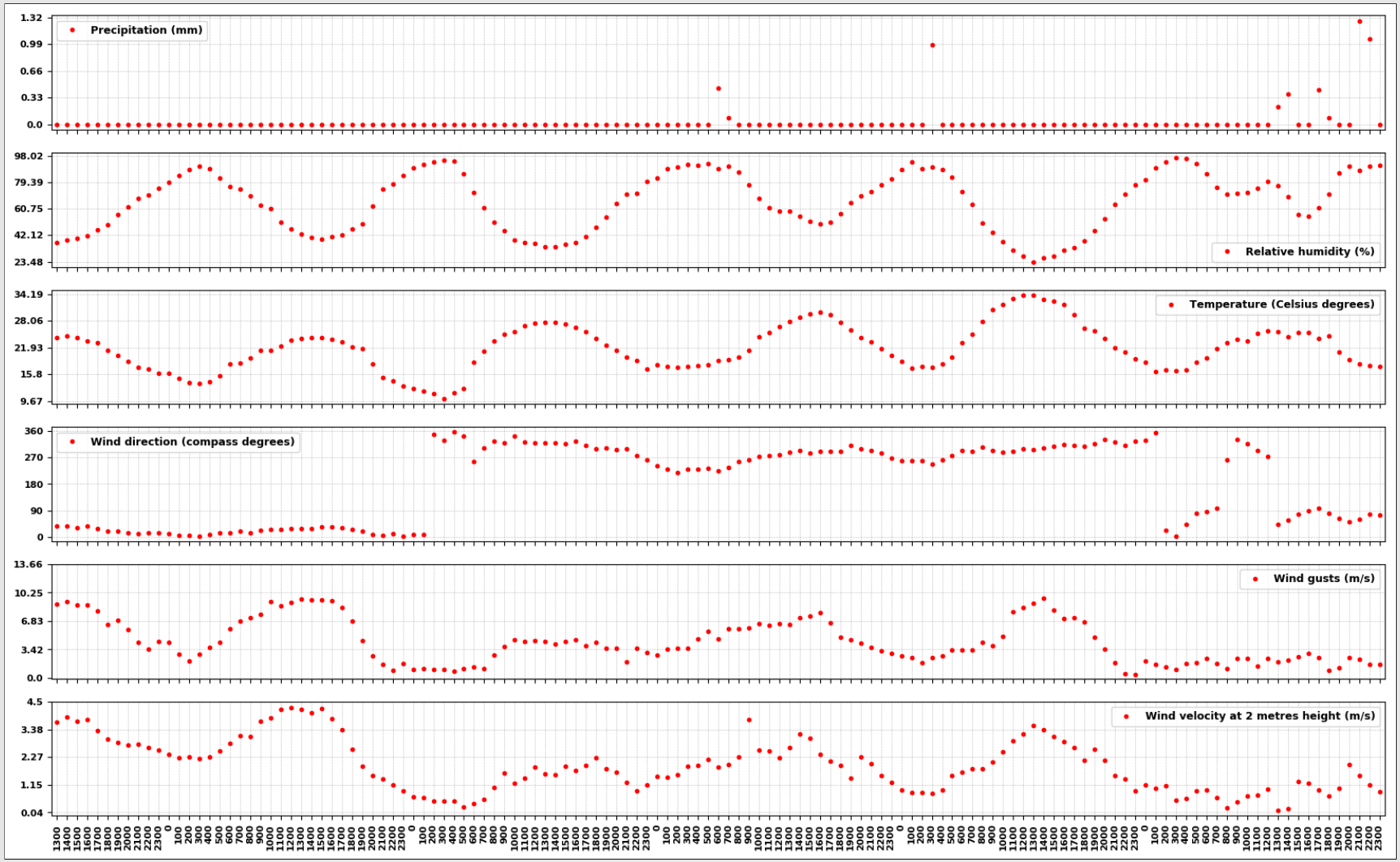

Figure C.11: Hourly variation of weather parameters, during the 2014 Västmanland wildfire, at MESAN data point ten (see figure C.1).

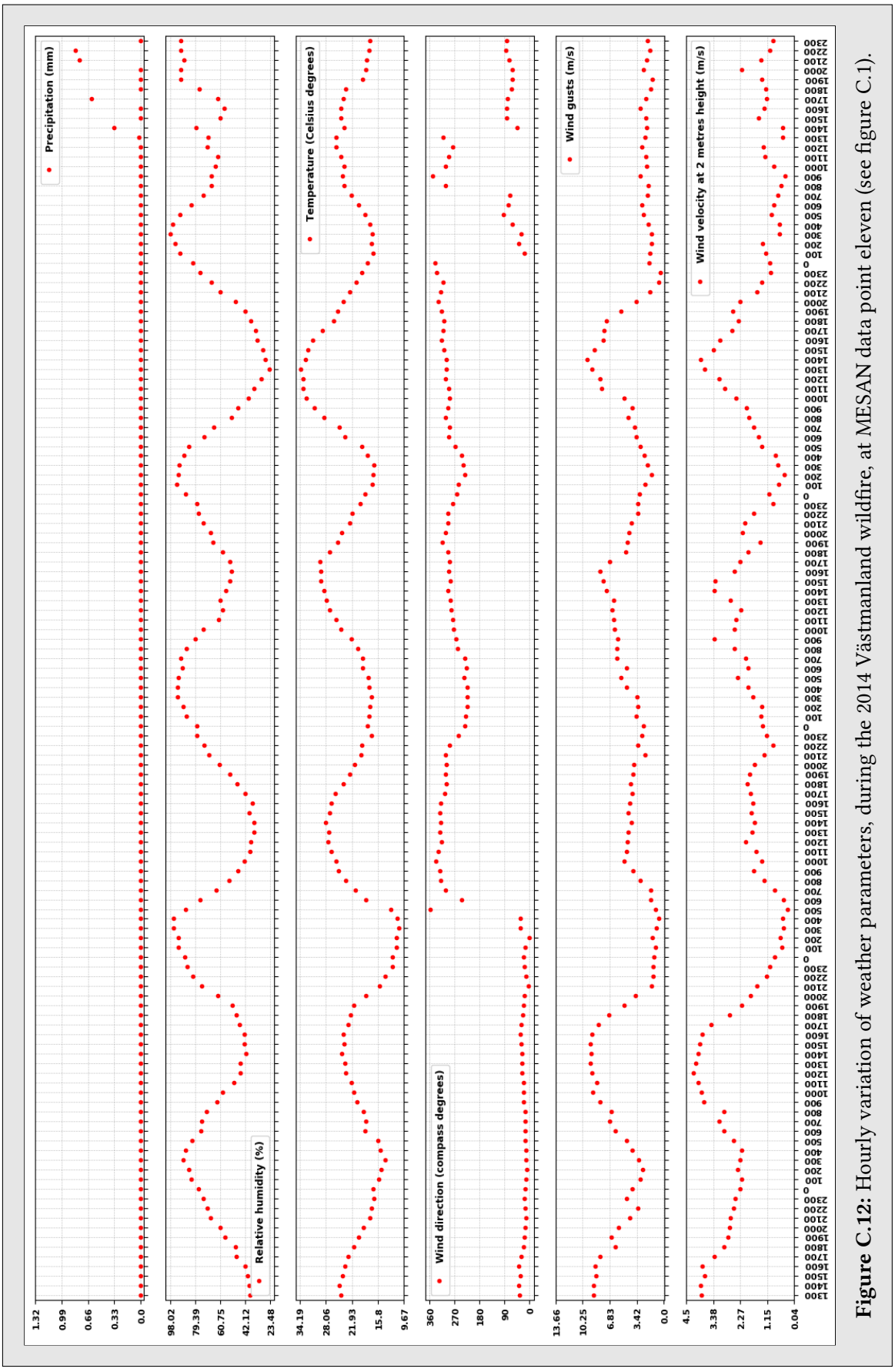

Figure C.12: Hourly variation of weather parameters, during the 2014 Västmanland wildfire, at MESAN data point eleven (see figure C.1).

MESAN data point twelve

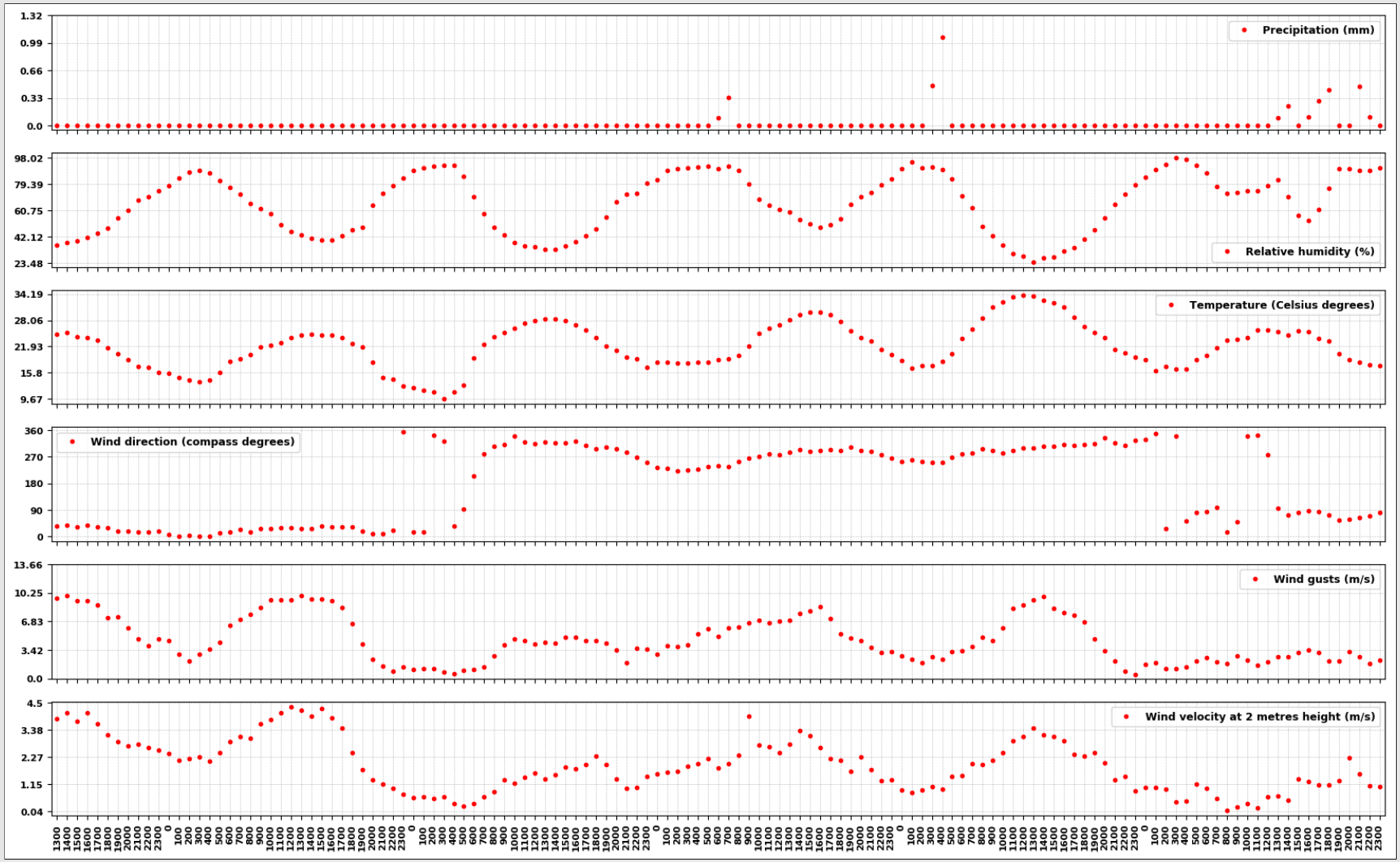

Figure C.13: Hourly variation of weather parameters, during the 2014 Västmanland wildfire, at MESAN data point twelve (see figure C.1).

MESAN data point thirteen

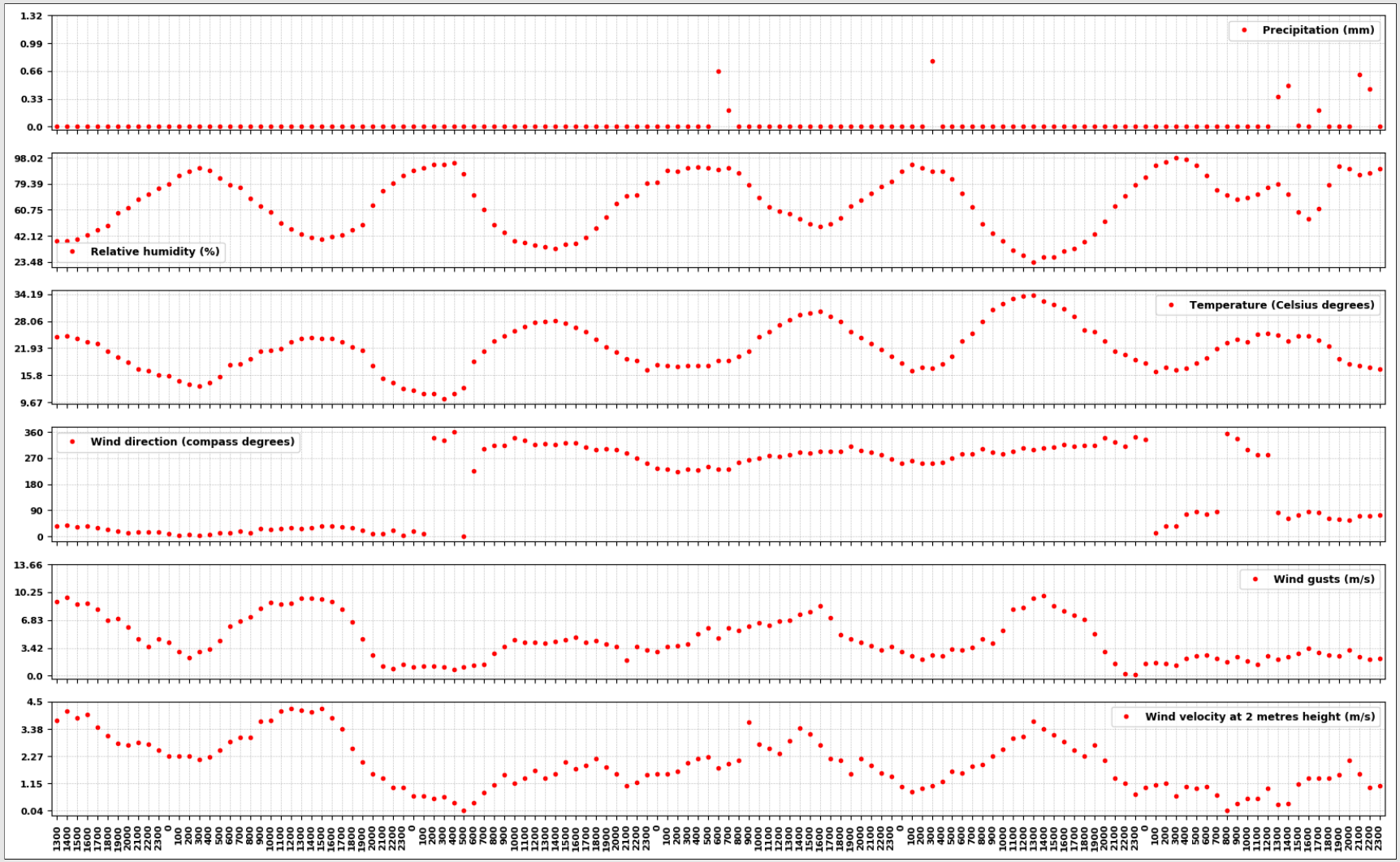

Figure C.14: Hourly variation of weather parameters, during the 2014 Västmanland wildfire, at MESAN data point thirteen (see figure C.1).

MESAN data point fourteen

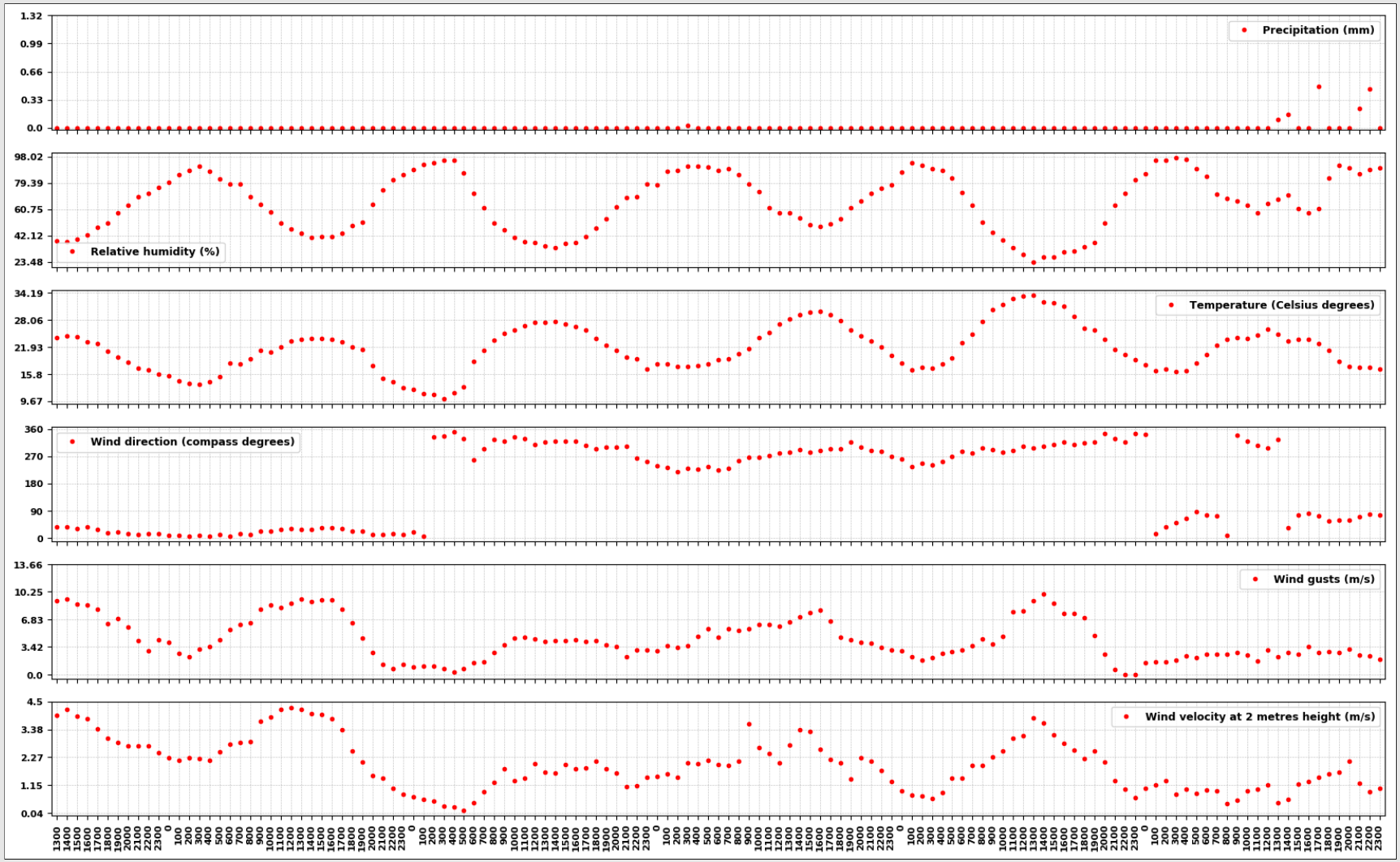

Figure C.15: Hourly variation of weather parameters, during the 2014 Västmanland wildfire, at MESAN data point fourteen (see figure C.1).

Series from Lund University

Department of Physical Geography and Ecosystem Science

Master Thesis in Geographical Information Science

1. *Anthony Lawther:* The application of GIS-based binary logistic regression for slope failure susceptibility mapping in the Western Grampian Mountains, Scotland (2008).
2. *Rickard Hansen:* Daily mobility in Grenoble Metropolitan Region, France. Applied GIS methods in time geographical research (2008).
3. *Emil Bayramov:* Environmental monitoring of bio-restoration activities using GIS and Remote Sensing (2009).
4. *Rafael Villarreal Pacheco:* Applications of Geographic Information Systems as an analytical and visualization tool for mass real estate valuation: a case study of Fontibon District, Bogota, Columbia (2009).
5. *Siri Oestreich Waage:* A case study of route solving for oversized transport: The use of GIS functionalities in transport of transformers, as part of maintaining a reliable power infrastructure (2010).
6. *Edgar Pimiento:* Shallow landslide susceptibility - Modelling and validation (2010).
7. *Martina Schäfer:* Near real-time mapping of floodwater mosquito breeding sites using aerial photographs (2010).
8. *August Pieter van Waarden-Nagel:* Land use evaluation to assess the outcome of the programme of rehabilitation measures for the river Rhine in the Netherlands (2010).
9. *Samira Muhammad:* Development and implementation of air quality data mart for Ontario, Canada: A case study of air quality in Ontario using OLAP tool. (2010).
10. *Fredros Oketch Okumu:* Using remotely sensed data to explore spatial and temporal relationships between photosynthetic productivity of vegetation and malaria transmission intensities in selected parts of Africa (2011).
11. *Svajunas Plunge:* Advanced decision support methods for solving diffuse water pollution problems (2011).
12. *Jonathan Higgins:* Monitoring urban growth in greater Lagos: A case study using GIS to monitor the urban growth of Lagos 1990 - 2008 and produce future growth prospects for the city (2011).
13. *Mårten Karlberg:* Mobile Map Client API: Design and Implementation for Android (2011).
14. *Jeanette McBride:* Mapping Chicago area urban tree canopy using color infrared imagery (2011).
15. *Andrew Farina:* Exploring the relationship between land surface temperature and vegetation abundance for urban heat island mitigation in Seville, Spain (2011).
16. *David Kanyari:* Nairobi City Journey Planner: An online and a Mobile Application (2011).
17. *Laura V. Drews:* Multi-criteria GIS analysis for siting of small wind power plants - A case study from Berlin (2012).
18. *Qaisar Nadeem:* Best living neighborhood in the city - A GIS based multi criteria evaluation of ArRiyadh City (2012).
19. *Ahmed Mohamed El Saeid Mustafa:* Development of a photo voltaic building rooftop integration analysis tool for GIS for Dokki District, Cairo, Egypt (2012).

20. *Daniel Patrick Taylor:* Eastern Oyster Aquaculture: Estuarine Remediation via Site Suitability and Spatially Explicit Carrying Capacity Modeling in Virginia's Chesapeake Bay (2013).
21. *Angeleta Oveta Wilson:* A Participatory GIS approach to unearthing Manchester's Cultural Heritage "gold mine" (2013).
22. *Ola Svensson:* Visibility and Tholos Tombs in the Messenian Landscape: A Comparative Case Study of the Pylian Hinterlands and the Soulima Valley (2013).
23. *Monika Ogden:* Land use impact on water quality in two river systems in South Africa (2013).
24. *Stefan Rova:* A GIS based approach assessing phosphorus load impact on Lake Flaten in Salem, Sweden (2013).
25. *Yann Buhot:* Analysis of the history of landscape changes over a period of 200 years. How can we predict past landscape pattern scenario and the impact on habitat diversity? (2013).
26. *Christina Fotiou:* Evaluating habitat suitability and spectral heterogeneity models to predict weed species presence (2014).
27. *Inese Linuza:* Accuracy Assessment in Glacier Change Analysis (2014).
28. *Agnieszka Griffin:* Domestic energy consumption and social living standards: a GIS analysis within the Greater London Authority area (2014).
29. *Brynja Guðmundsdóttir:* Detection of potential arable land with remote sensing and GIS - A Case Study for Kjósarhreppur (2014).
30. *Oleksandr Nekrasov:* Processing of MODIS Vegetation Indices for analysis of agricultural droughts in the southern Ukraine between the years 2000-2012 (2014).
31. *Sarah Tressel:* Recommendations for a polar Earth science portal in the context of Arctic Spatial Data Infrastructure (2014).
32. *Caroline Gevaert:* Combining Hyperspectral UAV and Multispectral Formosat-2 Imagery for Precision Agriculture Applications (2014).
33. *Salem Jamal-Uddeen:* Using GeoTools to implement the multi-criteria evaluation analysis - weighted linear combination model (2014).
34. *Samanah Seyedi-Shandiz:* Schematic representation of geographical railway network at the Swedish Transport Administration (2014).
35. *Kazi Masel Ullah:* Urban Land-use planning using Geographical Information System and analytical hierarchy processcase study Dhaka City (2014).
36. *Alexia Chang-Wailing Spitteler:* Development of a web application based on MCDA and GIS for the decision support of river and floodplain rehabilitation projects (2014).
37. *Alessandro De Martino:* Geographic accessibility analysis and evaluation of potential changes to the public transportation system in the City of Milan (2014).
38. *Alireza Mollasalehi:* GIS Based Modelling for Fuel Reduction Using Controlled Burn in Australia. Case Study: Logan City, QLD (2015).
39. *Negin A. Sanati:* Chronic Kidney Disease Mortality in Costa Rica; Geographical Distribution, Spatial Analysis and Non-traditional Risk Factors (2015).
40. *Karen McIntyre:* Benthic mapping of the Bluefields Bay fish sanctuary, Jamaica (2015).
41. *Kees van Duijvendijk:* Feasibility of a low-cost weather sensor network for agricultural purposes: A preliminary assessment (2015).

42. *Sebastian Andersson Hylander:* Evaluation of cultural ecosystem services using GIS (2015).
43. *Deborah Bowyer:* Measuring Urban Growth, Urban Form and Accessibility as Indicators of Urban Sprawl in Hamilton, New Zealand (2015).
44. *Stefan Arvidsson:* Relationship between tree species composition and phenology extracted from satellite data in Swedish forests (2015).
45. *Damián Giménez Cruz:* GIS-based optimal localisation of beekeeping in rural Kenya (2016).
46. *Alejandra Narváez Vallejo:* Can the introduction of the topographic indices in LPJ-GUESS improve the spatial representation of environmental variables? (2016).
47. *Anna Lundgren:* Development of a method for mapping the highest coastline in Sweden using breaklines extracted from high resolution digital elevation models (2016).
48. *Oluwatomi Esther Adejoro:* Does location also matter? A spatial analysis of social achievements of young South Australians (2016).
49. *Hristo Dobrev Tomov:* Automated temporal NDVI analysis over the Middle East for the period 1982 - 2010 (2016).
50. *Vincent Muller:* Impact of Security Context on Mobile Clinic Activities A GIS Multi Criteria Evaluation based on an MSF Humanitarian Mission in Cameroon (2016).
51. *Gezahagn Negash Seboka:* Spatial Assessment of NDVI as an Indicator of Desertification in Ethiopia using Remote Sensing and GIS (2016).
52. *Holly Buhler:* Evaluation of Interfacility Medical Transport Journey Times in Southeastern British Columbia. (2016).
53. *Lars Ole Grottenberg:* Assessing the ability to share spatial data between emergency management organisations in the High North (2016).
54. *Sean Grant:* The Right Tree in the Right Place: Using GIS to Maximize the Net Benefits from Urban Forests (2016).
55. *Irshad Jamal:* Multi-Criteria GIS Analysis for School Site Selection in Gorno-Badakhshan Autonomous Oblast, Tajikistan (2016).
56. *Fulgencio Sanmartín:* Wisdom-volkano: A novel tool based on open GIS and time-series visualization to analyse and share volcanic data (2016).
57. *Nezha Acil:* Remote sensing-based monitoring of snow cover dynamics and its influence on vegetation growth in the Middle Atlas Mountains (2016).
58. *Julia Hjalmarsson:* A Weighty Issue: Estimation of Fire Size with Geographically Weighted Logistic Regression (2016).
59. *Mathewos Tamiru Amato:* Using multi-criteria evaluation and GIS for chronic food and nutrition insecurity indicators analysis in Ethiopia (2016).
60. *Karim Alaa El Din Mohamed Soliman El Attar:* Bicycling Suitability in Downtown, Cairo, Egypt (2016).
61. *Gilbert Akol Echelai:* Asset Management: Integrating GIS as a Decision Support Tool in Meter Management in National Water and Sewerage Corporation (2016).
62. *Terje Slinning:* Analytic comparison of multibeam echo soundings (2016).
63. *Gréta Hlín Sveinsdóttir:* GIS-based MCDA for decision support: A framework for wind farm siting in Iceland (2017).

64. *Jonas Sjögren:* Consequences of a flood in Kristianstad, Sweden: A GIS-based analysis of impacts on important societal functions (2017).
65. *Nadine Raska:* 3D geologic subsurface modelling within the Mackenzie Plain, Northwest Territories, Canada (2017).
66. *Panagiotis Symeonidis:* Study of spatial and temporal variation of atmospheric optical parameters and their relation with PM 2.5 concentration over Europe using GIS technologies (2017).
67. *Michaela Bobeck:* A GIS-based Multi-Criteria Decision Analysis of Wind Farm Site Suitability in New South Wales, Australia, from a Sustainable Development Perspective (2017).
68. *Raghdaa Eissa:* Developing a GIS Model for the Assessment of Outdoor Recreational Facilities in New Cities Case Study: Tenth of Ramadan City, Egypt (2017).
69. *Zahra Khais Shahid:* Biofuel plantations and isoprene emissions in Svea and Götaland (2017).
70. *Mirza Amir Liaquat Baig:* Using geographical information systems in epidemiology: Mapping and analyzing occurrence of diarrhea in urban - residential area of Islamabad, Pakistan (2017).
71. *Joakim Jörwall:* Quantitative model of Present and Future well-being in the EU-28: A spatial Multi-Criteria Evaluation of socioeconomic and climatic comfort factors (2017).
72. *Elin Haettner:* Energy Poverty in the Dublin Region: Modelling Geographies of Risk (2017).
73. *Harry Eriksson:* Geochemistry of stream plants and its statistical relations to soil- and bedrock geology, slope directions and till geochemistry. A GIS-analysis of small catchments in northern Sweden (2017).
74. *Daniel Gardevärn:* PPGIS and Public meetings - An evaluation of public participation methods for urban planning (2017).
75. *Kim Friberg:* Sensitivity Analysis and Calibration of Multi Energy Balance Land Surface Model Parameters (2017).
76. *Viktor Svanerud:* Taking the bus to the park? A study of accessibility to green areas in Gothenburg through different modes of transport (2017).
77. *Lisa-Gaye Greene:* Deadly Designs: The Impact of Road Design on Road Crash Patterns along Jamaica's North Coast Highway (2017).
78. *Katarina Jemec Parker:* Spatial and temporal analysis of fecal indicator bacteria concentrations in beach water in San Diego, California (2017).
79. *Angela Kabiru:* An Exploratory Study of Middle Stone Age and Later Stone Age Site Locations in Kenya's Central Rift Valley Using Landscape Analysis: A GIS Approach (2017).
80. *Kristean Björkmann:* Subjective Well-Being and Environment: A GIS-Based Analysis (2018).
81. *Williams Erhunmonmen Ojo:* Measuring spatial accessibility to healthcare for people living with HIV-AIDS in southern Nigeria (2018).
82. *Daniel Assefa:* Developing Data Extraction and Dynamic Data Visualization (Styling) Modules for Web GIS Risk Assessment System (WGRAS). (2018).
83. *Adela Nistora:* Inundation scenarios in a changing climate: assessing potential impacts of sea-level rise on the coast of South-East England (2018).
84. *Marc Seliger:* Thirsty landscapes - Investigating growing irrigation water consumption and potential conservation measures within Utah's largest master-planned community: Daybreak (2018).

85. *Luka Jovičić:* Spatial Data Harmonisation in Regional Context in Accordance with INSPIRE Implementing Rules (2018).
86. *Christina Kourdounouli:* Analysis of Urban Ecosystem Condition Indicators for the Large Urban Zones and City Cores in EU (2018).
87. *Jeremy Azzopardi:* Effect of distance measures and feature representations on distance-based accessibility measures (2018).
88. *Patrick Kabatha:* An open source web GIS tool for analysis and visualization of elephant GPS telemetry data, alongside environmental and anthropogenic variables (2018).
89. *Richard Alphonce Giliba:* Effects of Climate Change on Potential Geographical Distribution of Prunus africana (African cherry) in the Eastern Arc Mountain Forests of Tanzania (2018).
90. *Eiður Kristinn Eiðsson:* Transformation and linking of authoritative multi-scale geodata for the Semantic Web: A case study of Swedish national building data sets (2018).
91. *Niamh Harty:* HOP!: a PGIS and citizen science approach to monitoring the condition of upland paths (2018).
92. *José Estuardo Jara Alvear:* Solar photovoltaic potential to complement hydropower in Ecuador: A GIS-based framework of analysis (2018).
93. *Brendan O'Neill:* Multicriteria Site Suitability for Algal Biofuel Production Facilities (2018).
94. *Roman Spataru:* Spatial-temporal GIS analysis in public health - a case study of polio disease (2018).
95. *Alicja Miodońska:* Assessing evolution of ice caps in Suðurland, Iceland, in years 1986 - 2014, using multispectral satellite imagery (2019).
96. *Dennis Lindell Schettini:* A Spatial Analysis of Homicide Crime's Distribution and Association with Deprivation in Stockholm Between 2010-2017 (2019).
97. *Damiano Vesentini:* The Po Delta Biosphere Reserve: Management challenges and priorities deriving from anthropogenic pressure and sea level rise (2019).
98. *Emilie Arnesten:* Impacts of future sea level rise and high water on roads, railways and environmental objects: a GIS analysis of the potential effects of increasing sea levels and highest projected high water in Scania, Sweden (2019).
99. *Syed Muhammad Amir Raza:* Comparison of geospatial support in RDF stores: Evaluation for ICOS Carbon Portal metadata (2019).
100. *Hemin Tofiq:* Investigating the accuracy of Digital Elevation Models from UAV images in areas with low contrast: A sandy beach as a case study (2019).
101. *Evangelos Vafeiadis:* Exploring the distribution of accessibility by public transport using spatial analysis. A case study for retail concentrations and public hospitals in Athens (2019).
102. *Milan Sekulic:* Multi-Criteria GIS modelling for optimal alignment of roadway by-passes in the Tlokweng Planning Area, Botswana (2019).
103. *Ingrid Piirisaar:* A multi-criteria GIS analysis for siting of utility-scale photovoltaic solar plants in county Kilkenny, Ireland (2019).
104. *Nigel Fox:* Plant phenology and climate change: possible effect on the onset of various wild plant species' first flowering day in the UK (2019).
105. *Gunnar Hesch:* Linking conflict events and cropland development in Afghanistan, 2001 to 2011, using MODIS land cover data and Uppsala Conflict Data Programme (2019).

106. *Elijah Njoku:* Analysis of spatial-temporal pattern of Land Surface Temperature (LST) due to NDVI and elevation in Ilorin, Nigeria (2019).
107. *Katalin Bunyevácz:* Development of a GIS methodology to evaluate informal urban green areas for inclusion in a community governance program (2019).
108. *Paul dos Santos:* Automating synthetic trip data generation for an agent-based simulation of urban mobility (2019).
109. *Robert O' Dwyer:* Land cover changes in Southern Sweden from the mid-Holocene to present day: Insights for ecosystem service assessments (2019).
110. *Daniel Klingmyr:* Global scale patterns and trends in tropospheric NO2 concentrations (2019).
111. *Marwa Farouk Elkabbany:* Sea Level Rise Vulnerability Assessment for Abu Dhabi, United Arab Emirates (2019).
112. *Jip Jan van Zoonen:* Aspects of Error Quantification and Evaluation in Digital Elevation Models for Glacier Surfaces (2020).
113. *Georgios Efthymiou:* The use of bicycles in a mid-sized city - benefits and obstacles identified using a questionnaire and GIS (2020).
114. *Haruna Olayiwola Jimoh:* Assessment of Urban Sprawl in MOWE/IBAFO Axis of Ogun State using GIS Capabilities (2020).
115. *Nikolaos Barmpas Zachariadis:* Development of an iOS, Augmented Reality for disaster management (2020).
116. *Ida Storm:* ICOS Atmospheric Stations: Spatial Characterization of CO2 Footprint Areas and Evaluating the Uncertainties of Modelled CO2 Concentrations (2020).
117. *Alon Zuta:* Evaluation of water stress mapping methods in vineyards using airborne thermal imaging (2020).
118. *Marcus Eriksson:* Evaluating structural landscape development in the municipality Upplands-Bro, using landscape metrics indices (2020).
119. *Ane Rahbek Vierø:* Connectivity for Cyclists? A Network Analysis of Copenhagen's Bike Lanes (2020).
120. *Cecilia Baggini:* Changes in habitat suitability for three declining Anatidae species in saltmarshes on the Mersey estuary, North-West England (2020).
121. *Bakrad Balabanian:* Transportation and Its Effect on Student Performance (2020).
122. *Ali Al Farid:* Knowledge and Data Driven Approaches for Hydrocarbon Microseepage Characterizations: An Application of Satellite Remote Sensing (2020).
123. *Bartlomiej Kolodziejczyk:* Distribution Modelling of Gene Drive-Modified Mosquitoes and Their Effects on Wild Populations (2020).
124. *Alexis Cazorla:* Decreasing organic nitrogen concentrations in European water bodies - links to organic carbon trends and land cover (2020).
125. *Kharid Mwakoba:* Remote sensing analysis of land cover/use conditions of community-based wildlife conservation areas in Tanzania (2021).
126. *Chinatsu Endo:* Remote Sensing Based Pre-Season Yellow Rust Early Warning in Oromia, Ethiopia (2021).

127. *Berit Mohr:* Using remote sensing and land abandonment as a proxy for long-term human out-migration. A Case Study: Al-Hassakeh Governorate, Syria (2021).
128. *Kanchana Nirmali Bandaranayake:* Considering future precipitation in delineation locations for water storage systems - Case study Sri Lanka (2021).
129. *Emma Bylund:* Dynamics of net primary production and food availability in the aftermath of the 2004 and 2007 desert locust outbreaks in Niger and Yemen (2021).
130. *Shawn Pace:* Urban infrastructure inundation risk from permanent sea-level rise scenarios in London (UK), Bangkok (Thailand) and Mumbai (India): A comparative analysis (2021).
131. *Oskar Evert Johansson:* The hydrodynamic impacts of Estuarine Oyster reefs, and the application of drone technology to this study (2021).
132. *Pritam Kumarsingh:* A Case Study to develop and test GIS/SDSS methods to assess the production capacity of a Cocoa Site in Trinidad and Tobago (2021).
133. *Muhammad Imran Khan:* Property Tax Mapping and Assessment using GIS (2021).
134. *Domna Kanari:* Mining geosocial data from Flickr to explore tourism patterns: The case study of Athens (2021).
135. *Mona Tykesson Klubien:* Livestock-MRSA in Danish pig farms (2021).
136. *Ove Njøten:* Comparing radar satellites. Use of Sentinel-1 leads to an increase in oil spill alerts in Norwegian waters (2021).
137. *Panagiotis Patrinos:* Change of heating fuel consumption patterns produced by the economic crisis in Greece (2021).
138. *Lukasz Langowski:* Assessing the suitability of using Sentinel-1A SAR multi-temporal imagery to detect fallow periods between rice crops (2021).
139. *Jonas Tillman:* Perception accuracy and user acceptance of legend designs for opacity data mapping in GIS (2022).
140. *Gabriela Olekszyk:* ALS (Airborne LIDAR) accuracy: Can potential low data quality of ground points be modelled/detected? Case study of 2016 LIDAR capture over Auckland, New Zealand (2022).
141. *Luke Aspland:* Weights of Evidence Predictive Modelling in Archaeology (2022).
142. *Luís Fareleira Gomes:* The influence of climate, population density, tree species and land cover on fire pattern in mainland Portugal (2022).
143. *Andreas Eriksson:* Mapping Fire Salamander (Salamandra salamandra) Habitat Suitability in Baden-Württemberg with Multi-Temporal Sentinel-1 and Sentinel-2 Imagery (2022).
144. *Lisbet Hougaard Baklid:* Geographical expansion rate of a brown bear population in Fennoscandia and the factors explaining the directional variations (2022).
145. *Victoria Persson:* Mussels in deep water with climate change: Spatial distribution of mussel (Mytilus galloprovincialis) growth offshore in the French Mediterranean with respect to climate change scenario RCP 8.5 Long Term and Integrated Multi-Trophic Aquaculture (IMTA) using Dynamic Energy Budget (DEB) modelling (2022).
146. *Benjamin Bernard Fabien Gérard Borgeais:* Implementing a multi-criteria GIS analysis and predictive modelling to locate Upper Palaeolithic decorated caves in the Périgord noir, France (2022).

147. *Bernat Dorado-Guerrero:* Assessing the impact of post-fire restoration interventions using spectral vegetation indices: A case study in El Bruc, Spain (2022).
148. *Ignatius Gabriel Aloysius Maria Perera:* The Influence of Natural Radon Occurrence on the Severity of the COVID-19 Pandemic in Germany: A Spatial Analysis (2022).
149. *Mark Overton:* An Analysis of Spatially-enabled Mobile Decision Support Systems in a Collaborative Decision-Making Environment (2022).
150. *Viggo Lunde:* Analysing methods for visualizing time-series datasets in open-source web mapping (2022).
151. *Johan Viscarra Hansson:* Distribution Analysis of Impatiens glandulifera in Kronoberg County and a Pest Risk Map for Alvesta Municipality (2022).
152. *Vincenzo Poppiti:* GIS and Tourism: Developing strategies for new touristic flows after the Covid-19 pandemic (2022).
153. *Henrik Hagelin:* Wildfire growth modelling in Sweden - A suitability assessment of available data (2023).